

# **Chapter 1: Introduction**

**1.1. Introduction**

**1.2. UAE Sustainability Scenario**

**1.3. Importance of the Study**

## 1.1 Introduction

The construction industry in the UAE has been and continues to be influenced by a raft of building methodologies and design principles from diverse parts of the globe. As buildings in the UAE rise higher and reflect more aesthetic and iconic aspirations, an interest in sustainability has also become increasingly prevalent.

In a global context, energy consumption is one of the biggest environmental concerns which translate to carbon emissions and fossil fuel depletion. In the US alone, buildings consume almost 37% of energy and 68% of electricity (USGBC, 2007). Consequently, the UAE's energy consumption per capita is twice that of the US. (Kazim, 2005)

In a hot humid climate like in the UAE, cooling loads escalate to maintain liveable conditions in indoor spaces. The building envelope which serves as external protection therefore plays a critical role in controlling building energy consumption. Unlike building active systems installation, architectural elements are inanimate solutions that do not depend on energy to maintain optimum performance. These however should be designed and resolved early since not only do they affect aesthetics, but they are also a permanent element which stays through the lifetime of the building.

The industry in the UAE is able to learn from the experiences of other regions. Instead of focusing on future conceptual solutions and unrealized building systems and materials, current available technology should be harnessed and utilized. Double skin façade has shown itself to be highly beneficial in various areas of building performance in other

parts of the world, particularly in temperate zones. The double skin façade has proved its usefulness in these regions, offering up to 30% reduction in energy consumption (Arons & Glicksman, 2001). However, the double skin façade has been rarely used in the desert climate, thus a case starting point for this research.

## 1.2 UAE Sustainability Scenario

Early industries whose main economic activities include farming herding, dates, coasts- fish, pearl diving and trading form much of the UAE's early industries. After its independence in 1971, the UAE diversified economy into petrochemicals, tourism, real estate, banking, and aviation International Economic Data Bank (2000 cited in Kazim, 2005)

The UAE is one of the largest consumer of water at 90gallons/capita which is about 12% of the world's total desalinated water. Water desalination typically requires 86 kWh/m<sup>3</sup> or 5kWh/m<sup>3</sup> through reverse osmosis. 70% of total potable water is acquired through desalination. In Figure 1.1, from 1990 – 2001, energy consumption per capita is about 6 – 9 times greater than Middle East and the world respectively. Consequently, energy consumption is 4 to 2 folds more than EU countries and US, respectively. Carbon emission per capita is at least twice of the developed countries like US and EU countries as seen in Figure 1.2.

“According to energy information administration (US DOE EIA, 2004), the UAE's maximum crude oil production capacity is estimated to be around 2.0–2.5 million barrels per day (bbl/d). Generally, the country plays an essential role in the world energy market because it possesses roughly 100 billion barrels of proven oil reserves, which is nearly 10% of the world's crude oil supply” (Kazim, 2005:427).

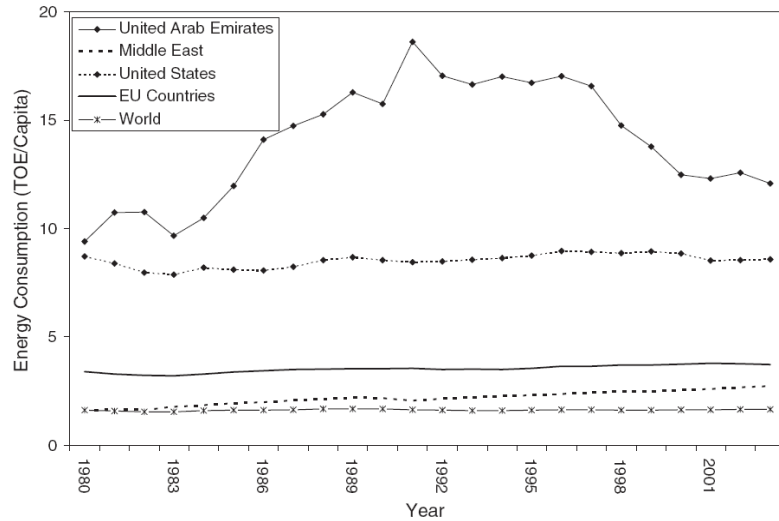


Figure 1.1 UAE's energy consumption per capita compare to other regions from 1980 to 2003 (Kazim, 2005:434)

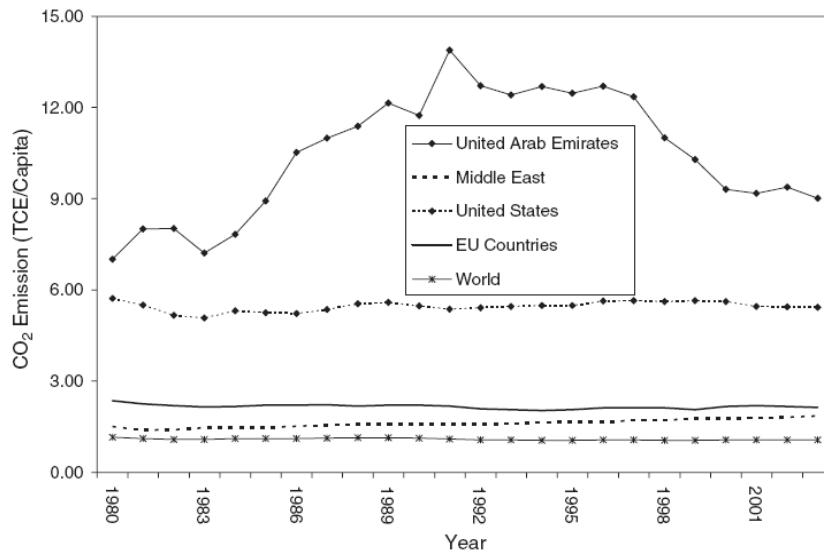


Figure 1.2 UAE's carbon emission in comparison to other regions from 1980 to 2003. (Kazim,2005:434)

There are several projects underway to manage the overwhelming surge in energy consumption. As part of Abu Dhabi's drive to relieve dependence from hydrocarbon power generation, the government is set to build a \$350m solar power plant. This 500 megawatt plant is anticipated to commence operations for 2009. The first wind generated power plant in the Arabian Peninsula has recently been set up on Sir Baniyas Island, UAE (Middle East Electricity, 2008).

In other related projects, seven solar-powered wind measurement towers were built to measure the wind statistics potential of various parts of the emirate of Fujairah back in 2002. Three towers with computerize sensors and detectors to be able to record wind data were constructed in Al Siji, Masafi and Dhadnah while four other were erected at the mountains fo Habhab, Tawiyeen, Jareef and Al Halat (UAE Interact, 2003).

Some solar photovoltaic applications have also been started in the country. A hotel project used solar energy and has proven to reduce cooling loads to a third. Also visible in the city of Dubai are several parking meters that are powered through photovoltaic cells (Middleeast Electricity, 2008)

In Abu Dhabi, a visionary project called Masdar City is aimed be the world's first sustainable development. This will be first zero carbon and zero waste city that is entirely powered by renewable energy. The city scale project has attracted several prominent designers and incorporates infrastructure with state of the art green technologies (Masdar, 2008).

The rapid growth of the UAE has inevitably taken its toll on the environmental situation of the country. Only recently, the sustainability race has been more clamored on the international scene, and locally it imposes its presence, as seen from the programs and commencing initiatives. Since there is a wide interest amongst various sectors and evidently, there is more pressure to develop expertise. At this stage, the supply of knowledge needs to catch up to the demand for environmental solutions.

### **1.3 Importance of the Study**

Double skin facades have been applied and studied in actual built structures, mostly in temperate climates. Yet increasingly, it is being considered in other climatic zones. The chief feature of the system is its thermal benefit. The major end result is the reduction of energy usage for heating or cooling loads, and the corresponding cost savings.

Double skin facades serve as an external shading device for year-round temperature control. The ability to reclaim heated air into the space through ventilation is very suitable for cold conditions in temperate countries. Some applications also demonstrate the use of the design in both summer and winter seasons in temperate climates.

Apart from the thermal benefits advantages in acoustics and lighting are known. It can serve as an acoustic barrier in cities or noisy environments. Indoor lighting can be supplemented by enhanced daylight penetration through the transparent double glazing.

However, some concerns with envelope systems such as double skin facades focusing on cost, maintenance issues and glare, need to be addressed. There is a higher initial investment for the additional exterior glazing, which could double the cost compared to a typical curtainwalling system. Façade maintenance is a major concern, since surfaces to be cleaned are almost tripled additionally due to increased exposure to dust, rain and pollution. Depending on the cavity dimension, the façade typically utilizes the maximum floor area of the building, offsetting leasable space for high density areas. Consuming the perimeter space may also have implications for exit and emergency escape routes. At the

same time, care may have to be taken to minimize glare in certain solar locations.

Most applications have been in new buildings however, the technique can also be used as an applied retrofit as presented by Ballestrini et al (2004) which studied a rehabilitation of a disused factory that incorporated a second glazed skin with the original external walls.

Categorizations based on climatic examples from temperate and exported to arid and humid locations are too broad to allow useful generalized analysis. As noted by Arons and Glicksman (2001), context is crucial:

Before analyzing the potential for transfer of technologies such as double skin facades] to different continents (climates, cultures and economies) it is important to understand what the systems are and how they work in their original context

(Arons and Glicksman 2001:3)



## **Chapter 2: Literature Review**

- 2.1. Definitions and History of Double Skin Facades**
- 2.2. Classifications and Typologies**
- 2.3. Technical Description**
- 2.4. Other Applications**
- 2.5. Double Skin Façade Examples**
- 2.6. UAE Climatic Profile**
- 2.7. Examples in the Desert Climate and UAE**
- 2.8. Findings of Literature Review - Water Spray**
- 2.9. Dissertation Aims and Objectives**

## **2.1 Definitions and History of Double Skin Facades**

### **Definition**

The double skin façade assembly has been named with different tags and characterization to illustrate the assembly. Based on function or configuration, different meanings are attempted to describe satisfactory this system.

Saelens (2001) referred to double skin facades with various associations such as active envelopes, twin facades or second skin facades. He described the system to consist of two panes with a cavity in between, where air flows and a shading device is installed. There is a distinction between naturally and mechanically ventilated façades, and according to the air flow path, various ventilation strategies are applicable.

Gan (2005) described a double skin façade as consisting of an inner and outer skin. This aids thermal and sound insulation as compared to traditional glazing, and can be used for natural ventilation.

Hamza (2007) defined double skin facades as two layers of façade separated by an air gap that varies in its depth and creating a solar chimney effect where warm air rises by buoyancy.

Ding et al (2004) described a double skin façade to be composed of an external façade, an intermediate space and an inner façade. The study further described that the outer faced layer provides protection against

weather and improves acoustics insulation while adjustable sunshading devices like blinds are usually installed.

The Belgian Building Research Institute (2002) describes a double skin façade as follows:

- a. Exterior glazing which can be a fully glazed exterior façade and is usually a hardened single glazing.
- b. Interior glazing is most likely an insulating double glazing unit (low E coating, clear with incorporated solar controls). This layer is typically this is not fully glazed.
- c. There is an air cavity between the two panes which can be natural driven, fan assisted or mechanically ventilated. The width dimension influences the maintenance and performance of the system and may range from 200mm to more than 2 meters.
- d. An operable interior window is integrated if natural air flow into the space is preferred
- e. Solar shading devices automatically controlled can be added into the cavity.
- f. Heating radiators can be installed adjacent to the façade according to climate variations. (BBRI, 2002)

## **History**

De Ruiter (1998) cited in Saelens (2002) narrated that the director of the industrial Museum in Brussels Jean-Baptiste Jobard in 1849 described a mechanically ventilated multiple skin façade. He explained that in summer, cold air should be circulated within the two glazing surfaces while in winter, it should be warm air. A similar idea emerged again after 65 in Scheerbaert's (1914) book "Glasarchitectur." (Saelens, 2002)

Crespo claims that that first double skin curtain wall was seen at Steiff Factory in Giegen, Germany in 1903 and was designed by the factory owner's son, Richard Steiff. According to Crespo, the system focused on daylight while responding to the cold weather and strong winds. The structure is a three storey building used as storage in the ground, and work areas in the upper floors. The success of the system was followed by two more buildings in 1904 and 1908 which alternated timber instead of steel. At present, the buildings mentioned are still being used.

Crespo also mentioned a design competition by Otto Wagner in 1903 for the Post Office Savings Bank in Vienna, Austria. A steel structure supports glass and aluminium skylight in the main hall occupying three naves of the building. It was built in two phases from 1904 to 1912. With renovations in the 70's, it is still currently used by the same owner

In 1928 Russia, Moisei Ginzburg experimented using double skin stripes in the communal housing blocks of Narkomfin building. While the project is regarded as representation of communism, the designer wanted to test the window idea through the use of a vertical truss system that supports a curtain wall hanging inside and outside the building (Crespo, 1999).

Still in the 1920's, Le Corbusier incorporated what he referred to as "murnneutralisant," which was a system of ventilated double glazing often regarded expensive and impractical to build. Le Corbusier was also designing in Moscow the Centrosoyus around this time and eventually started in Paris, the design for the Cite de Refuge (1929) and the Immeuble Clarte (1930). Similarities between Narkomfin and Cite de

Refuge could have been influenced by Le Corbusier's consecutive visits to Moscow and the eventual acquaintance of Ginzburg (Crespo, 1999).

In 1978 Cannon Design and HOK designed the Hooker office Building in Niagara Falls, New York where Le Corbusier's ventilation ideas were incorporated. A solar reactive bank of louvers, tilts and collects solar radiation within an 8 inch cavity. The induced stack effect is either collected in cold weather or flushed out during summer. Around the same time, the Solar Dairy at Mysen Norway used a similar configuration Harrison (2001).

In the 80's, double skin façades were applied due to aesthetics and environmental considerations. Arup Associates in 1984 design the offices of Leslie and Godwin or the Briarcliff House in Farnborough, England. Herzog and De Meuron in 1993 designed the SUVA Building in Basel, Switzerland which focused on the aesthetic effect of a glass louver envelope for a renovation project. (Crespo, 1999)

The 90's, environmental concerns and the desire for enhanced iconic or corporate image influenced the call for green buildings. Computer tools for calculations drove the design of the façade. Notable examples both in 1997 Germany include RWE AG Headquarters by Ingenhove, Overdiek Kahlen un Partner and Commerzbank HQ by Foster and Partners. In 1998, Renzo Piano Building workshop of the Debis Tower in the Potsdamer Platz development has also undergone a comprehensive facade analysis to achieve the flexibility in the assembly layers.

## 2.2 Classifications and Typologies

Several studies have different ways of categorizing double skin facades. The means of classification vary depending on factors such as assembly configuration, air movement or construction to mention a few.

Arons (2000) distinguished two main types of facades, Airflow façade and Airflow window. “An Airflow façade is a double-leaf façade that is continuous for at least one story, with its inlet and flow level of one story and its exhaust at least as high as the floor level above. On the other hand, “an Airflow window is a double-leaf façade that has an inlet and outlet spaced less than the vertical spacing between floor and ceiling.”

Arons (2000) classify double skin facades based on Primary and Secondary Identifiers. Primary identifiers describe the airflow pattern and building height relationship, while Secondary identifiers include factors such layering, materials, operability and cavity dimensions.

*Table 2.1 Primary Identifiers Arons (2000)*

Primary Identifiers	
Airflow Patterns	Building Height
<ul style="list-style-type: none"> <li>• <b>Outside ventilated</b> outside air enters the cavity and vents outside</li> <li>• <b>Inside ventilated</b> indoor air enters the cavity and exhausts to plant</li> <li>• <b>Hybrid Systems</b> outdoor or indoor air enters the cavity and exits the opposite side</li> </ul>	<ul style="list-style-type: none"> <li>• <b>mid-rise</b></li> <li>• <b>high-rise</b> allows windows to be openable even at high external wind pressure</li> </ul>

Table 2.2 Secondary Identifiers Arons (2000)

Secondary Identifiers					
Layering Composition	Depth of Cavity	Horizontal extend of cavity	Vertical extent of cavity	Operability	Materials
<ul style="list-style-type: none"> <li>• glass</li> <li>• gases</li> <li>• shading device</li> </ul>	<ul style="list-style-type: none"> <li>• <b>Compact Style</b> 200 to 1400mm</li> <li>• <b>Wide Style</b> 1000mm</li> <li>• <b>Expanded Style</b> atrium spaces or buildings in buildings</li> </ul>	<ul style="list-style-type: none"> <li>• <b>box window</b> covers only the extent of windows on opaque walls</li> <li>• <b>corridor facade</b> are continuous glass &amp; or uninterrupted cavity                             <ul style="list-style-type: none"> <li>• walkway can be grated for airflow</li> <li>• walkway can be closed but horizontally uninterrupted</li> </ul> </li> </ul>	<ul style="list-style-type: none"> <li>• <b>atria</b> if relatively wide; <b>flues</b> if narrower</li> <li>• <b>double skin façade</b> if full storey height</li> <li>• <b>double skin window</b> if partial height with spandrels or other windows</li> </ul>	<ul style="list-style-type: none"> <li>• <b>automated</b> or <b>occupant</b> operated inner pane</li> <li>• form varies tilt-turn inset full height</li> <li>• <b>slide</b> - full height access</li> <li>• <b>pivot</b> - may restrict sun shading elements</li> </ul>	<ul style="list-style-type: none"> <li>• care in material selection due to increased temperatures within the cavity</li> </ul>
<i>(depends on air movement strategy)</i>		<i>(divided in relation to interior partitions)</i>	<i>(refers to the distance between air supply to cavity and final exhaust from cavity without interference)</i>		

Saelens (2002) classify facades based on the geometry of the cavity.

Table 2.3 Classification based on Cavity Geometry by Saelens (2002)

Box Window Type	Shaft Box Type	Corridor façade	Multi storey Double Skin façade
<ul style="list-style-type: none"> <li>• horizontal and vertical partitioning divides into modular boxes</li> </ul>	<ul style="list-style-type: none"> <li>• box window elements are connected through vertical shafts for stack effect</li> </ul>	<ul style="list-style-type: none"> <li>• horizontal partitioning into corridors ideal for acoustics, fire security, ventilation</li> </ul>	<ul style="list-style-type: none"> <li>• clear of partitioning, opening placed near floor and roof</li> </ul>

Poirazis (2004) provides an extensive literature review describing different approaches in classifying double skin facades. The following authors have been extracted from this compilation. Battle McCarthy, a British engineering firm grouped double skin facades in five primary types

with subcategories based on façade configuration and manner of operation as seen in Table 2.4. Table 2.6 however showed how Magali (2001) distinguished two main categories based on the horizontal partitioning per floor while sub-categories describe airtightness associated with the opening. Kragh (2000) on the other hand categorized three types according to the ventilation function of the cavity as illustrated in Table 2.7.

The Belgian Building Research Institute Sourcebook (2002 cited in Poirazis, 2004) detailed characterizations similar to the above, and added a louvers façade type where the exterior skin has mechanized transparent louvers that closes for airtightness and opens to allow ventilation.

*Table 2.4 Five Primary Types by Battle McCarthy*

<b>Category A</b>	<b>Category B</b>	<b>Category C</b>	<b>Category D</b>	<b>Category E</b>
Sealed inner skin	Openable Inner and Outer Skin	Openable Inner Skin	Sealed Cavity	Acoustic Barrier
<ul style="list-style-type: none"> <li>• mechanically ventilated, controlled flue intake</li> <li>• ventilated and serviced thermal flue</li> </ul>	<ul style="list-style-type: none"> <li>• single storey cavity</li> <li>• full building cavity</li> </ul>	<ul style="list-style-type: none"> <li>• mechanically ventilated, controlled flue intake</li> <li>• ventilated and serviced thermal flue</li> </ul>	<ul style="list-style-type: none"> <li>• zoned floor by floor</li> <li>• full height cavity</li> </ul>	<ul style="list-style-type: none"> <li>• massive exterior envelope</li> <li>• lightweight exterior envelope</li> </ul>

*Table 2.5 Classification by Uutu*

<b>Building - High</b>	<b>Storey-high</b>	<b>Box Double Skin</b>	<b>Shaft Facades</b>
<ul style="list-style-type: none"> <li>• cavity extends the whole building height without separation</li> </ul>	<ul style="list-style-type: none"> <li>• separated horizontally at each floor</li> </ul>	<ul style="list-style-type: none"> <li>• horizontal partitioning on each floor and vertical partitions in each window</li> </ul>	<ul style="list-style-type: none"> <li>• storey high cavities are connected to a central building high cavity that induces air flow through stack effect</li> </ul>



Table 2.6 Categories by Magali

Category A		Category B
no horizontal partitioning		horizontal partitioning at each floor
A1	2 façades are airtight	B1
A2	non-airtight internal façade - airtight external façade	B2
A3	non-airtight external façade - airtight internal façade	B3
A4	non-airtight internal and external façade	B4

Table 2.7 Wall types by Kragh

Naturally Ventilated Wall	Active Wall	Interactive Wall
<ul style="list-style-type: none"> <li>• extra skin is added outside the building envelope</li> <li>• solar heat gain drives natural bouyancy within the façade cavity</li> <li>• not recommended for hot climates</li> </ul>	<ul style="list-style-type: none"> <li>• extra skin is added inside the building envelope</li> <li>• return air passes through the cavity, blinds inside absorb solar radiation</li> <li>• solar energy is removed by ventilation or recovered by heat exchangers for indoor occupant comfort</li> <li>• recommended for cold climates</li> </ul>	<ul style="list-style-type: none"> <li>• similar to naturally ventilated wall except ventilation is forced, does not rely on stack effect alone</li> <li>• ventilation can be minimized in cold weather</li> <li>• possible use of operable windows even in high-rise</li> <li>• ideal for hot climates since it does not depend on stack effect alone</li> </ul>

Table 2.8 Classification by BBRI

Type of Ventilation	Origin of Airflow	Destination of Airflow	Airflow Direction	Width of the air cavity	Partitioning
<ul style="list-style-type: none"> <li>• natural</li> <li>• mechanical</li> </ul>	<ul style="list-style-type: none"> <li>• inside</li> <li>• outside</li> </ul>	<ul style="list-style-type: none"> <li>• inside</li> <li>• outside</li> </ul>	<ul style="list-style-type: none"> <li>• to the top</li> <li>• to the bottom (only in mechanical ventilation cases)</li> </ul>	<ul style="list-style-type: none"> <li>• narrow (10-20 cm)</li> <li>• wide (0.5-1m)</li> </ul>	<ul style="list-style-type: none"> <li>• horizontal (at each level)</li> <li>• no horizontal partitioning</li> </ul>

The various types and classifications of double skin facades show the complexity of configuring this assembly. At times it may be difficult to incorporate combinations of strategies where features could double functions or at times even contrast each other. Specific configurations rely on careful design discretion and should be evaluated individually and per case, based on parameters and combinations of these mentioned categorizations.

## **2.3 Technical Description**

### **Construction Elements**

Uuttu (2001, cited in Poirazis 2004) divides the structures of double skin facades into three main groups: Primary, Secondary and Tertiary structures. Primary structures are load bearing elements that include columns, walls, floors and brackets that carry loads. Secondary structures include floors that are not part of the primary system, partitions, roof structures and built-in items. Tertiary structures are those which are not critical to the stability of the secondary structure such as windows within the façade.

Kallioneimi (1999, cited in Poirazis 2004) described that the connection types of steel-glass facades. These include putty glazing, glass holder list, pressed fastening, point supported glass panes and structural silicone glazing.

### **Opening Principles**

The air movement within the cavity of the double skin façade may be natural, fan supported (hybrid) or mechanical. The depth may vary from 10cm to 2m and this may influence the façade's physical properties and manner of maintenance. (Streicher et al, 2007)

Faist (1998, in Poirazis 2004) compared a double skin façade that used natural room ventilation and an airtight façade. Faist explained that cavity depths are not critical in air tight facades and that although windows are usually closed, it does not ensure good room ventilation. The canal or cavity is also open at the bottom with controlled top valves while a height limitation of 3 to 4 levels is considered to allow air temperature increase.

Ventilated façade depth on the other hand has to be designed accurately. Room ventilation is engaged by corresponding floor to floor valves. Its cavity is closed at the bottom and extends above the uppermost floor for a limit of 10 to 15 storeys to allow air temperature increase. (Faist, 1998, in Poirazis 2004)

Oesterle et al (2001) explained in Poirazis (2004) that when the cavity is shallow (around 40cm) that considerable pressure losses will occur due to air flow resistance. In ventilating functions, the effectiveness of inner façades depends on the opening operation of the windows. The authors further added that the same concept in air intakes also are applicable to air extracts.

## **Material Choice**

### Glass

The selected glazing is purely dependent on the chosen facade typology. In an outdoor ventilated façade, an insulating sealed double glazed unit is placed at the interior side while a single pane is placed on the exterior. An indoor ventilated façade however has the insulating pane outside and a single pane at the interior side. (Streicher et al, 2007)

Lee et al (cited in Poirazis, 2002) said that heat strengthened safety glass or laminated safety glass is the most common type of exterior glass while the interior layer is a fixed or operable double or single pane casement or hopper windows with low emittance coatings to reduce heat transfer.

## Shading Device

Shading devices like venetian blinds are usually placed inside the cavity for protection. Their position and characteristics affect the performance of the cavity since they absorb or reflect radiant energy. Careful selection of the shading device against the pane type and cavity geometry and ventilation strategy has a high impact on indoor daylight. (Streicher et al, 2007).

Lee et al (2002) and Oesterle et al (2001) as cited in Poirazis (2004) both suggested that the position of the shading device is critical in double skin design. Essentially, the shading design should be placed at the outer half of the intermediate space but not too close to the outer glass, about 15 cm between the sun shading and external skin.

## **Fire Issues**

Poirazis (2004) stated that fire protection might be a critical issue in double skin facades. Depending on the design, double skin façade designs can reach a depth of about two meters and may have a continuous clearance throughout the height of the building. In such cases the propagation of fire between floors could be critical since there may be no thermal breaks or fire stoppers within the cavity between floors. Also, the induced air movement due to convection can spread and feed the flames due to continuous venting of combustion. It is not yet clear if the assembly can be advantageous or not. Poirazis (2004) further noted that some authors stressed the possibility of adjacent room smoke transmission in the occasion of fire.

Chow et al (2005b) studied the behavior of a double skin façade assembly in the occasion of fire. The research, conducted in a testing facility in Northeast China, studied the relationship of smoke movement

causing glass damage in relation to the cavity depth of a double skin façade assembly. The authors found that even in a scenario of fire reaching a temperature of only 110 °C, there was a high possibility of cracking or breaking big glass panels. This means that even at a low threshold, it is difficult for double skin façades to be compliant with fire regulations.

Chow and Hung (2005a) also noted that several new projects in Hong Kong incorporating the use of double skin facades failed compliance with safety and fire codes. They also stressed that very few studies showed a large-scale burning test to study or predict the performance of double skin facades during fires. The same study compared smoke behavior in the three depth scenarios of 0.5, 1.0, and 1.5, and found out that the 1 meter depth has proven to be more dangerous. It was observed that smoke further propagates closer towards the inner glazing, and spreading to the floors above.

Chow et al (2005b) also noted that the damage caused by fire to the outer glazing could be dangerous to pedestrians. They suggested that strong outer skin using thicker glass or tempered glass could be used. However the cost implications need to be considered when using such type.

## **2.4 Other Applications with the Double Skin Facade**

### **Integration to HVAC Strategies**

In the analysis of the integration of HVAC strategies to double skin façades, the compilation and work of Poirazis (2004) is used as a foundation for this section. This work has exhibited a comprehensive and comparative collection of different literature on double skin technology.

Stec and Paasen (2003) conducted a study where different HVAC strategies are integrated in various double skin typologies. Considerations in design included the definition double skin function, selection of type, and the optimization of HVAC design and selection of control strategy. The study also stressed that thin cavities are more suitable in cold season to enhance the increase of temperature, however in hot seasons, the double skin should work as a screen from solar radiation.

Stec et al (2003 cited in Poirazis, 2004) described three ways that an HVAC can be incorporated in a double skin façade. These ways describe whether the double skin contributes to the HVAC system, Full, Limited or No HVAC where the later means that the double skin façade performs the entire HVAC system

There are different types according to Stec et al (2003) where the double skin façade can be integrated in the HVAC system.

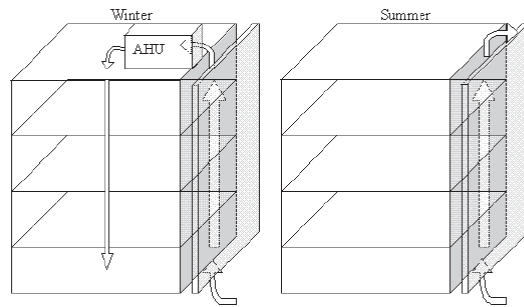


Figure 2.1a DSF Pre-Heater

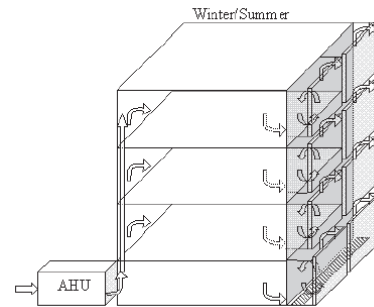


Figure 2.1b DSF Exhaust

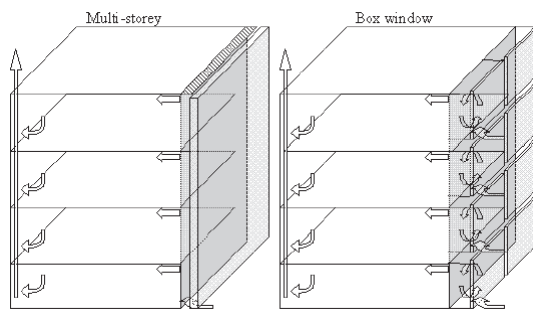


Figure 2.1c DSF Supply of Pre-Heated Air Exhaust

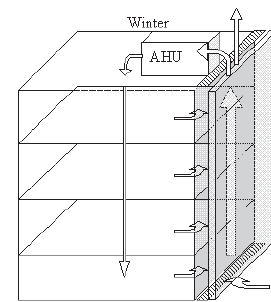


Figure 2.1d DSF Central Exhaust

In winter, (Figure 2.1a) fresh air can be preheated when it enters first through the façade. In Summer, air can be extracted through the upper extract of the double skin. In Figure 2.1b, the double skin is used exclusively as an exhaust duct. It is also possible to directly introduce into the space the preheated air from the double skin façade with some variable air volume control as shown in Figure 2.1c. This however is not advisable during summer since air within the double skin façade is usually warmer. Figure 2.1d on the other hand shows that the double skin façade can be used as a channel for HVAC extract.

Essentially, supply facades function better in winter for preheating purposes, while in summer it is more useful for cooling the cavity.



## **Solar Chimney**

Ding et al (2004) studied the natural ventilation performance of a double-skin façade with a solar chimney. Their paper highlighted the performance of a double-skin façade with a thermal storage space called a solar chimney above the double skin space to strengthen stack effect occurring in the intermediate rooms to encourage natural ventilation between the rooms. Their experiment was an 8-storey building tested through a 1/25 scaled prototype model and a CFD analysis. One of their conclusions mentions that increasing the solar chimney height generally increases ventilation with recommendations to make it more than two floors high.

Gan (2005) studied the numerical simulation of buoyancy – induced flow in open cavities for natural ventilation using technologies like the solar chimney, double facade and trombe wall. The same paper studied 3 types of solar chimney configurations with a height of 6m and applied on a building two storeys high. It concludes that (1) buoyancy in open cavities increases with solar gains; (2) buoyancy induced ventilation rate also increases with cavity width up to a point; (3) optimum width for open cavity was found to be between 0.55m and 0.6m for a solar chimney of 6m.

## **Vegetation Skin / Green Skins**

Incorporating vegetation within the double skin façade has been explored in various contexts. The benefit of having greenery in buildings is not only for aesthetic image, but also for the purpose of producing a healthy environment. The information below provides some indication these benefits and its integration to a double skin assembly.

Kaplan (2007) using a survey and photo-questionnaire, asked employees along a major business corridor about their nearby natural setting, satisfactions, preferences, and desired changes to the landscape. Findings consistently showed preference to scenes of forested and other natural areas. Kaplan also noted that having bigger trees strongly affected the employees' satisfaction with their workplace area.

Papadakis et al (2000) investigated the effect of using plants for solar control of buildings through shading. This paper showed the influence of trees on the heat transfer between a building façade and the environment. A space was compared against another space with tree shading, showing several benefits on the vegetation shaded area. Plants manage to keep their own temperature lower than the surrounding air through transpiration, or by evaporating great amounts of water. The temperature of a conventional sunscreen on the other hand rises higher than the ambient air which induces thermal radiation that burdens the wall.

Papadakis et al (2000) noted however that the refresh rate of the air between the wall and the trees is lower than in the unshaded area since trees block the air movement, as supported by their findings. Also, a negligible increase in temperature was observed with the shaded wall at night due to the presence of the trees inhibiting radiative cooling.

Stec et al (2004) studied the application of vegetation on the double skin façade as shown in Figure 2.2. The author stated that such proposals on facades may bring additional benefits like:

1. improved thermal insulation
2. improved acoustic conditions

3. air filtering from dust, chemicals
4. oxygen production and CO<sub>2</sub> reduction
5. psychological positive effect that may reduce the risk of sick building syndrome, healing effects and reduced stress
6. aesthetic stimulant to people However, this paper noted that disadvantages may occur due to maintenance and problems of light transmission control.

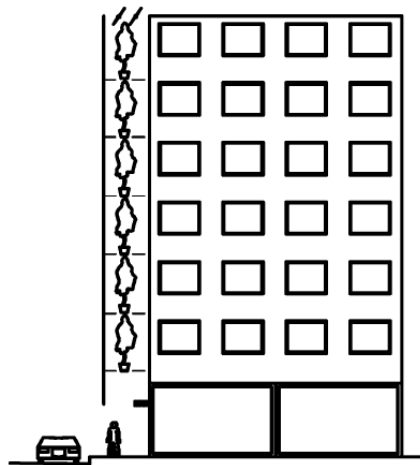


*Figure 2.2 DSF with Plants*

Further on, Stec et al (2004) modelled a building double skin façade with plants. It was found to have the ability to dissipate absorbed solar radiation into sensible and latent heat, about 60%. In the experiment, plant species was carefully chosen since it needs to withstand strong solar radiation and temperatures varying from 10 - 40 °C. The crawling plant ivy (*hedera helix*) was chosen for this climate and context study. Installation considerations include flower pots, adequate spacings, and using plants that shed in winter.

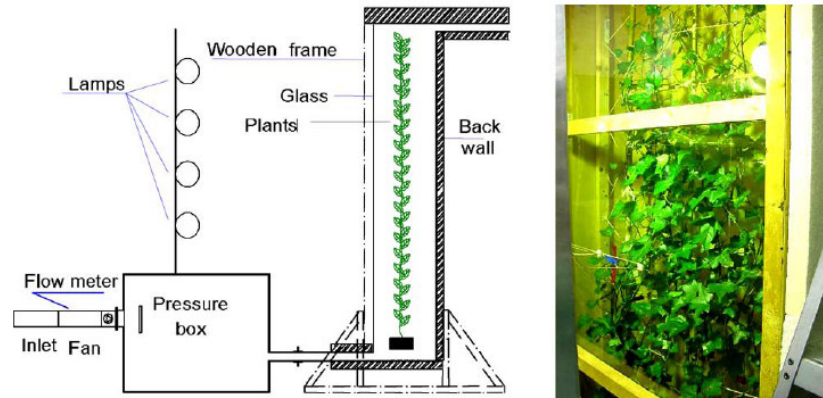


Figure 2.3 Lab test facility of double skin with plants

Stec et al (2004) conducted their study through laboratory tests and computer simulations as illustrated in Figure 2.3. The study found that it create more effective shading system than blinds since temperature of the double skin façade layers were much lower and that the cooling capacity reduced by almost 20%



Fig 2.4a Atriplex halimus



Fig 2.4b Lantana camara

Vegetation can potentially reduce the cooling load of buildings. However, transpiration requires much water to aide in lowering the temperature in the cavity. The selection of appropriate plant species will also be a challenge in the UAE context. There are a couple that may be able to withstand the conditions in the hot – humid desert climate. Atriplex halimus (Fig. 2.4a) is often cultivated as forage because tolerating severe conditions of drought, and it can grow up in very alkaline and saline soils. Additionally, Lantana camara (Fig. 2.4b) has become naturalized in

tropical and warm regions worldwide. In the Kenyan highlands it grows in many areas that receive even minimal amounts of rainfall.

Of course more appropriate species should be properly consulted. Such climbers like the above mentioned heder helix that can keep its adherence to the wall. However, most plant species can attract insects or birds specially if flowering or bearing fruit implying added maintenance concerns.

### **Controls**

Any building system working in sync with different mechanisms on varying conditions must have an integrated building management system or controls that allow user control or intelligent automation. According to Stec et al (2003 in Poirazis, 2004) “efficient control systems need to be applied to manage rapidly changing outside conditions. A successful application can only be achieved when the contributions of all the devices can be synchronized by an integral control system.”

Stec and Passen (2004) mentioned that control strategies should prioritize the use of passive components like valves, windows and blinds. Natural ventilation should be used whenever possible which improves higher energy savings.

It was explained that occupants must be able to have control even if such intervention can disrupt energy savings. Controls must also take advantage of outside conditions first before engaging HVAC systems with the focus on providing comfort with the lowest energy usage. (Paasen, 1995 in Poizaris, 2004)

## 2.5 Double Skin Façade Examples

Three buildings incorporating a double skin façade are highlighted in this section. It exhibits the opportunities and early issues associated with this application and shows information on actual building performance.

### 2.5.1 The Occidental Chemical Center (Hooker Building)

Location: Niagara Falls, New York

Architect: Cannon Design Inc.

Consultants: Hellmuth, Obata & Kassabaum

Completion: 1980

Floors: 9 storeys

Type: Full height buffer Façade



(a)

(b)

Figure 2.5 Occidental Chemical Building Exterior

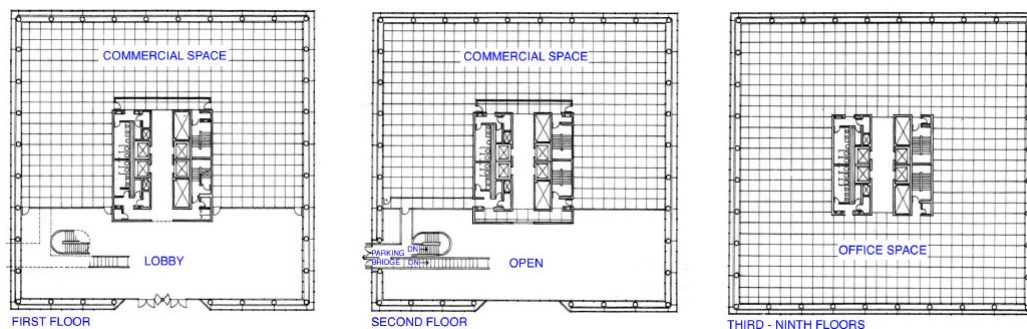


Figure 2.6 Occidental Chemical Building Floor Plans

Occidental Chemical Center or otherwise known as Hooker Building was the first double skin façade example in North America. It has been identified as one of the most energy efficient commercial buildings in the world with citations for design excellence from AIA and EPA Star. Being one of the oldest examples of modern double skin façade buildings, performance information has been found both valuable and controversial. The nine storey cube floor layout (Fig. 2.6) incorporates a continuous façade with motorized dampers for ground level floor intake while a top outlet exhausts at roof level. The façade allows warm air to act as buffer between the glass and interior spaces. (Fig. 2.9)

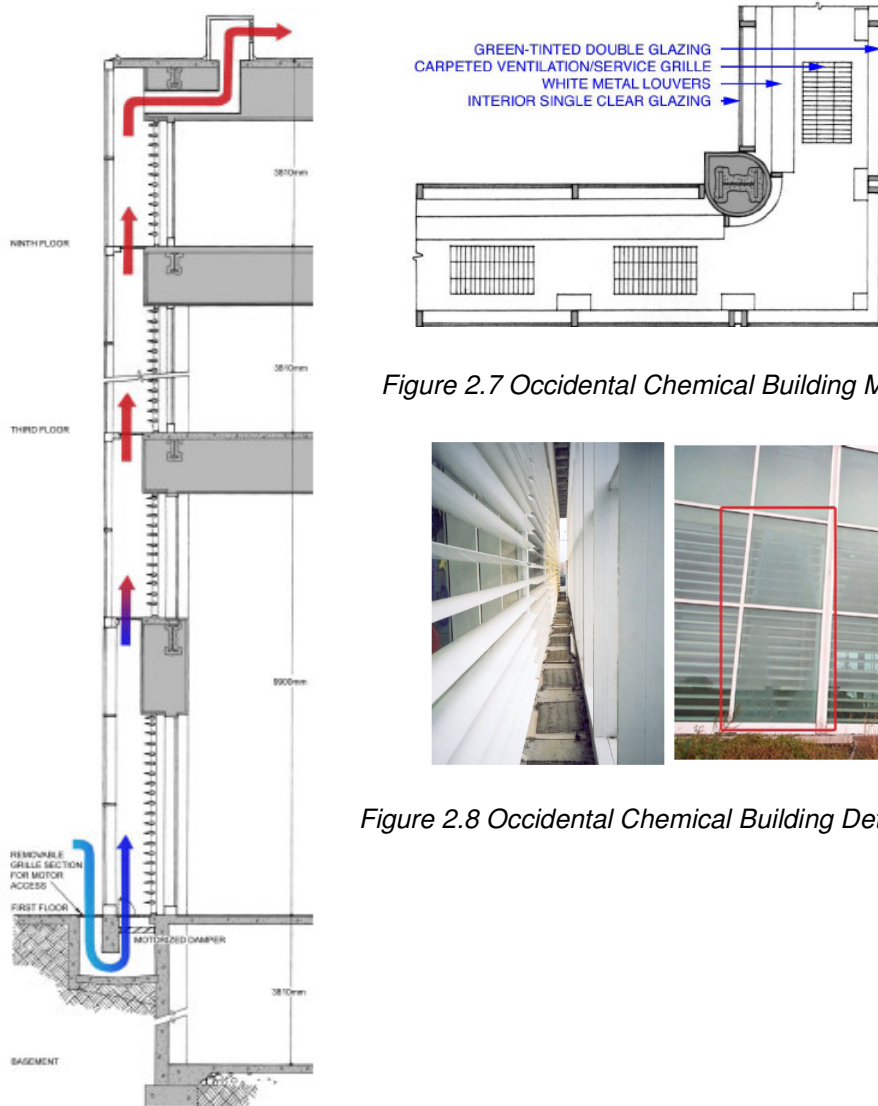


Figure 2.7 Occidental Chemical Building Materials

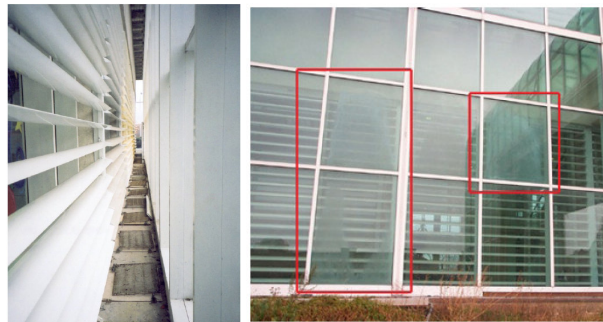


Figure 2.8 Occidental Chemical Building Details

Figure 2.9 Occidental Chemical Building Exterior

The envelope is comprised of an exterior green tinted insulating glass with 80% solar penetration. It is followed by a 1200 mm air space with 15-foot span hollow metal air-foil shaped louvers while also incorporating service grilles. A layer of clear glass then separates the interior. (Figure 2.7)

The acclaim for this building however was touted with issues in performance. The initial assumption of the double skin assembly offsetting the mechanical systems requirements to half, was complicated by occupational patterns. Cooling loads increased significantly such that the boilers were never required to heat the building even in extreme winter conditions. (Harrison, 2001).

Harrison (2001). reported one of the adjacent excavations, the intake grilles at ground level have been covered with particulates and dust that accumulated the cavity. The blockage was unable to draw air and led to overheating in the upper floors. Louver operations also ceased operation and got stuck in a horizontal position that prevents only 50% of solar south radiation, and lesser on the east and west. The current maintenance issues caused tenants complaining either from too much heat or cold. Some clouding formation also occurred within the façade causing a visually stained appearance as shown in Figure 2.8.

At present, only certain areas of the building façade are still functioning. Problems heavily relied on the façade's inadaptability and the static status of a failed buffer cavity. In the future, longevity and repairs highly contribute to the life cycle cost of this type of façade. Such consideration allows optimal function long throughout the building's usage and occupancy. (Harrison, 2001).



## 2.5.2 RWE AG Headquarters

Location: Essen, Germany

Architect: Ingenhoven Overdiek and Partners

Completion: 1996

Floors: 29 (127m; 162m including antenna)

Type: Transparent and interactive façade on the whole building envelope



(a)

(b)

Figure 2.9 RWE AG Headquarters



(a)

(b)

Figure 2.10 RWE AG Headquarters Façade Features

RWE Tower one of the highest in Germany and considerably the tallest structure in the Ruhr area. The building (Fig.2.9 a&b) utilized the double skin façade in all sides of the building. The inner and outer facades are separated by 50cm incorporating 80mm wide aluminum louver blinds that can be remotely controlled. Another set of roller shades are also installed. The outer façade however not only provides shading and heat reflecting effects but also helps protect against wind and rain. (Nippon, 1999)

In warm conditions, the operable inner glazing that can open up to 15 cm to allow natural ventilation (Fig 2.10b). It is mentioned that it is possible to occupy the building without artificial cooling or heating 70% of the year. The actual measured energy savings from however was 30-35% which was accompanied by building sensors that manage adjustments in sunshade and ventilators based on the external conditions. (Nippon, 1999)

Sound transmission is also insulated by the outer glazing. Special “fish mouths” (Fig 2.10a) mediating floor to floor height however hinders vertical sound transmission. This same feature prevents diagonal streaming of air and helps suppress spreading of fire. For maintenance, the cavity inner glazing is also accessible for regular cleaning. With the external glazing, project targeted a highly transparent building. This was achieved by carefully selecting an altered glass composition where 97% of the iron oxides is removed, leaving green physical tint. (Nippon, 1999)

## 2.5.3 Gemeinnützige Siedlungs-und Wohnbaugenossenschaft

### (GSW) Headquarters

Location: Berlin, Germany

Architect: Sauerbruch Hutton Architekten

Completion: 1995-1999

Floors: 22 storeys

Area: 47,873 square meters (515,000 square feet)

Type: Cross ventilation & double skin thermal flue on the west façade.



(a)

(b)

Figure 2.11 GSW Headquarters



Figure 2.12 GSW Headquarters Façade Features

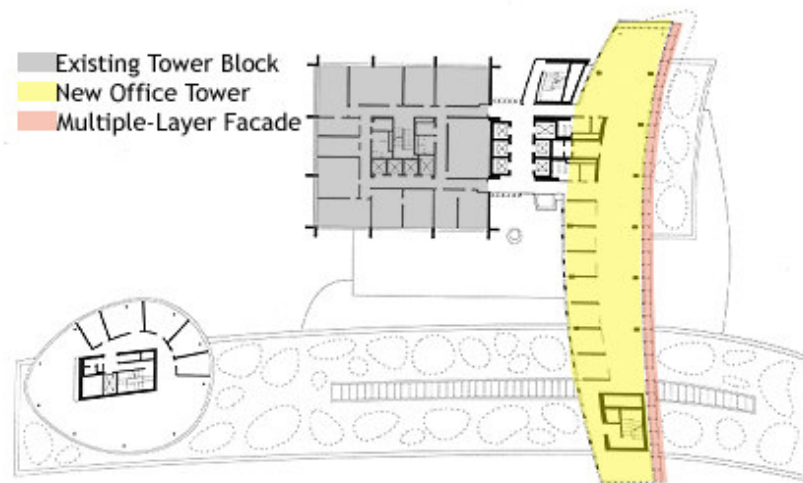


Figure 2.13 GSW Headquarters Floor Plan

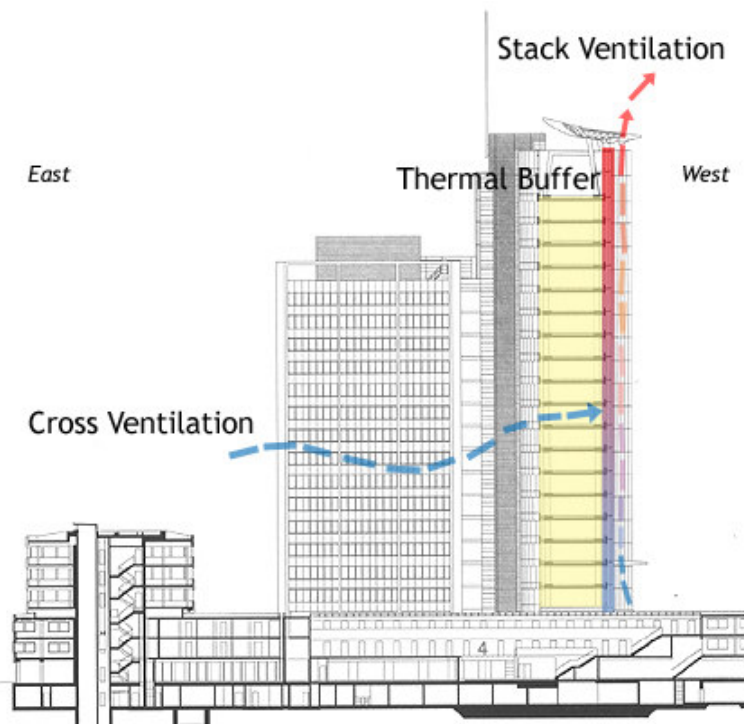


Figure 2.14 GSW Headquarters Section showing cross ventilation

Arup and Sauerbruch/Hutton architect worked together for this competition building. GSW Headquarters is one of Berlin's most distinguished building. A refurbishment extended the building as shown in Figure 2.13, added innovative engineering concepts using natural ventilation. The project's aim was to achieve an energy savings of 30-40% relative to a typical building. (Arup)

The 11 meter wide building allows cross ventilation through the use of automatic and manually operated triple glazed windows with between-pane blinds that are incorporated on the east façade. At the same time, louvered metal panels are installed to admit fresh air even without windows.

The west double skin façade consists of manually and automatically operable interior double pane windows while being sealed by a 10mm exterior glazing layer. Also, wide automatic and manually adjustable perforated aluminum louvers are deployed on the 0.9 m wide cavity space.

Basically, the east façade allows outside air to cross ventilate towards at the west façade. The west double skin façade is a full 20 storey high shaft that allows airflow through thermal buoyancy (Fig 2.14).

For heating purposes, the cavity is sealed to allow the accumulation of heat. The warm air produced is then returned to the central plant for heat recovery. (High Performance Commercial Building Façade)

## 2.6 UAE Climatic Profile

### The UAE



Figure 2.15 UAE Map

United Arab Emirates is located at 22°50' and 26°N and between 51° and 56°25' E and along the south-eastern part of the Arabian Peninsula. The country has a total area of about 83,600 sq km. The capital and the largest city of the federation is , Abu Dhabi. (Emirates.org)

“The UAE lies in the arid tropical zone extending across Asia and North Africa. Climatic conditions in the area are strongly influenced by the Indian Ocean, since the country borders both the Arabian Gulf and the Gulf of Oman. This explains why high temperatures in summer are always accompanied by high humidity along the coast. There are noticeable variations in climate between the coastal regions, the deserts of the interior, and mountainous areas..” (Emirates.org)

In winter months from November to March, daytime temperatures average  $\approx 24^{\circ}\text{C}$ . Night-time temperatures are slightly cooler, averaging  $13^{\circ}\text{C}$ . Summer temperatures can be as high as  $48^{\circ}\text{C}$  inland, but are a few degrees lower in the coastal area. Humidity in coastal areas averages between 50 and 60 per cent, touching over 90 per cent in summer and autumn. Inland it is far less humid.

Average rainfall is low at less than 6.5 centimeters annually, more than half of which falls in December and January.

*Table 2.9 UAE Temperature*

<b>Abu Dhabi</b>	Jan	Feb	Mar	Apr	May	Jun	Jul	Aug	Sep	Oct	Nov	Dec
Rainfall (mm)	16	28	23	8	0	0	1	0	0	1	2	13
Rainfall (inches)	.5	1	1	0	0	0	0	0	0	0	0	.5
Min Temp ( $^{\circ}\text{C}$ )	14	15	17	20	24	27	29	30	27	24	19	16
Max Temp ( $^{\circ}\text{C}$ )	24	25	28	33	37	39	41	41	39	35	31	26
Min Temp ( $^{\circ}\text{F}$ )	57	57	62	68	75	81	84	86	81	75	68	57
Max Temp ( $^{\circ}\text{F}$ )	75	77	82	91	98	102	106	106	102	95	89	78

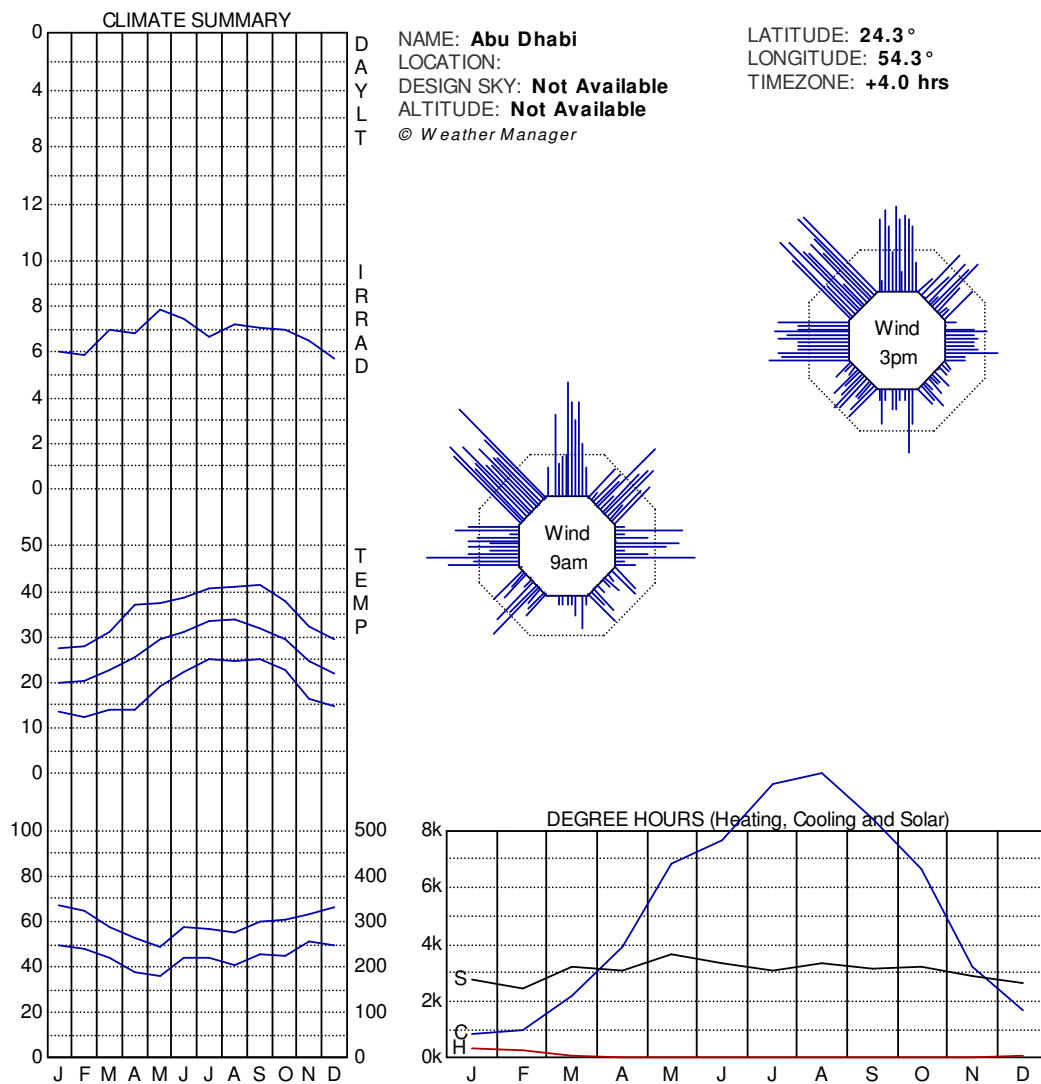


Figure 2.16 Ecotect Abu Dhabi Climate Summary

Table 2.9 and the Ecotect weather file for the UAE capital Abu Dhabi (Fig. 2.14) shows the rise in temperature during starting April and peaks through the months of July and August. The Peak in radiation occurs during mid-May where summer temperatures also start to rise. It is important to note however that the highest temperature readings do not correspond to the same time as the highest values in radiation. Humidity values rise at inverse proportion to temperature as can be seen during



the months of Nov – Jan. Low values of relative humidity occur around May, but slightly rises in the summer months of June – July.

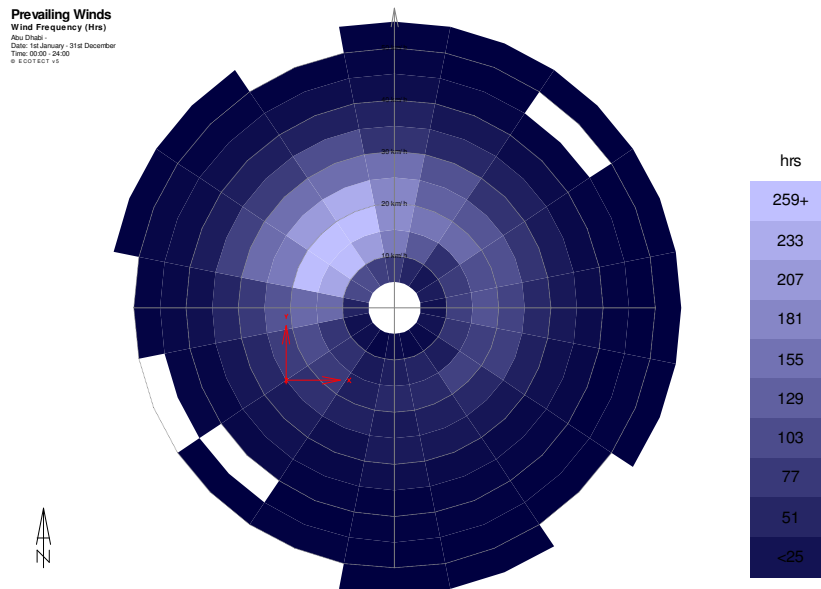


Figure 2.17 Ecotect Abu Dhabi Prevailing Winds  
 Date: 1<sup>st</sup> Jan – 31<sup>st</sup> December

Local north-westerly winds (shamal) frequently develop during winter, bringing cooler windy conditions. Prevailing winds, which are influenced by the monsoons, vary between south or south-east, to west or north to north-west, depending upon the season and location.

## **2.7 Examples in the Desert Climate and UAE**

### **2.7.1 Studies in Similar Climate**

A study of double skin facades in Cairo, Egypt was conducted by Hamza & Underwood (2005) using CFD supported modelling. Unlike most studies about double skin facades that focuses on enhancing ventilation rates, this paper focuses on air conditioning load reduction in a hot arid climate.

The literature review of Hamza & Underwood (2005) mentioned that according to Hamza (2004) and Afifi (1999), “on hot days, the exterior leaf of a double façade would reduce direct solar heat gain in rooms; the trapped heat in the gap induces natural buoyancy which in turn would reduce elevated air temperatures away from the inner building skin.” Also, the review of Hamza (2004) stressed that “a reflective outer surface on the double skin façade is predicted to decrease the annual cooling load by 40%.” It may however reduce daylight levels that can partially offset cooling load reductions due to lighting loads.

According to Hamza & Underwood (2005) “the buoyancy driven channel flow rate is dependent on the temperature difference between the discharge and inlet of the channel.” It further stated that “the flow development through the channel increases with increasing solar intensity but reduced with increasing external air temperature at any given value of solar intensity.” These relationships and other variable like surface convection, air flow rate and temperature were simulated using a CFD package in IES V 5.1. It was concluded that a reflective double skin façade may have a significant effect in reducing cooling loads but an absorptive glazing was more promising. “The CFD simulations

calculated that heat conducted into the cavity from an absorptive glazing combined with higher ambient temperatures leads to increasing the mass flow rate (also heat removal rate) within the cavity.” It was further added that “the effects of changing the mass flow rates in the range of 0.5kg/s – 0.9 kg/s has minor effect on room sensible cooling loads which was only 2%. (Hamza & Underwood, 2005)

Wong et al (2006) used CFD analysis to determine a new type of double skin façade to improve thermal comfort conditions in the hot and humid climate. The study focused on natural ventilation strategies applied an 18 storey high rise buildings. Their study was conducted using Airpak design tool and analysis which uses FLUENT CFD solver engine for thermal and fluid-flow calculations.

### **2.7.2 Examples in the UAE**

An ideal way to research a building typology would be to observe built structures. As opposed to the examples present in moderate climates, the actual performance of this application is not well recorded in the hot and humid context of the United Arab Emirates. Finding buildings with double skin facades has proven to be a challenge. However, there are prestigious examples underway that prove this system is considered in this climate.

#### ADNOC Headquarters

One of the examples of a double skin façade construction in the UAE is the ADNOC Corporate Headquarters. Designed by HOK, it consists of more than 65 floors with an Office Tower, Corniche Club, SPC and Crisis Management Centre, Heritage Museum and other supporting facilities. (ADNOC 2008).

The ADNOC Headquarter main tower is comprised of solid frames where mechanical cores are located. It also contains a monolithic glass tower inside. The solid frames act as a shield against the Western and Eastern sun and allow the office spaces more flexibility with interior layouts. The north façade has special feature elements that gives a high tech impression while the south facade is a double skin façade incorporating a photovoltaic glazing. At present, the construction has already started in planned phases. Demolition is underway for the A1 building where the current office is located. (ADNOC 2008)

### Sowwah Square



In Abu Dhabi 2008, Goettsch and Partners has publicized a design of an environmentally responsive and energy-efficient building relying heavily for its success on the exterior walls. Keeping in mind the extreme conditions in the desert climate, the building façade does not only mitigate the extremes in diurnal temperature, but is also able to protect the building from the corrosive wind influenced by the coast and with consideration for the resistance to sandstorms (Soberg, 2008).

*Figure 2.18 Sowwah Square Facade*

The Sowwah Square by Goettsch and Partners consists of a five-building, 3 million square foot development. Two buildings are 31 storey and the other two are 37 storey structures. The main feature of this structure is that the building envelope consists of a ventilated cavity double skin façade system that covers the majority of the building elevation.

The designer has recognized that the double skin façade for the desert climate should be a different version of the more common designs in moderate climates. The ultimate function of the double skin façade in cooler regions is to promote heat gain and supply this accumulated warmer air to the interior spaces. The design distinguishes the reverse function of the double skin façade which is to minimize radiant heat gain from the exterior environment from penetrating in to the interior spaces (Soberg, 2008).

The designed double skin façade runs throughout the entire building height starting from fourth floor all the way up to the penthouse mechanical levels. Within this cavity are installed active solar shading devices which is designed adjustable in order to maintain and control the optimal angle for improved solar protection. However, it has been recognized that the mechanism that controls this device could be damaged due to corrosion and sand infiltration. Therefore, in order to preserve the long-term functionality of this system, the designers have decided to seal the double skin totally from the exterior environment unlike the typical double skin facades that encourages the flow of outdoor air into the cavity. By doing so, the shading device and mechanisms are protected from the elements that would hinder the proper operation of the shading device (Soberg, 2008)

Additionally, exhaust air is directed to the double skin façade in order to maintain a cool cavity. Controls and sensors determine modulating dampers at the building top for flushing out air and help redirect areas where cooling is necessary. Although the cavity is sealed from entry from outdoors, options for opening using dampers are used specially for night cooling. (Soberg, 2008)

ADNEC Capital Gate (RMJM, 2008)

Another promising example that uses the double skin façade system is the Abu Dhabi National Exhibition Center (ADNEC) Capital Gate in Abu Dhabi, UAE, designed by RMJM Architects (RMJM, 2008). The mixed use tower with five star hotel facilities is located at the end of the National Day Parade Grandstand in Abu Dhabi. This project is still under construction and will be finished around 2009.

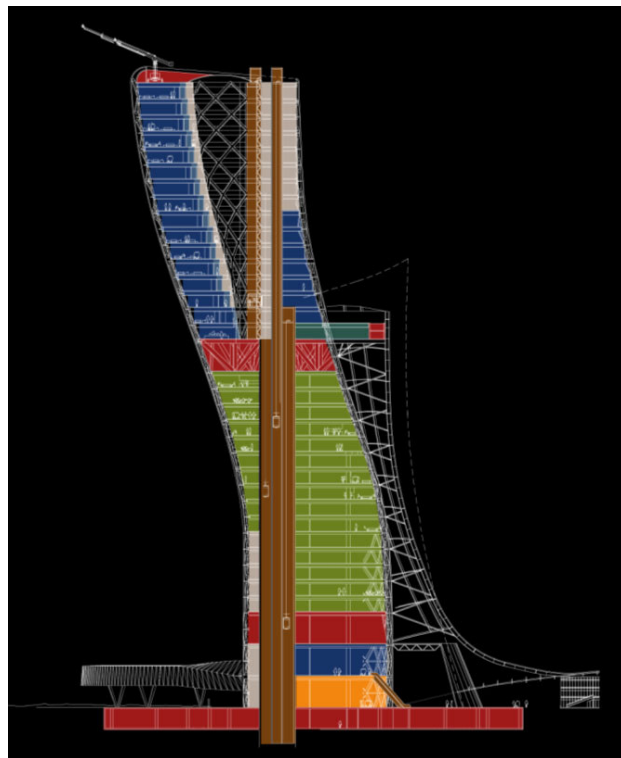


*Figure 2.19 ADNEC Section*

The building is a 160 m high structure that consists of a basement, ground floor, mezzanine and 33 floors (1B+G+M+33). The architecture is based on an irregular oval shaped floor plan where each floor plate marginally increasing in size as towards the succeeding floors up the building. Each floor is marginally off-set from the floor below to create in

cross-section a stretched S-shape profile. The central vertical core that contains the lift shafts and stair well runs throughout the building and occupies the common overlapping areas of each floor.

Part of the exterior is covered with a false screen, located on the opposite side of the tower and visually balancing the overhang. This screen stops at Level 19 but continues from the tower by means of a transition curve to form an elliptical arch over the Grandstand with a circular curved front and rear to back cross-section profile. This screen and the Grandstand roof structure is intended to employ a perforated metal sheet finish. At the Ground and Mezzanine Floor the open space created by this screen is filled in or occupied as residential, commercial or hotel space.

The general building exterior structure is a steel tower housing glass diamond and triangular glazing. The main feature on this structure is the incorporation of a double skin façade system.

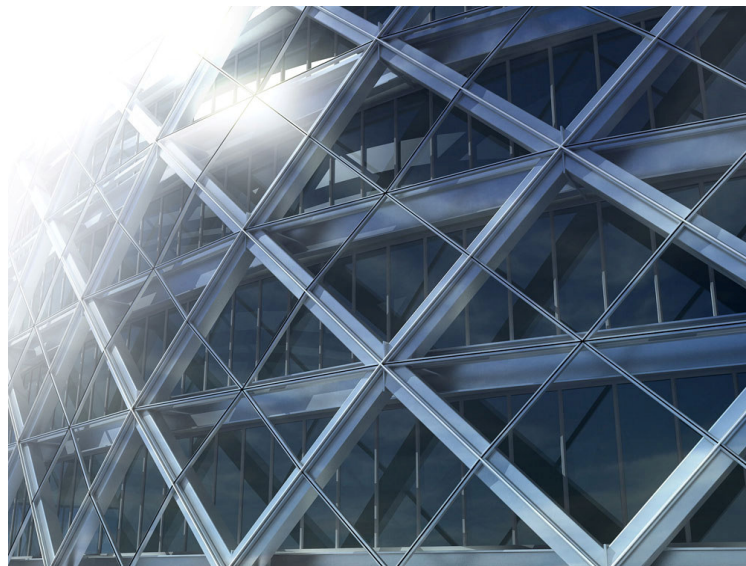


*Figure 2.20 ADNEC Facade*

The tower envelope is a double façade, with a double-glazed thermal curtain wall outside layer, and a single-glazed partition inside layer. The air gap formed serves as a buffer between the hot air outside and the cool air inside. In context to the desert climate, the system should ideally cool the air in the cavity, rather than warm the air which typical in European double facades. The project proposes to do this by circulating the conditioned air from the living spaces into the cavity, through grilles at the base of the single glazing, which rises to the top through convection, where it is recovered in the ceiling plenum and then re-circulated back through the room.

The main tower structure is a diagrid, a triangular network of metal tubes woven in a net pattern all around the exterior of the cylinder which enables its rigidity. This diagrid is based on the 4-meter floor heights, which follow the curved geometry of the tower shaft.

The preliminary studies projected that the double façade should significantly reduce energy needs for the building. It is estimated that supply air volume required for a hotel room would be about 12-15% less than with a typical curtain wall envelope, and the cooling requirements would be reduced by about 5%, resulting in smaller fan coil units. This would enable the load reduction on the building's mechanical system, and eases the need for chilled water which is supplied by district cooling. The following section details these projections.

ADNEC Capital Gate Façade Heating and Cooling Schematics:



Contained in the ADNEC Capital Gate design report, RMJM (2007) conducted a basic analysis which compared the solar heat gain expected between two facade options. Option 1 is the double façade while Option 2 is a typical double glazing. The study assumed internal heat gain of 3 kW in both cases while 46 degrees Celsius (Dry Bulb) was used as outside temperature in summer conditions.

The two options comparisons are based on the same glass types using common U-values as per municipality requirement and shading coefficients from Pilkington glass:

Single glazing:      Optifloat clear    4 mm U=5.9 W/m<sup>2</sup>K,    SC=0.99

Double glazing:      Glass 1 – Suncool HP Neutral 53/40 6mm

                                 Glass 2 – Optifloat Clear 4mm U=1.8, SC 0.35

RMJM (2007) calculated that the cooling requirements of the double façade are more favourable. Option 1 (Fig 2.21) generates about 5.8 kW of solar heat gain, requiring approximately 5% less cooling than the Option 2 (Fig 2.22) double glazing which generates about 6.1 kW of heat gain. The analysis in also mentioned that the other advantage of option 1 is that the 12-15% reduction of supply air volume to the space will mean relatively small fan coil units.

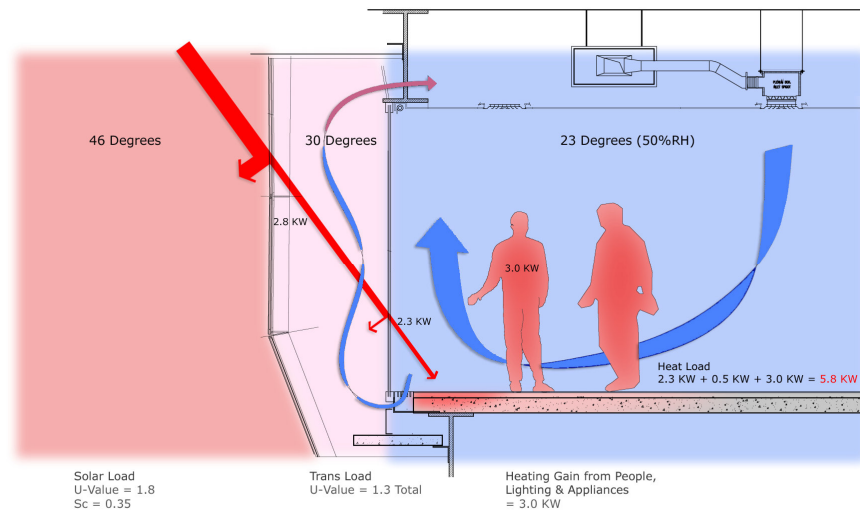


Figure 2.21 ADNEC Option 1 Double Façade

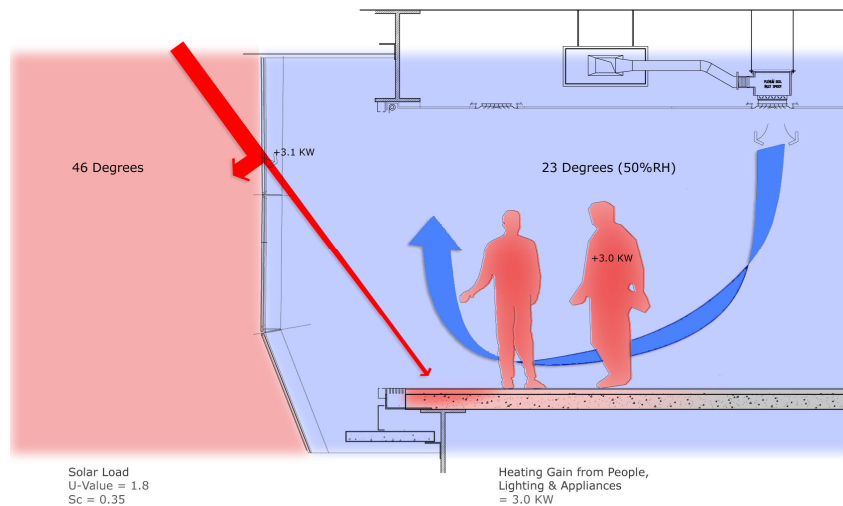


Figure 2.22 ADNEC Option 2 Single Façade

With the Option 1, an obvious benefit of the double skin façade is through its characteristic as an external shading device which directly alleviates solar exposure by filtering direct solar radiation into the building. At the same time, the volume of return air within the cavity that ends up more exposed to heat accumulation is relatively small and is separated from the general liveable space and breathing area. The project stipulates lessened cooling load by targeting only the warmed air within the higher heat concentrated cavity (RMJM, 2007).

## **2.8 Findings of Literature Review**

The vast literature and studies for double skin facades have been presented in the literature review. It showed in summary, the various types, applications and tests on different configurations. There are some commonalities and there are various contradictions and dependencies.

The original context studies have been mentioned. However, it is not sufficient to represent the multitude of variations necessary to generalize the double skin concepts in this climate. Some future and ongoing projects were also highlighted. These have adapted concepts from its original predecessors by responding to the desert climate. In the future, these will serve as an opportunity for reviews where its operational performance can be tested.

For the findings of the literature review, the building physics and technical description will be revisited. This section will analyze the concepts and ideas that are particularly appropriate to a double skin façade in the desert context. With some critique and analysis, the various concepts will be discussed and redefined.

### **Precedents**

ADNOC Headquarters double skin façade functions more of an external shading device to screen from radiation. It has also incorporated PV panels on the façade which is a good combination of technology, but is not an innate a double skin specific function.

Sowwah Square on the other hand, chose to seal the double skin façade and restrict airflow from the outside in order to protect shading device. HVAC exhaust is used to feed air into the double skin façade, allowing it to cool without outdoor intervention similar to the proposal of Stec et al (2003 cited in Poirazis, 2004). Option for flushing out air is also considered to release accumulated warm air. This scheme is more likely to be applicable and operational in terms of achieving the function of a double skin façade in the desert climate.

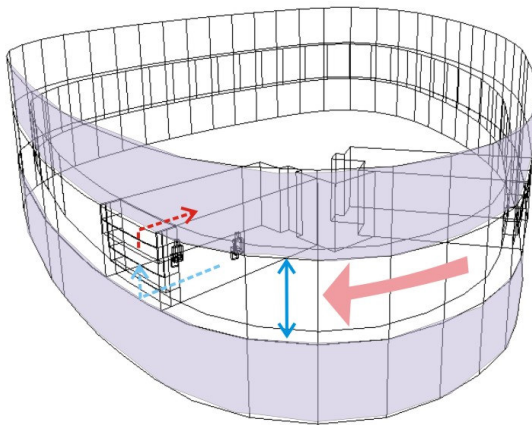


Figure 2.23 Schematic Air Flow

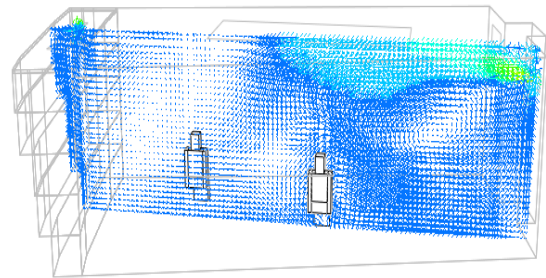


Figure 2.24 Façade CFD

The initial design of the ADNEC Capital Gate double skin design (Fig 2.23) is an elliptical modified corridor type facade where the void cavity is not open through the entirety of the building. The cavity is sealed and partitioned between floors, therefore limiting the convection height within the floor to floor clearance. It is also an ‘inside ventilated cavity’ (Fig 2.24) travelling through passages near the floor and returning to the fan coil units near the ceiling.

In this double skin façade, it is also very likely that the heat within the cavity may reach extreme temperatures especially during summer. Such an accumulation in temperature can create a reverse air flow due to the

pressure induced temperature difference between the cavity and indoor spaces. Essentially, the same fan coil unit cools the double skin cavity having higher temperatures and less volume, together with the occupied space having less heat gain but greater volume. Due to this relationship, the initial assumed energy savings might end up negligible.

As an initial critique, it is analyzed that there is air movement however, around the elliptical floor plan cavity perimeter. This is likely to occur due to the temperature difference between the shaded and the sun-exposed portions of the façade. The lower temperature areas of the cavity can serve as a heat sink and encourage ant axial movement. However, this same behavior serves indeterminable benefits since it can either alleviate the cooling load of one side, or burden the other areas not necessarily exposed to direct heat gain. At present, the updated design of the ADNEC Capital Gate has addressed this concern by installing vertical partitioning within the cavity.

### **Opening Principles**

Even in extreme temperatures, the double skin façade should be able to vent to outside otherwise, any protection through glazing properties will still be insufficient to keep the cavity cooler. Any enclosure with glass that is exposed to sunlight will inevitably have increased temperature higher than outdoors, and may even be in danger of retaining heat even if solar radiation has declined.

Kragh (2000 in Porazis, 2004) mentioned that naturally ventilated walls are not recommended for the hot climate. The most favorable temperature that a naturally ventilated cavity can achieve is to equal the outdoor ambient temperatures. All other situations will most likely have

increased temperature within the cavity. Therefore, even the inner glazing should be closed as well. The only promising behavior within the cavity is the opportunity for stack effect where self driven heat gain would allow air mass flow exchanges which in turn can reduce surface temperatures.

For the purpose of analyzing the complexity of a naturally driven façade, fan supported ventilation will not be considered. However the possibility of mixed-mode operation for operable windows will be tested for its benefits in night cooling or for day direct cooling during favorable condition like winter season.

### **Technical Description**

Construction Elements can be similar to the mentioned original structures. Additional thermal stops between connected fittings however, should be incorporated to assure that warm air will not infiltrate the building space. This will also help in the possibilities where heat conduction can travel along the structural framing supports.

### Dimensions

Only when the cavities are shallow (around 40cm) that air flow resistance causing pressure losses will occur (Oesterle et al, 2001 cited in Poirazis, 2004). Otherwise, depth is not critical for the temperature inside the cavity in an airtight façade where the double skin does not provide room ventilation. In mixed mode, opening windows doesn't assure good room ventilation. (Faist,1998 in Poirazis, 2004) Therefore determining depth will be highly dependent on the function of a mixed mode system in order to make the double skin façade beneficial in both scenarios.

Adding a solar chimney on top of the double skin façade improves stack effect (Ding et al, 2004). The same author further recommends in making the solar chimney height to more than two floors. Gan (2005) also mentioned an optimum depth of 0.55 to 0.6 m for a 6 meter high solar chimney.

There is an obvious variation in the selection of double skin façade dimensions for optimum performance. Due to this, varying depths will be tested separately to obtain the ideal configuration.

### Glass

In the selection of glass for an outdoor ventilated facade, (Streitcher et al, 2007) suggested an insulating double sealed glazing unit on the interior while using a single pane glass on the exterior. Lee (2002) or Poirazis, (2004) mentioned that strengthened safety or laminated safety glass for exterior while internal windows with low e coatings are necessary to reduce heat transfer. Hamza (2004) on the other hand, suggested a reflective outer glazing that is predicted to reduce cooling loads by 40%, however partially offsetting daylight levels.

Having high shading coefficient will ultimately reduce solar heat gain. The double skin façade has double opportunities to block solar radiation. The external glazing will be a low e coating but transparent enough not to impair daylight. High shading coefficient, insulated, with low U value glass will be applied to the internal glazing to ultimately prevent heat transmission. The solar chimney however will be applied with transparent clear glazing that allows all radiation to penetrate into the upper cavity.

This allows the top portion to accumulated heat that drives and induces stack effect.

### Shading Device

Shading devices are typically place inside the cavity whose installation affects the double skin performance by either reflecting or absorbing heat while at the same time, impacting daylight. (Streitcher et al, 2007)

Heat absorption should be avoided as much as possible since thermal retention is released after solar radiation has waned. If the shading devices are placed outside, it would reflect radiation before it even enters the cavity, while its thermal lag will be released directly outdoors by radiant cooling. However shading devices are known to improve energy reductions, this will not be incorporated in the simulations studies. Its performance can function separately and may complicate to the findings of the simulation since it serves as an added shading feature. The study merits on the focus of the isolated effect of glazing in mass air flow and energy reduction.

### **Cooling the Cavity**

Most of the double skin examples in temperate climates highlight the possibility of utilizing and enhance direct ventilation. This however is not recommended for high external temperatures. A cavity with sealed inner panes has the potential to either prevent direct solar gain, or enhance air flow as heat removal medium. Through the simulations of Hamza and Underwood (2005), doubling the mass air flow with initial value 0.5 to the enhanced 0.94 kg/s predicted the effect to only contribute in 2% energy reduction. There should ideally be a more substantial heat sink within the



double skin cavity since mass air flow in reality would only displace cavity air with the same high outside temperature.

### Integration with HVAC

Stec et al (2003 in Poirazis, 2004) suggested that double skin facades can be used as an exhaust duct that in essence would help cool the cavity. The configurations suggested for winter is essentially not relevant in the desert climate since dominant winter temperatures are tolerable enough to be directly applied into the space and preheating is not necessary.

In most buildings, the exhaust air is used with a recovery wheel to couple and pre-cool air intake and helps in the direct reduction of cooling loads. The remnants of exhausted air coupled through thermal wheel may still be passed on to the cavity but will essentially have less efficiency as compared to a direct room exhaust.

This manner of operation is still highly applicable for this climate and has been done by Sowwah Square (Soberg, 2008) among others.

### Vegetation or Green Skins

In cooling the double skin façade using vegetation, Stec et al (2004) found it difficult to simulate the plants function based on its properties which may lead to unpredictable actual performance. Controls will be rather tricky since vegetation is immobile and not user operative. Its applicability may also be integrated into the building landscape or ideally,

in locations where maintenance will not be hindered by height or other constraints.

### Water Spray – Direct Evaporative Cooling

Discussed earlier are several features that can be integrated with the double skin façade. These approaches are adapted from the precedent examples and manipulated to be more conducive to this climate. Incorporating solar chimneys while exploring configurations and careful material selection can optimize its performance. Certain features like blinds and louvers are also helpful, but in essence can work independent to a double skin façade system.

Some of the examples earlier mentioned namely, ADNOC Headquarters, Sowwah Square and ADNEC Feature Tower incorporated the use of double skin façade in this climate. With a strong emphasis on Sowwah Tower (Soberg, 2009) and ADNEC (RMJM, 2008), the envelope assembly was modified to be a means of temperature insulator by carefully designing the cavity to contain cooled exhaust or re-circulated air. The double skin façade in essence serves as a function of a buffer zone to protect or reduce the conduction of external heat towards the interior spaces.

In using these precedent directions, cooling the double skin façade cavity air is a means to improve the thermal resistance of the assembly by providing a heat sink and enhancing air mass flow exchanges. Obviously, recovering exhaust air is an effective means of cooling the air cavity. This scheme has already been shown in literature and applied on a real building. On the merit of using a different approach, direct

evaporative cooling in consideration has this potential to lower air temperature.

When warm air passes over water, the liquid evaporates and in the process, absorbs a substantial amount of heat which cools the air and increases its humidity. (Konya, 1980). Every gram of water that is evaporated consumes in the process about 58kcal (0.145 Btu), which is the latent heat of vaporization (Givoni, 1976).

Several vernacular principles have been applied using water evaporation for cooling in buildings. Vegetation has been used in front of windows facing the path of natural ventilation and evidently humidifies and dampens the air while filtering out dust. Wind catchers in oriental courtyard houses of Iraq channels wind to pass through beds of wet charcoal or porous water jugs located indoors before the air is introduced to livable spaces. . (Konya, 1980)

Konya (1980) emphasized that similar means of channeling air over a pond or water spray can also be used, and stressed that a spray is more effective than a still pond. The author explained that sprays do not only cool the air directly, but it can also wash out air particulates since dust could easily stick to water droplets preventing it from being airborne. Givoni (1976) also mentioned that in some coal mines, wetting is used for dust suppression with a vapour pressure of above 40 mm Hg.

Givoni (1976) on the other hand added that cooling by spraying presents some drawbacks in a practical point of view. The effect of evaporative cooling is maximized in arid regions which observably are places where water could be restricted and oftentimes costly.

## **Effect on Fire Hazard and Maintenance**

Much concern has been stressed regarding double skin facades during the occasion of fire. The possibilities of propagation may be aggravated due to enhanced air flow between floor of the full height cavity aside from the added damage due to the failure of external glazing. On the contrary, the proposal of incorporating water sprays however can help fire suppression by the use of evaporative sprays. Valves that regulate water vapor can also enhance its rate by introducing added volume of water into the air stream.

Self cleaning facades can be incorporated into the double skin assembly. These are a type of glass where through natural processes, the surfaces are able to eradicate dirt and debris. To elaborate, one of the main manufacturers of this type of glass explains 2 main processes involved in this material. Prior actual performance, the coating is activated by UV light through an initial exposure of 5-7 days after installation. The first process or the photocatalytic stage is where solar reaction and even daylight in overcast skies, reacts and breaks down organic dirt where its adherence to the surface is weakened. Secondly at hydrophilic stage, water application like rain touches the surface and is evenly spread. It runs down the glass as a thin sheet which takes away loose dirt while quickly drying without any streaks. (Pilkington)

Through the application of this self cleaning property, the double skin façade cleaning maintenance will be reduced. Also, the most advantageous synthesis of these features is due to the spray proposal into the cavity. The mechanism for evaporative spray and cleaning reaction at hydrophilic stage is well incorporated to take away surface grime like dust or sand that is a common problem in this region.

## **Problem Statement**

This research explores the suitability of a particular type of double skin façade in a desert climate. It looks at current literature and examples and applies environmental modeling techniques to a proposed adaptation of a double skin façade system.

Particularly, the intervention of direct evaporative cooling using spray component is introduced into the double skin cavity. With this intent, the performing properties of the proposed design can alleviate envelope heat gains and reduce energy consumption.

This research has the following Aims:

- Understand the dynamics of the double skin façade assembly
- Assess the suitability and performance of the double skin façade system in the hot and arid/humid desert climate.
- Explore system adaptation to suit local conditions
- Incorporate an evaporative cooling spray within the cavity
- Identify and quantify the benefits of using the proposed double skin.

With these aims in mind, the Objectives set for this study is as follows:

- CFD simulation to show air flow patterns
- Interpolation of literature findings
- Thermal modeling to predict and estimate energy consumption based on studied parameters

- Calculations of evaporative cooling effect using latent heat equations
- Comparisons of energy simulations and savings

This research hypothesizes that the double skin facade can be adapted in desert climates by the use of an evaporative cooling spray within the cavity assembly.

## **Chapter 3: Methodology**

**3.1. Building Physics**

**3.2. Spray Components**

**3.3. Research Methodology**

**3.4. Selection of Software and Training**

### **3.1 Building Physics**

#### **Air flow**

Shiou Li (2001 in Poirazis, 2004) describes that the double skin façade is either naturally or mechanically ventilated. In naturally ventilated facades, air movement is induced even without wind due to stack effect by allowing air to flow in, become heated and less dense, and thus buoyant. Although naturally ventilated façades propose a highly environmental image, the dynamics of wind pressure and stack effect have to be carefully studied. In mechanically assisted ventilation, air is forced into the cavity and is expelled or recirculated due to the continual rise of heated air. The sealed nature of the system from the outside ensures less condensation risk, minimal pollution penetration and reduced traffic noise.

Pasquay (2004) stated that “apart from the temperature difference, the wind speed and wind direction must have a significant influence on the ventilation of the façade gap.” The paper studied a detailed statistical analysis of a whole year measurement of the Siemens building in correlations between wind direction, speed and external environmental temperature. It was found that although the values determined are not equal at the same time, it is evident that the influence of wind speed is at least as much as the influence of the temperature difference.

#### **Air flow simulations**

Manz (2002) said that the prediction of internal and external flows with the use of computational fluid dynamics (CFD) has become an integral engineering tool, having a dramatically increased during the past two decades. He also noted that the building industry is left behind as compared with other sectors such as electronics and aerospace. The



obvious benefits of using CFD can help in applications for the field of construction which includes simulations for internal ventilation leading to indoor thermal qualities, or contaminant air flows like smoke in fire and pollutants, just to mention a few.

There are various approaches in calculating air flow inside the cavity. Djunaedy, Hensen and Loomans (2002 in Poirazis, 2004), categorized 3 main airflow modeling levels. The main categories include the (1) Building energy balance (BEB) that relies on airflow estimates (2) Zonal airflow network (AFN) that are based on zone mass balance and inter-zone flow-pressure relationships usually for the entire building; and (2) CFD that is based on energy, mass and momentum conservation in cells that comprises the flow domain that typically uses a single zone.

In Poirazis (2004), Hensen, Bartak and Drkal (2002) explained that air flow simulations are focused on two main approaches. (1) Computational fluid dynamics of (CFD) which uses conservation equations for mass, momentum and thermal energy are calculated for nodes of a 2 or 3D grid while (2) the Network method considers the building and included fluid flow systems as network of nodes which denotes rooms and sections of systems.

Most authors as mentioned in Poirazis (2004) agree that CFD approach is more beneficial in the study of double skin façade physics. Champagne (2002) said that CFD is an approach that is both informative and saves time and money. Jaros et al (2001) stressed the popularity and capability to model details in temperature and air flow patterns. Gan (2001) emphasized the advantage of CFD technique to apply performance evaluation of air flow windows. Manz and Simmler (2003) used

FLOVENT for calculations and found that analysis of air flow patterns and energy flow is only possible with CFD. Also, Hensen et al (2002) explained that CFD and network method can be combined with building energy simulations.

Tsou (2001) examined computational fluid dynamics (CFDs) in the evaluation of building performance. In computer simulation, a grid is used to represent continuous field phenomena. The accuracy and numerical stability of the simulation depend on the choice of this grid. The grid can be refined in the vicinity of critical areas by adjusting its density, although more refined grids will not necessarily give significant results.

CFD verification is possible but with cost implications. Tsou's (2001) study verified the CFD simulations using a boundary - layer wind tunnel test. Also, Manz (2002) mentioned that modelling fluid flow and heat transfer is a complex task that cannot be satisfactorily performed without continued reference to experimental validation

### 3.2 Spray Components

The cooling effect may be influenced by 3 main processes: (1) contact with cooler surface, (2) mixing with cooler air, and (3) expansion from rising air currents or adiabatic cooling. Dew and fog formation occurs from the first two processes while large scale precipitation occurs from the third. Air in contact with cold surface beyond its dew point causes condensation while fog is formed it air is not in contact with any surface. Givoni (1976)

Belarbi (2006) mentioned that several researches (Ford and Hewitt, 1996, Cunningham and Thompson, 1986; Camargo et al., 2005; Santamouris, 1995) on low energy cooling of buildings as an alternative means for summer thermal comfort and airconditioning used evaporative cooling with sprays injected in the air stream. It was explained that while water droplets evaporates the air temperature lowers and increases humidity ratio.

Wu et al (2006) stated that key process of transferring heat and moisture between air and water through evaporative cooling systems like cooling towers, evaporative condensers are a well-known technology and widely used in industry. They wrote in their research a development of an effective and simple method in numerical simulation of the heat and mass transfer in the direct evaporative cooler.

Erell et al (2005) assessed the cooling efficiency of spraying system installed in a tower. The study mentioned two types of sprays which include the Mist DECT and the Shower DECT (down draft evaporative cooling tower). A Mist DECT involves a very fine mist of water that is generated at the top of a tower, it evaporates rapidly and cools the

surrounding air. Restricting water supply would guarantee full evaporation but may not produce favorable results since in a hot and dry climate, evaporation exceeds water supply. Also, this type would consume more energy to produce enough pressure.

A Shower DECT on the other hand produces larger droplets of water sprayed at the top of the tower and does not fully evaporate by the time it hits the ground. Due to the volume of water applied beyond the potential for evaporation, chilled water is also produced with the cooling air (Rodriguez et al, 1991 or Erell, 2005). Maximum evaporation would also be ensured through excessive spraying. This type of spray is a rather simpler and more reliable device than mist since there is no pressurization required for the nozzle heads, is cheaper and is less prone to clogging. The water reservoir however requires frequent maintenance through cleaning and filtration of recycled water. (Erell et al, 2005)

A typical down-draft evaporative cooling tower (DECT) would have dry air drawn at the tower top while the cooler air is at the bottom. The experimental DECT that the study has used looks like two overlapping cones with the top one inverted, has two air inlets located at different levels and is assisted by a 1.1 kW electric fan as contingency for low wind speed conditions. The other mechanisms include a 750 watt pump, individual controls for two circuits of sprayers, primary and secondary inlet. The circuits contain control valves, pressure regulators, pressure transducer, water meter and sprayers. (Erell et al, 2005)

The study results found a nominal cooling output of up to 70kW which is quite substantial. It is also further noted that the application of

evaporative cooling towers is a practical means for cooling, suitable dry and warm weather. (Erell et al, 2005)

Sureshkumar et al (2007a) presented a paper for the application of evaporative cooling by water sprays under two ambient conditions namely hot-dry and hot-humid climates under dry bulb temperature range of 35 to 47°C. The experiment tested a parallel flow and counter air flow spray effects on a wind tunnel facility made out of a transparent material Perspex. Different air flow representative of a hot humid conditions were simulated by heaters while the varying nozzle size, temperature and wind velocity were modified and recorded. The conclusion draws that for any given water flow rate, a smaller nozzle produces more cooling that reaches up to 14°C in a hot and dry climate.

A follow-up paper by Sureshkumar et al (2007b) simulated a model for two-way heat and mass transfer coupling between water droplets in air that would predict its cooling effect. The prediction in cooling and moisture addition agree with the experiments within  $\pm 15\%$  for parallel flow configuration, but within  $\pm 30\%$  for counter flow configuration.

Belarbi et al (2006) proposed sizing model for a spraying system installed in a building equipped with a shower tower in Catalina (Italy). The models were experimented using a built passive down draught evaporative cooling (PDEC). The same models were also used to size the distance between the nozzle and the distance needed for complete evaporation and can also be used to estimate the temperature reduction as a result of evaporative cooling.

### **3.3 Research Methodology**

#### **Literature Review**

In order to study and understand the performance of double skin facades, related literature and studies associated to the topic is analyzed in their original context. A couple of studies and building examples in the desert climate are also presented to be able to comprehend the dynamics of adapting this concept. Operational features in temperate climate examples and existing proposals of structures shows the points for critique and in defining the dissertation problem. These are the basis of the building design parameters where objectives are drawn and assumptions are tested.

#### **Software Simulation Method**

Since incorporating double skin facades in this climate is a relatively new concept, notable structures are still under construction and are not yet available for real time testing and field studies. A scaled miniature model of the building is not considered since as per the literature review, there are definitive characteristics in dimensions that ultimately affect double skin façade functions and operations.

Air flow is an important issue in building design since it is one of the criteria for human comfort within a space. Tsou (2001) noted that it is difficult to predict the complex and dynamic behavior of wind and air. Wind tunnel tests and smoke movement can represent the behavior, but this method may not be cost-effective especially during the early design stages.

Software simulations therefore, can best replicate the conditions of an actual building tested close to the real environment. It provides detailed results regarding the thermal performance of the structure at particular times of the year while varying parameters to optimize building design and to understand operational flaws.

The task in this section is to be able to find the appropriate software within the resource range of cost and time necessary for learning. Concurrently, the software selected should satisfy the user criterion while exhibiting the competency of the chosen software tool.

### **Software Validation**

A basic software validation helps test the reliability of the chosen program. Pedrini et al (2002) and Carriere et al (1999) of Hamza (2007) listed out a three-tier approach for software calibration. This includes: (1) Analysis of buildings and documentation; (2) Walk through and audits, and (3) End-use energy measurement. In following this approach, simulation results should be comparably close to the end-use measurements to achieve confidence with the software capability.

### **Design Parameters**

#### Materiality

The build-up of the building case model is based on the prevalent building codes. A stringent building code is issued by Dubai Administrative

Resolution No. (66) of 2003. This regulation is otherwise entitled “Approving Regulations on the Technical Specifications for Thermal Insulation Systems and Control of Energy consumption for Air-conditioned Buildings in the Emirate of Dubai” (Appendix A), Using this materiality allows the building to be performing in buildable specification. However, this regulation is already good quality practice consideration which results to high performance benchmarks. With this in mind, savings or improvement for the proposed system could be relatively lower.

Specifications below are materials chosen and available from the software database or materials library.

*Table 3.1 Simulation Materials*

<b>Construction</b>	<b>IES ID</b>	<b>Description</b>	<b>CIBSE U-value</b>
<b>Opaque</b>			
Roof	FROOF2	Flat roof (2002 regs)	0.2497
Ground/Exposed Floor	STD_FL02	Standard floor construction (2002 regs)	0.3487
Ceiling	CEIL4	False ceiling with insulated slab above	0.1678
External Wall	W25	Type2 Metal clad wall	0.3488
<b>Transparent</b>			
External Glazing	LWDB0000	low-3 double glazing (6mm+6mm) (2002 regs)	1.95
Internal Partition	W251	Type2 – Metal clad wall	0.342
Internal Glazing	LWDB0000	low-3 double glazing (6mm+6mm) (2002 regs)	1.7546

The general external glazing are all constructed to low-e double glazing in order to further resist thermal transmission since the inner double skin glazing or windows will also be subjected to the same, if not increased temperatures. A solar chimney is tested to the top exposed part of the



double skin façade. This designed to drive thermal stack effect similar to the proposal of Gan (2004) and Ding et al (2004).

### Prototype Double Skin Facade

The findings from the literature review are used to identify the base case model layout. A relatively conservative floor plan layout of 25 x 25 meters with 8 storeys is utilized, which is almost the same dimensions as the prototype model of Gan et (2004). This presents manageable simulation costs necessary for testing different parameters. The floor to floor height on the other hand is 3.5 m which is similar to Hamza (2007) and close to Gan et al (2004) with 3.75m. The building envelop is 52% glazing, the same proportion as the software validation model, Dubai Convention Tower and close to Cairo World Trade Center, the verification model of Hamza (2007) .

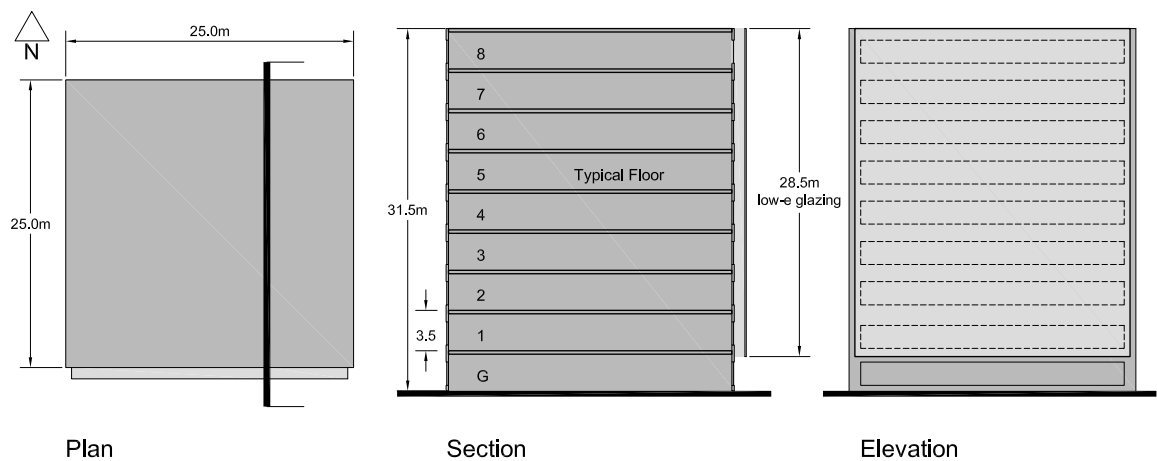
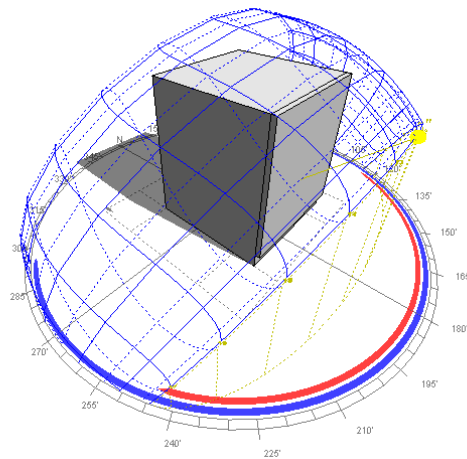


Figure 3.1 Prototype Specification

## Simulations

Testing different parameters is undergone to identify the more optimized configuration and its implications on the assembly performance. Two Day Scenarios are also assumed to study the behavior of air flow based on the extreme positions of the sun. These dates are June 21, and December 21 corresponding to the summer and winter solstice respectively. This period is also when the tilt of the Earth's axis is most at an angle away or towards relative to the Sun. Its location will seem at the position which is northernmost or southernmost in the sky, to contribute the effect of solar location in extreme scenarios.



*Figure 3.2 June 21 Design Day Solar Path*

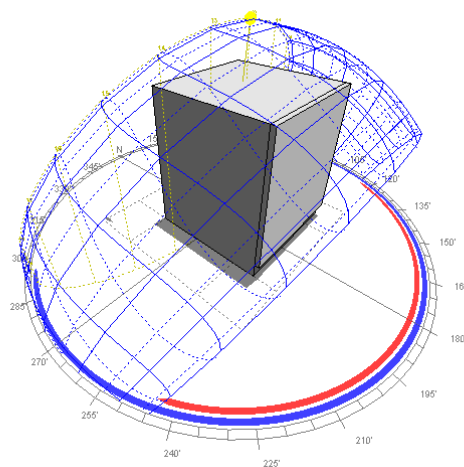


*Figure 3.3 December 21 Design Day Solar Path*

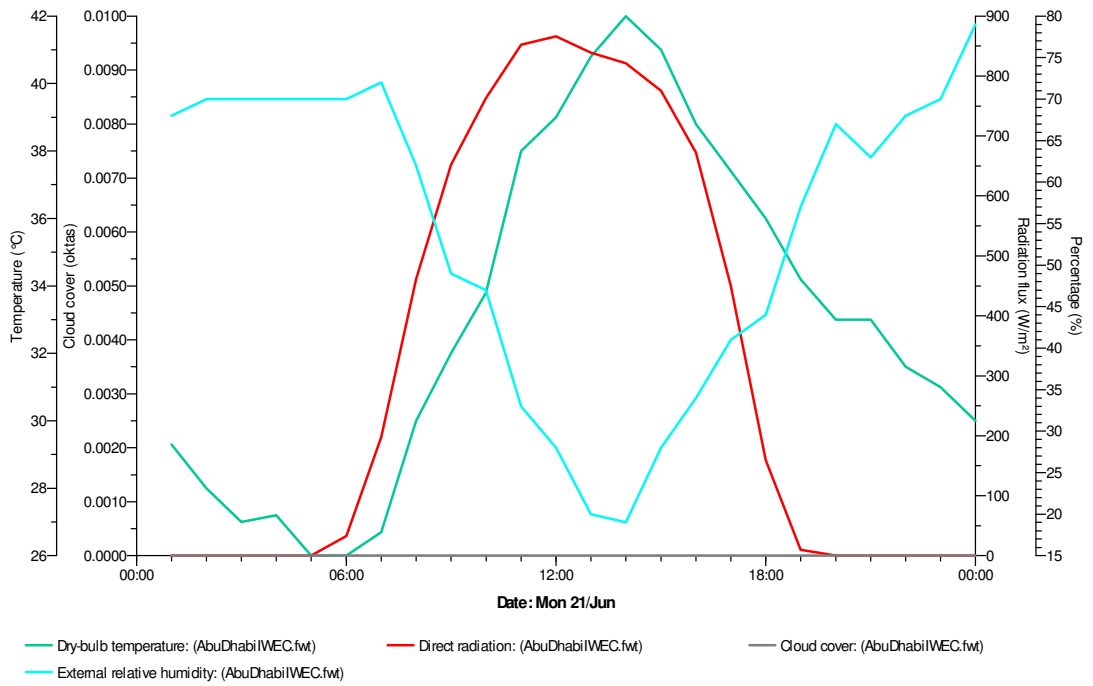


Figure 3.4 (a) June 21 Design Day Weather Readings

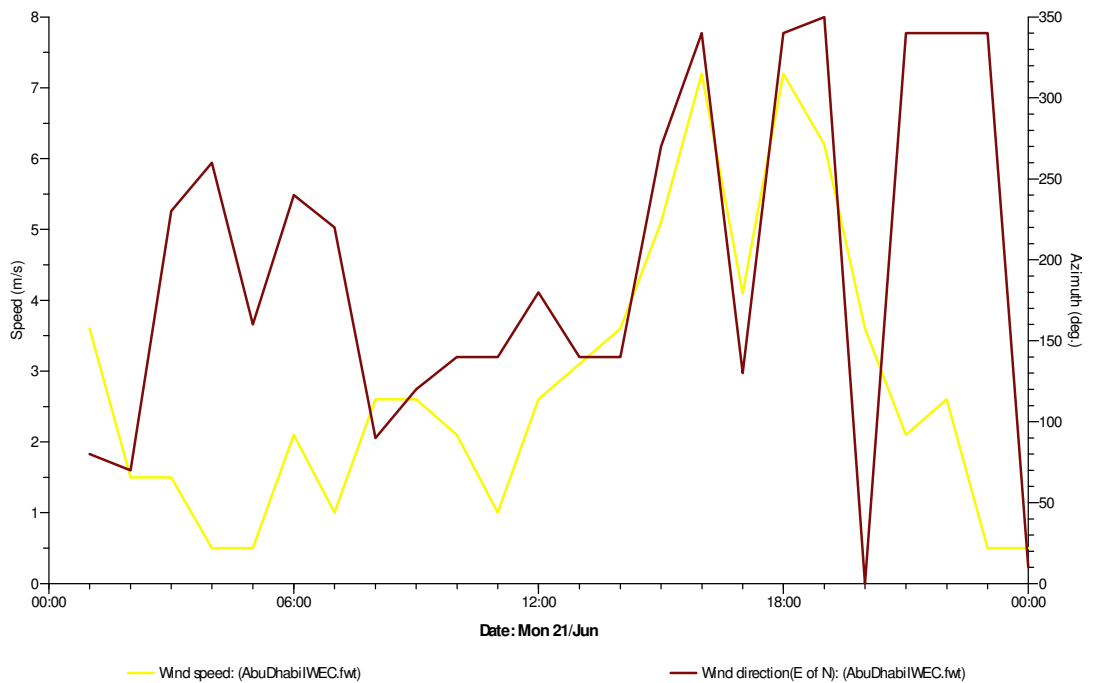


Figure 3.4 (b) June 21 Design Day Weather Readings showing Wind

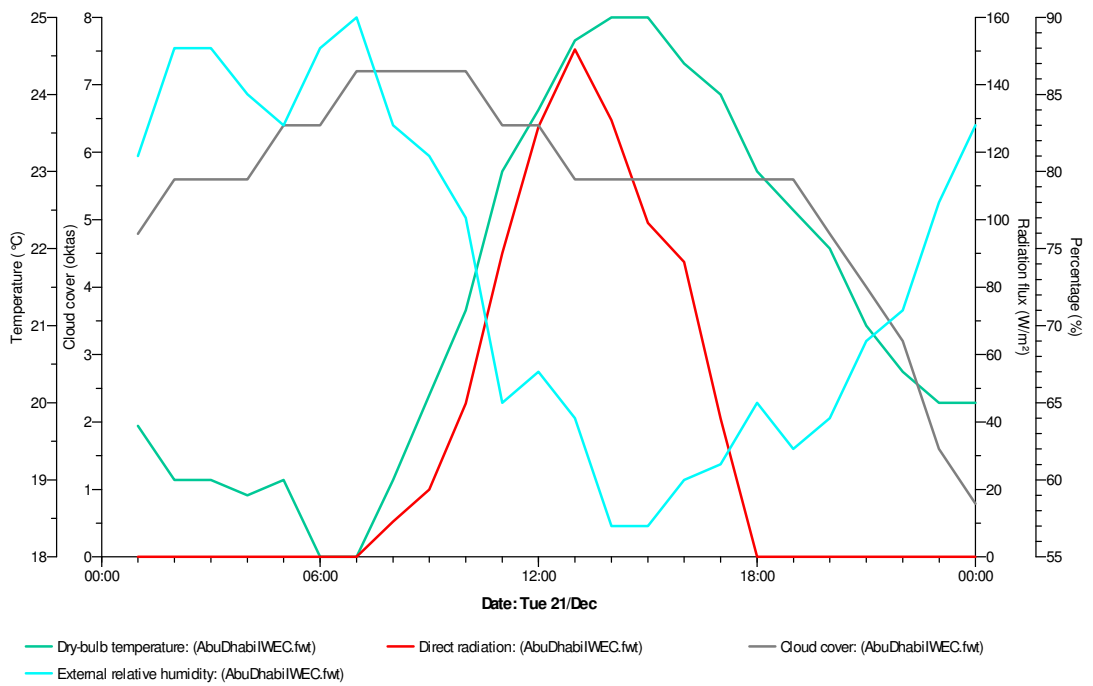


Figure 3.5 (a) December 21 Design Day Weather Readings

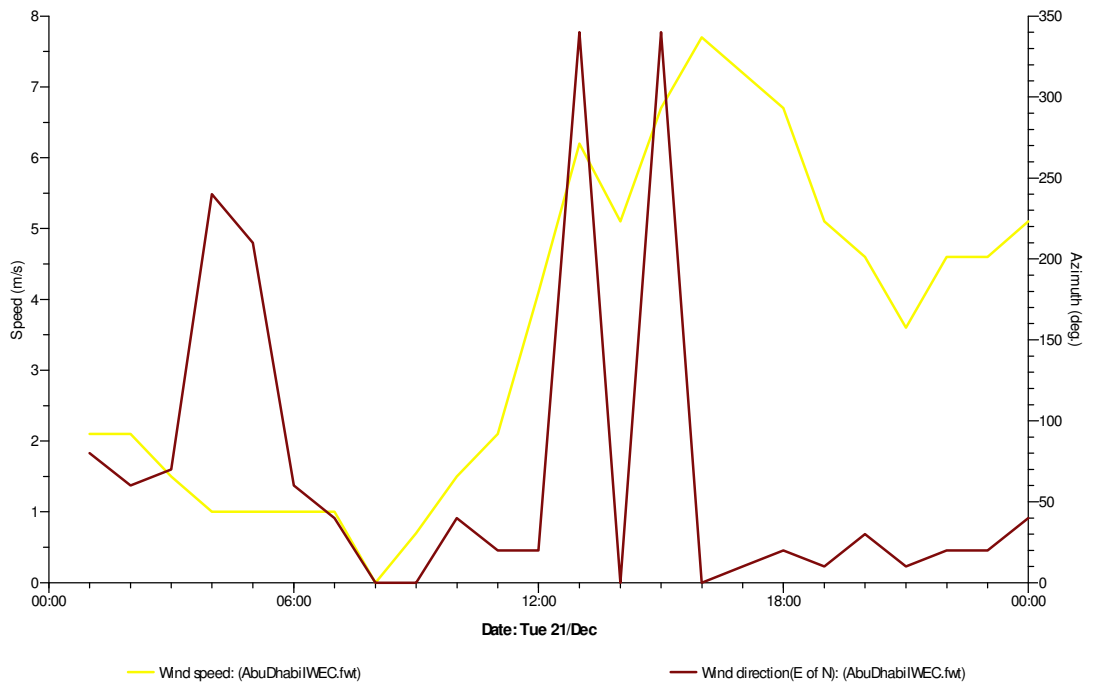


Figure 3.5 (b) December 21 Design Day Weather Readings showing Wind

In reading the graphs, colored legend at the bottom indicates the variables or data used. Horizontal axis refers to the time of the day while the vertical axes relate to the values of data plotted. In reading wind direction however, azimuth values refer to the horizontal angle measured clockwise from a north base line. Readings appear apart in the line graphs when it indicates values around 360° and 0° degrees which are basically north or close to north orientation. Since north reads 360° and 0°, east is 90°, south 180° and west 270°.

A Basic matrix of the double skin façade exploration is illustrated below in order to graphically map around the variables of the simulation run.

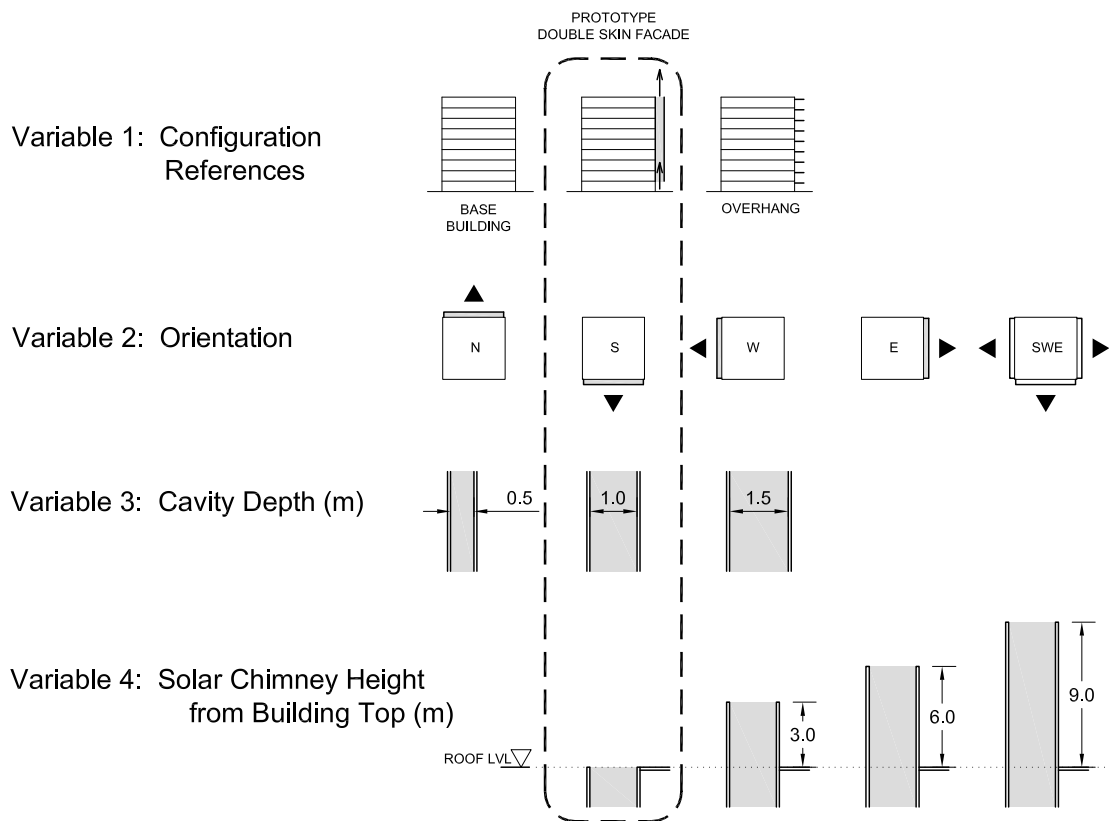


Figure 3.6 Simulation Matrix

#### Variable 1: Air Passage

Prototype model simulation is run to determine the annual energy consumption and air mass flow. Two other scenarios are tested against it, the Base Building that doesn't have a double skin façade, and a building with a south facing Overhang.

#### Variable 2: Orientation

Further iterations containing a double skin face in one side of the model is also simulated in four different orientations. Placing the assembly in one side of the elevation helps isolate the effects of contributed by orientation.

#### Variable 3: Depth

Optimal double skin façade dimensions are identified. The double skin façade assembly is altered to different depths of 0.5, 1.0 and 1.5 meters.

#### Variable 4: Height

Various double skin tops or chimney heights are tested. The solar chimney is altered to different heights, 3.0m (1 Storey), 6.0m (2 Storey) and 9.0m (3 Storey) meters relative to the height of the building top.

In all simulation runs, results are compared against the Base Case and different tested variables to identify which ones can best impact or where savings can be influenced in terms of annual energy reduction and enhanced mass air flow.

## **Calculations**

Aside from computer simulation, an alternative calculation method is introduced in identifying the evaporative cooling effect of the double skin assembly. Basic equations are used to determine the double skin performance while a Psychrometric Chart provides the value characteristics of air necessary to input in these equations. These methods are further explained below.

### Psychrometric Chart

There are innate principles in which air behaves relative to its other properties. For example, the capacity of air to hold water vapor increases with its temperature. Also, the moisture holding capacity is reduced when the air containing a certain amount of water is cooled down. In lower temperature, the air becomes saturated and reaches its dew-point which at a given atmospheric pressure is widely dependent on the vapor pressure of the air. Furthermore, condensation occurs if any cooling goes beyond the dew-point. Givoni (1976)

A Psychrometric Chart best describes the air properties relationship by providing a graphic representation of the state of condition of the air at any particular time. It relates to a temperature along the horizontal axis and moisture content on the vertical scale. This is an essential tool to be able to derive the energy absorbed or utilized by any adiabatic processes.

## Psychrometric Chart

Barometric Pressure: 101.36 kPa  
© Psycho Tool '06

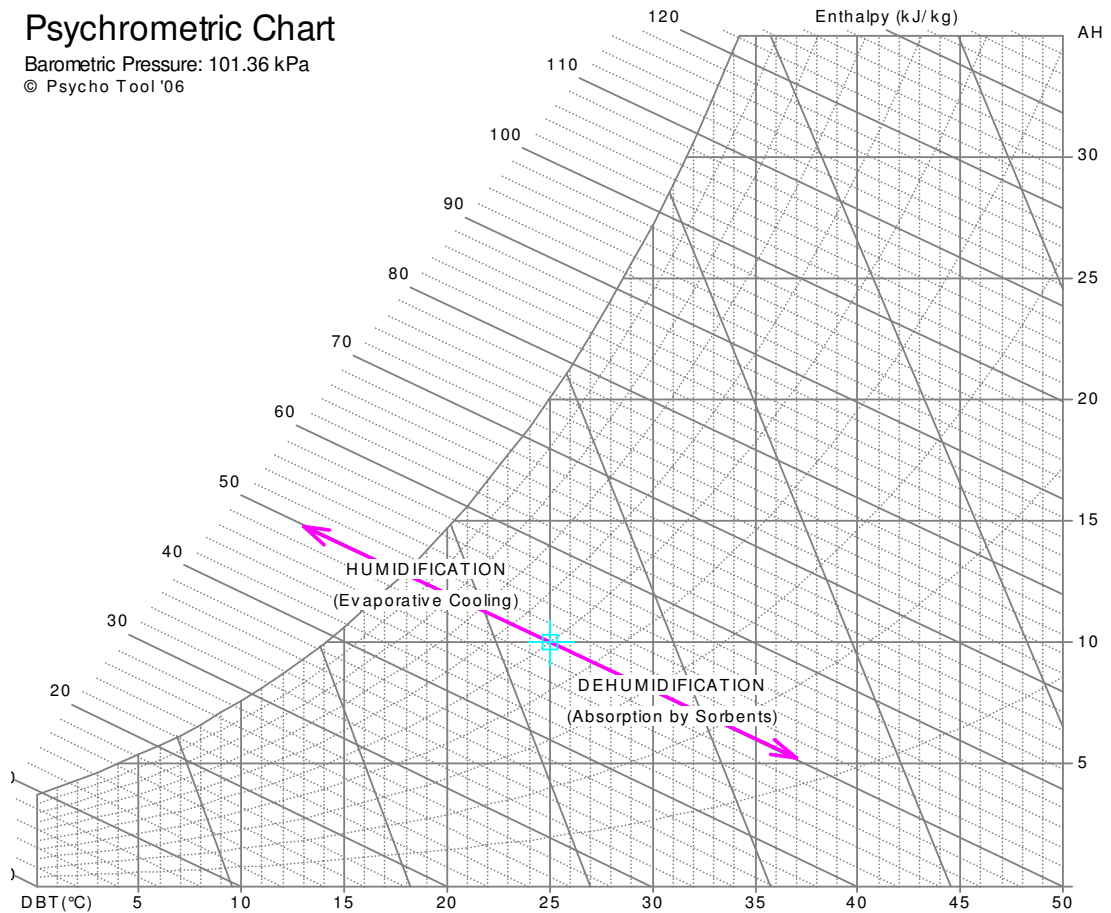


Figure 3.7 Ecotect Psycho Tool - Psychrometric Chart

The properties of air that can be extracted from Psychrometric Chart among others are:

- Dry Bulb Temperature (DBT) – refers to the ambient air temperature measured with a standard thermometer. ( $^{\circ}\text{C}$ ,  $^{\circ}\text{F}$ , K)
- Wet Bulb Temperature (WBT) – refers to the temperature a volume of air would have if cooled adiabatically to saturation at constant pressure by evaporation of water. ( $^{\circ}\text{C}$ ,  $^{\circ}\text{F}$ , K)
- Relative Humidity (RH) – refers to the amount of moisture vapour in a specific volume of air. It also the ratio between absolute



humidity of air at its current state compared to its maximum capacity or dew point. (%)

- Vapour Pressure (VP) – refers to the number of water vapour molecules per cubic meter caused by expansion of evaporated water, it is also linearly related to Absolute Humidity (vp, Pa)
- Enthalpy Values (h) – refers to the energy content of the air; each gram of water represents around 2400 Joules of latent heat energy, enough to raise 1 kilogram of air by around 2.4 °C. (kJ/kg)

Although the chart in itself is indicative enough for analysis, the values necessary to satisfy formulae are in a sensitive range that requires certain level of accuracy. Due to this, an interactive program called CTYSoft Psychrometric Chart is used to calculate and provide more accurate values to determine the various conditions of air. The trial software was downloaded last April 30, 2009 with 30 days validity. (CTYSoft)

#### Governing Equations:

The equations derive the energy absorbed by the incorporation of water vapor in the double skin façade air. For the purpose of these calculations, there are two basic conditions or certain state properties of air that are under consideration. The Initial condition is the state of air prior the spray application while the Final condition is the point after spray is applied, and is differentiated by a value of increased Relative Humidity (***RH***).

At Initial condition, the software simulations determine properties of the air within the double skin cavity. With a given dry bulb temperature (***DBT***) and Relative Humidity (***RH***) values, the initial enthalpy value (***h<sub>i</sub>***) and

Absolute Humidity ( $W_i$ ) in that state is determined through the Psychrometric Chart.

At Final condition, continuous supply of water spray increases vapor in the air up to a point where air reaches near saturation or near the maximum amount of moisture the air can hold. For the purpose of this study, this point is where Relative Humidity ( $RH$ ) reaches 90% or if maximum potential is assumed, ( $RH$ ) can be 100%. At this state, final enthalpy value ( $h_f$ ) and the Absolute Humidity ( $W_f$ ) is determined through the Psychrometric Chart.

Given the change in enthalpy  $\Delta h$  or ( $h_f - h_i$ ) from the psychrometric chart, and the mass flow rate ( $\dot{m}$ ) from the simulations, the Energy formula below is satisfied. It represents the amount of energy absorbed or released to raise moisture between these two conditions:

$$\Delta E = \dot{m} \cdot \Delta h \quad (1)$$

Where:

$\Delta E$  is the amount of energy absorbed during the change of phase of a substance

(kJ/s) also in kiloWatts (kW)

$\dot{m}$  Air mass flow rate is the mass of air passing through a given surface per unit time. Its unit is mass divided by time

(kg/s)

$\Delta h$  change in enthalpy ( $h_f - h_i$ )

enthalpy is also known as the heat of vaporization or heat of evaporation which is the energy required to transform a given quantity of a substance into gas.

(kJ/kg)

Consequently, the difference of Absolute Humidity between the Initial and Final Conditions corresponds to a certain amount of moisture induced into the air stream given as  $\Delta W$  or  $(W_f - W_i)$ . Amount or mass of water consumed between these two conditions is determined by satisfying the equation below:

$$\dot{m} = \dot{m} \cdot \Delta W \quad (2)$$

Where:

$\dot{m}$  is the mass flow rate of water

(g<sub>H2O</sub> /s)

$\dot{m}$  Air mass flow rate is the mass of air passing through a given surface per unit time. Its unit is mass divided by time

(kg/s)

$\Delta W$  change in Absolute Humidity ( $W_f - W_i$ )

(g<sub>H2O</sub> /kg<sub>Air</sub>)

Having the mass flow rate of water in (g<sub>H2O</sub> /s), it can be multiplied to 3600s to determine the total mass of water an hour. It is noted that 1 liter weighs 0.994 kilograms at 35°C in determining the volume in liters (Cengel and Boles, 2008).

In studying the relationships of Equations [1] and [2], it is observable that

- an increase in any values of  $\Delta h$ , change in enthalpy and  $m$ , mass air flow will increase the energy reduction potential of the spray. However, change in enthalpy is a given parameter since the assumptions of this study establishes the Final Conditions at 90% RH. The mass air flow however is a value that is a variable result dependent on the Simulation results. It is therefore important to observe the double skin façade performance that has higher net mass air flow.

Equations (1 and 2) will be tabulated (sample in Appendix I) against hourly readings of the two established Day Scenarios, June 21, and December 21. The results are used to determine the potential energy savings and amount of water used to achieve it. The same equations are prepared in a spreadsheet table with corresponding formulae and input data that helps automatically update repetitive calculation.

### **3.4 Selection of Software and Training**

#### **Selection of Software**

In determining the functionality of a double skin façade, it is important to utilize an appropriate tool in performance analysis. There are several available software in the market with varying capabilities. Its characteristics should be narrowed down using the researcher's user preference criterion.

A user friendly program interface is ideal to a non-engineering discipline while at the same time having sufficient detail necessary to conduct this research. Inter-software operability is also essential to take advantage of other software strengths through data sharable file formats. Exhibiting compliance with standards used for similar building performance studies is crucial for credibility. In possible cases, usage of prior accepted academic paper will strengthen the validity of the tool for study.

One of the challenges of building performance tools is scientific visualization, using color to represent numerical values of temperature and pressure. This kind of output used to be only available using supercomputers, but with faster computer processors and software development, visualization systems have become more practical. (Tsou, 2001)


According to Tsou (2001), architecture students are not very enthusiastic about using CFD tools since they are often laborious, non-intuitive and non-graphical. However the importance of applying these studies early in the design process would greatly improve building design. The same

author developed an online teaching tool that students could follow using a step-by-step interface on a sample project. This method makes the technology more accessible to users with less technical backgrounds and aids in the understanding of basic CFDs.

A basic comparison table extracted from RMJM (2008) Environmental Design Rules of Thumb guide compares several software capabilities. The software under consideration were Envest 2, EDSL Tes, Radiance, EnergyPlus, ESP-r, LT Europe, Ecotect and IES Virtual Environment. The table highlights each of the program's strength through the inclusion of specific areas of study such as, solar, thermal, daylight, CFD (computed fluid dynamics) and lifecycle analysis. IES or Innovation Environmental Solutions Software showed most comprehensive against the other software mentioned.

[a] Computational Analysis

**v. Software Matrix**

RED Rules of Thumb 

General Information  
 \* Table of software available within RMJM end applications

Software Title	Windows/ Linux	Licence	RED?	Solar	Daylight	Thermal	CFD/ Airflow	Lifecycle
IES Virtual Environment	Win	Commercial	✗	✗	✗	✗	✗	✗
Ecotect	Win	Commercial	✗	✗	✗	✗		
LT Europe	Win	Beta	✗			✗		
ESP-r	Lnx	Freeware	✗			✗	✗	
EnergyPlus	Win	Freeware				✗	✗	
Radiance	Both	Freeware	✗	✗	✗			
EDSL Tes	Win	Commercial		✗	✗	✗	✗	
Envest 2	Win	Commercial						✗

Figure 3.8 Software Selection Matrix

## IES Software Compliance

IES is used for domestic and non-domestic compliance assessment for building energy and carbon emissions in the UK and Republic of Ireland which includes Energy Performance Certificate (EPC), Display Energy Certificate (DEC) and Building Energy Rating (BER) capabilities. In Australia, IES offers detailed performance studies for NABERS Energy, Green Star and BCA Part J assessments for thermal performance, energy, CFD, carbon emissions and lighting/daylighting.

In the US, compliance paths for IES includes state building code requirements for federal incentives likes utility rebates and other forms of energy trust programs of sustainable strategies. Assessment for Architecture 2030 Challenge carbon dioxide emission reduction targets can also be used through this program. Furthermore, IES is ASHRAE 140-2004 compliant and can be used for several of the US Green Building Council's LEED rating system credits. ASHRAE 140-2004 is the Standard Method of Test for the Evaluation of Building Energy Analysis Computer Programs, which has a set of guidelines and procedures for the evaluation of the technical capabilities of computer software that calculates thermal and HVAC systems performance.

## IES Software Features

The software has various capabilities built within the IES Virtual Environment Interface. A breakdown of all its features is listed in Appendix B: IES Modules. Specific modules or features integral to this research are ApacheSim (thermal), Suncast (solar), Macroflo (bulk air flow) and Microflo (CFD).

ApacheSim is a thermal simulation program that calculates the heat movement and processes within the building and its perimeter where results are viewed using program Vista. Sunecast on the other hand gives and understanding of the sun's effect on a building while generating information in graphics visuals or numerical values.

MacroFlo analyzes infiltration and natural ventilation within a building using zonal airflow to calculate building air movement that is commonly influenced by buoyancy pressures and wind. The process is run through ApacheSim and is viewable using program Vista

Similarly, Microflo predicts the computed fluid dynamics of air flow in a building using an intuitive and simplified method of setting boundary conditions which reduces time consumed in data entering and preparation. This is distinct from Macroflo since CFD's generate information in graphical or numeric format typically within a span of a few minutes. Macroflo shows the overall effect of natural ventilation due to this air exchanges set up in an annual or specified time frame.

Several of its software tools are integrated to the central 3D model and connects directly with Google SketchUp™, Autodesk® Revit® and through gbXML with other 3D design tools. For example, direct access allows the usage of modelling capabilities and features of Sketchup, which is a common architectural and designer tool. The energy, carbon, daylight and solar analysis of IES are also easily integrated to produce early environmental assessment in concept design.



## **Training and Software Procurement**

There are available trainings online to introduce the software to potential users. The software website also contains features for posting queries in a forum that is made available for users.

The researcher has attended a face to face training with an IES training representative focusing on the IES Virtual Environment ModellIT (3D modeling) module on April 29, 2008. A follow-up face to face training was later held on May 26, 2008 for modules ApachSim (thermal) and FlucsDL (daylight) (Appendix C: RGV\_IES certificate).

The IES software was eventually procured through the IES online website on June 25, 2008 specifically for this research. The purchased student Package contains all of the features of the full version of IES. It is operable for one year and costs £50.

## **Chapter 4: Computer Simulation**

### **4.1. Software Validation**

### **4.2. Exploration of Configuration**

## 4.1 Software Validation

### Overview

A basic software validation is conducted to verify the simulation of energy consumption versus real time energy cost. Its purpose is to test the IESVE software capability to produce results close to the actual building performance. At the same time, it exhibits confidence to the researcher's proficiency in using the software which is integral to the conduct of this research.

The study attempted to validate the IESVE software against measured data from literature of Hamza (2005) where the same software was used to compare the performance of a double skin against a single skin façade in hot arid areas. For the purpose of this dissertation, the two simulated building models Cairo World Trade Center and the Research Case Model, of Hamza (2005) were tested for software validation. Both buildings were modeled using Google Sketchup and were exported to IESVE which simulated the annual energy consumption. The attempt however showed largely delineating and inconsistent results. This may be accounted for information not mentioned on the published paper that may include detailed architectural plans, specifications or varying occupancy patterns.

The third software validation model, Dubai World Trade Center Office Block showed more consistent building results from the IESVE ApacheSim annual energy simulation. Several factors may have contributed to this which may be due to proximity of study model location, regular occupancy patterns, and since more detailed architectural and other related information like specifications were readily available.



*Figure 4.1 DWTC Office Block Image*

The Dubai Convention Tower is a medium rise building consisting 14 floor of office space or G + 13. The building is design by RMJM and finished construction by 2003. This building is a part of the Dubai International Convention Center and was initially used as office space support for the 2003 International Monetary Fund meeting. At present, the building is leased out to different companies and institutions. Although it is connected to the Novotel and the Dubai Convention Concourse, its mechanical and electrical systems are separately designed.

### Weather Data

The weather data is provided by IES VE APLocate database. “APLocate is the weather and site location editor for the programs CIBSE Heat Loss & Heat Gains (ApacheCalc), ASHRAE Heat Balance Method (ApacheLoads), ApacheSim, SunCast and Radiance. It is possible to choose a location from an extensive database and guidance is given on defining weather data for various locations.”

## Building Model

The familiarity and proximity of this building to the location of the researcher also helped conduct informal site visits to visually analyze its perimeter and surroundings. The model is constructed to the dimensions of the architectural plans, details and information found in the appendix. See Appendix D: DWTC Plans.

The model is initially constructed using the program Google Sketchup, a common architectural software for basic modeling. The built-in link to IES VE has managed to assist input information for the building construction sets and functions within this program interface.

Building Properties tab allows the selection of the building location to set the climatic information. The Building Construction Set inputs the building type which affects occupancy patterns through its database. Basic Building HVAC Service type is also invoked to determine the building's cooling system. Another tab in identifying rooms is activated to differentiate between rooms as thermal zones and other objects as external obstructions like shading device.

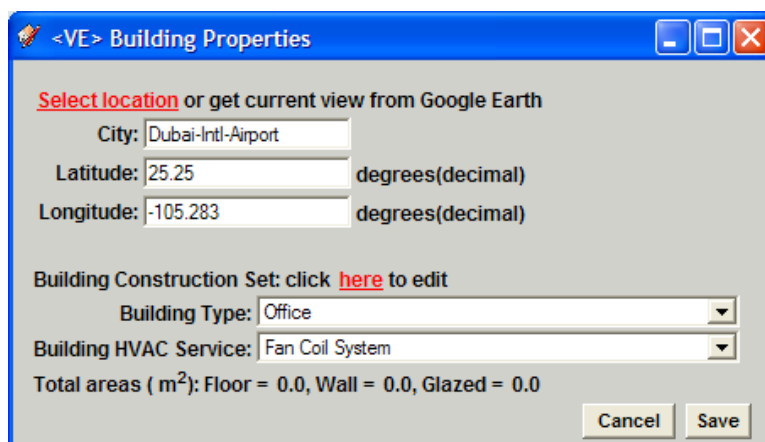


Figure 4.2 Google Sketchup – VE Building Properties

The program works in templates from its database to assume typical specifications based on building types with specific overrides to redefine, name and save construction presets.

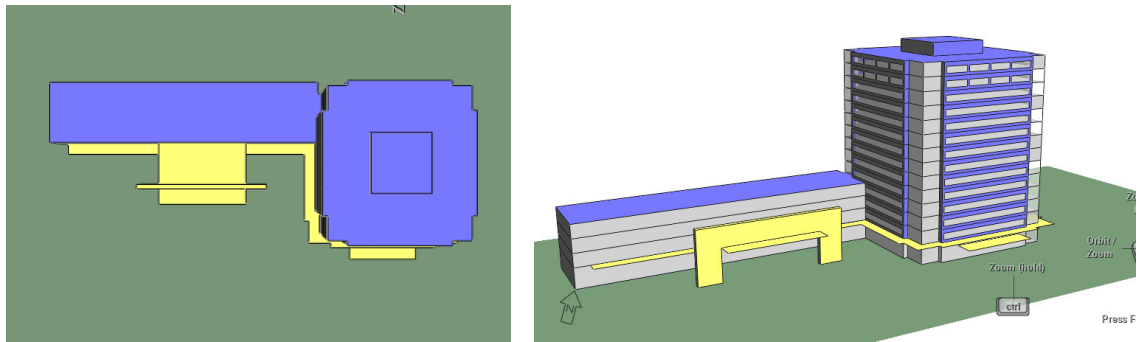


Figure 4.3 DWTC IES Simulation model

The constructed model is launched or exported to the IES Virtual Environment Software for the detailed environmental analysis. It is observed that some technical inconsistency with the earlier Sketchup location preset requires reinstatement of the location and Weather data within the IES VE interface using the APLocate Database.

Within IES VE, the module SunCast: Solar shading analysis is invoked to incorporate the effect of external obstructions within the site including the effects of solar shading elements.

Consecutively, Apache Thermal module is accessed and activates options for simulation. An annual energy consumption option is selected. Depending on the speed of the computer and complexity of the model, time required for simulation using an HP laptop with Intel (R) CPU T2500 @ 2.00 GHz, 3.00 GB of RAM took around two minutes.

### Data Comparison

A limited end-use energy measurement was collected for the months of April to August year 2006. Ideally, a whole year and several month readings of energy consumption is averaged. However, confidentiality constraint limited this information. Some projections are drawn based on this trend in order to estimate the consumption in the absence of readings in these months and is further explained in Appendix E.

*Table 4.1 DWTC Simulation Validation results*

DWTC Simulation Validation			
Actual Energy Consumption		IES Simulation	
Date	Total energy (MWh)	Date	Total energy (MWh)
Jan		Jan	684.16
Feb		Feb	634.28
Mar		Mar	708.20
Apr	826.65	Apr	722.19
May	1029.00	May	838.08
Jun	1077.63	Jun	880.53
Jul	1163.49	Jul	965.22
Aug	1129.39	Aug	961.94
Sep		Sep	902.35
Oct		Oct	841.79
Nov		Nov	722.24
Dec		Dec	657.68
		Sum/Total	9518.65

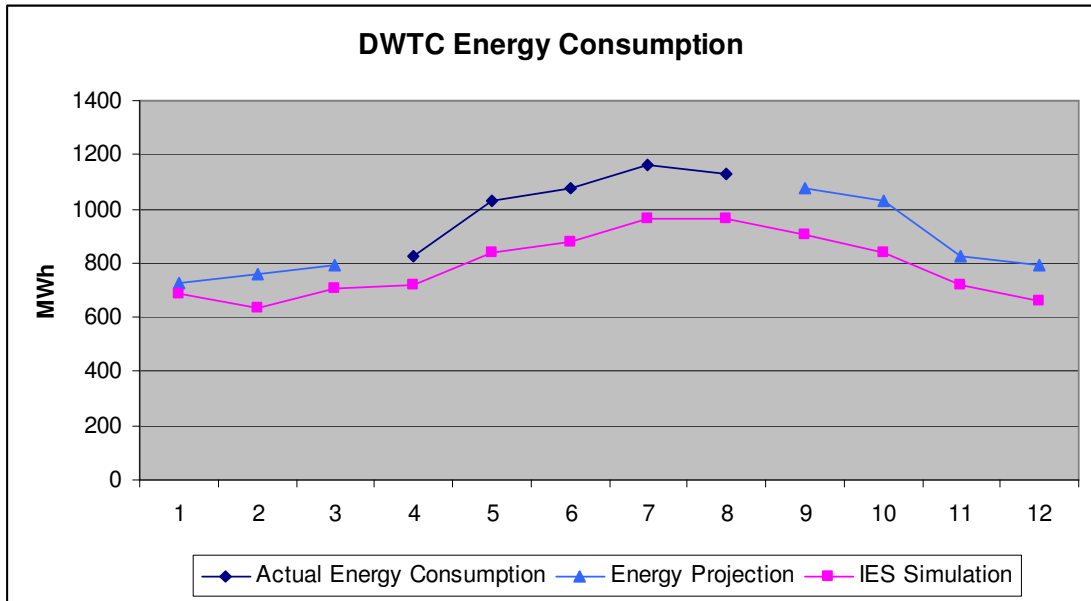


Figure 4.4 DWTC Energy Consumption

In Table 4.1 and Figure 4.4, it is observed that the combined Actual Energy consumption and predicted Energy Projection follows the same trend as the results of the IES Simulation. However there is a substantial difference on the actual readings against the simulated values. This could be accounted for the different occupational patterns of a restaurant – bar that is located in the ground floor and the allowance of usual occupant misuse. Also, the podium part of the office block is open to the Convention concourse. There is no separation between these areas, and thus there is a high possibility that the supply air is spilling through these spaces.



## 4.2 Simulation Results

Building Prototype Model

Storey: G+8

Floor Height: 3.5 m

Dimension: 25 x 25

Orientation: South Facing

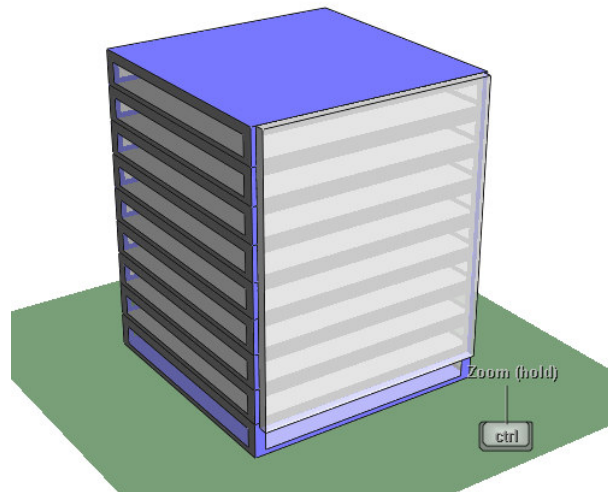


Figure 4.5 Prototype IES Model

Initially, the model is constructed using Google Sketchup in order to get the basic building form. However due to some complications in exporting issues, the entirety of the modeling was finally constructed through IES Modelit. Depending on the simulation variable, each model is altered to identify the results necessary for the research.

In IES, the location setting is established using APLocate which uploads weather data from a library. In the UAE, Abu Dhabi weather file is available for simulations. Construction materials are then assigned to the building which indicate the materiality of the built model. A thermal template per zone is assigned to the rooms in order for the software to identify typical occupational profiles where a Building Type Office Default is selected.

Some surfaces are assigned as opening through Macroflo. This is critical in identifying which window is open for air flow, in this case, the top vent

and bottom inlet of the double skin façade. SunCast is then run to identify the effect of solar obstruction and location.

The ApacheSim module simulates both energy consumption and mass air flow on the cavity. It is run with selected variables corresponding to the Design Days established, or annually for a whole year energy consumption. Results appear in graphs and as spreadsheet values.

CFD modeling however identifies air movement on a particular time. This is invoked using MicroFlo internal (for room air movement) and external (for whole site CFDs). Boundary conditions are set by importing values or specific time from the ApacheSim results which dictates the surface properties like temperature on the CFD boundary condition model. The grids are automatically generated however, at certain occasions, it needs to be simplified to due by increasing grids on areas not critical, specially in external CFDs. This however requires a couple of hours to process but produces graphical representation of air movement

### Variable 1: Configuration References

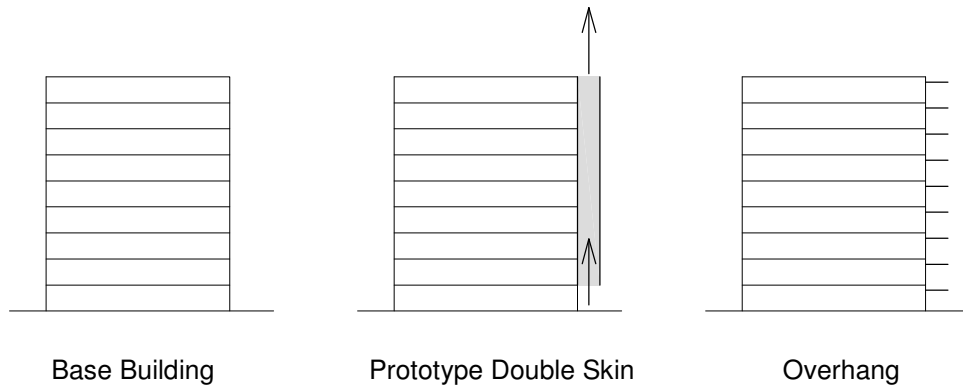


Figure 4.6: Variable1 Configuration References Diagram

In order to determine the energy savings contributed by the incorporation of a double skin façade, the annual energy consumption is compared with and without the double skin assembly. In the simulation model, these refer to the Prototype Double Skin and the Base Building respectively.

An alternative configuration using an Overhang on the south Base Building is also simulated in order to compare the effect of a typical passive strategy. The overhang has two different cases under consideration, a 1 meter and a 2 meter projection. Simulation details can be found in Appendix E.

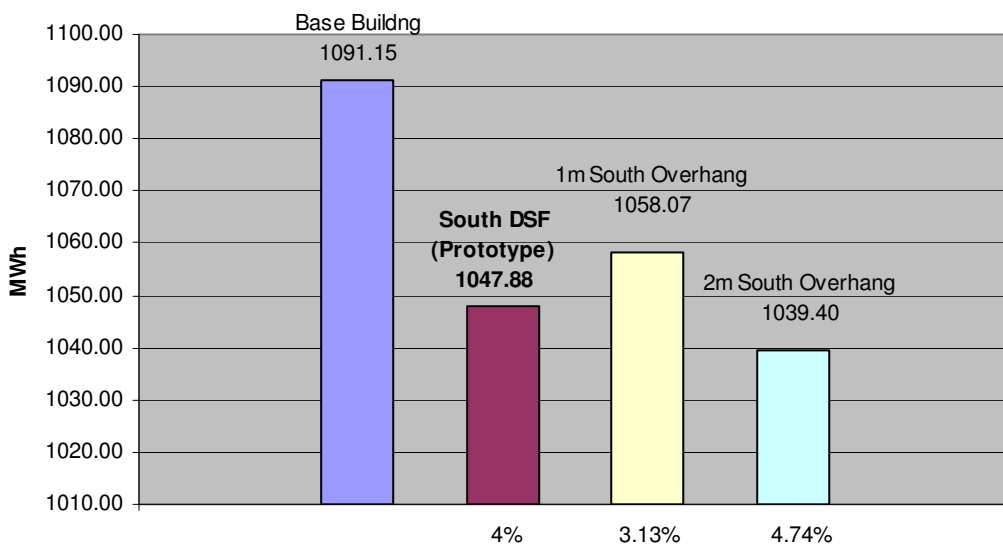


Figure 4.7: Variable1 Configuration Reference Annual Energy Consumption

Using a double skin façade through the Prototype models shows an energy reduction of 4% relative to a building of the same specifications without it. The alternative configuration of a 1 meter South Overhang is close with 3.13%. The 2meter South Overhang however has the highest energy reduction in the set with 4.74% savings.

This suggests that a 1 meter depth south double skin performs better than a 1 meter south overhang. However, an increase in overhang projection performs best in this simulation. Subsequent findings with the increase in double skin depth will be covered in Variable 3.

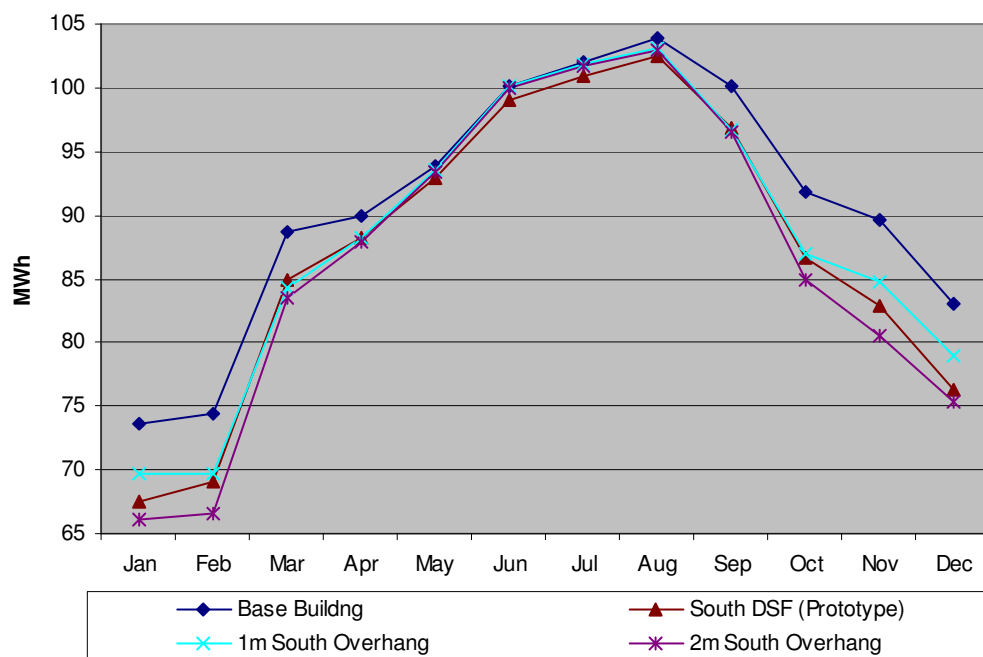


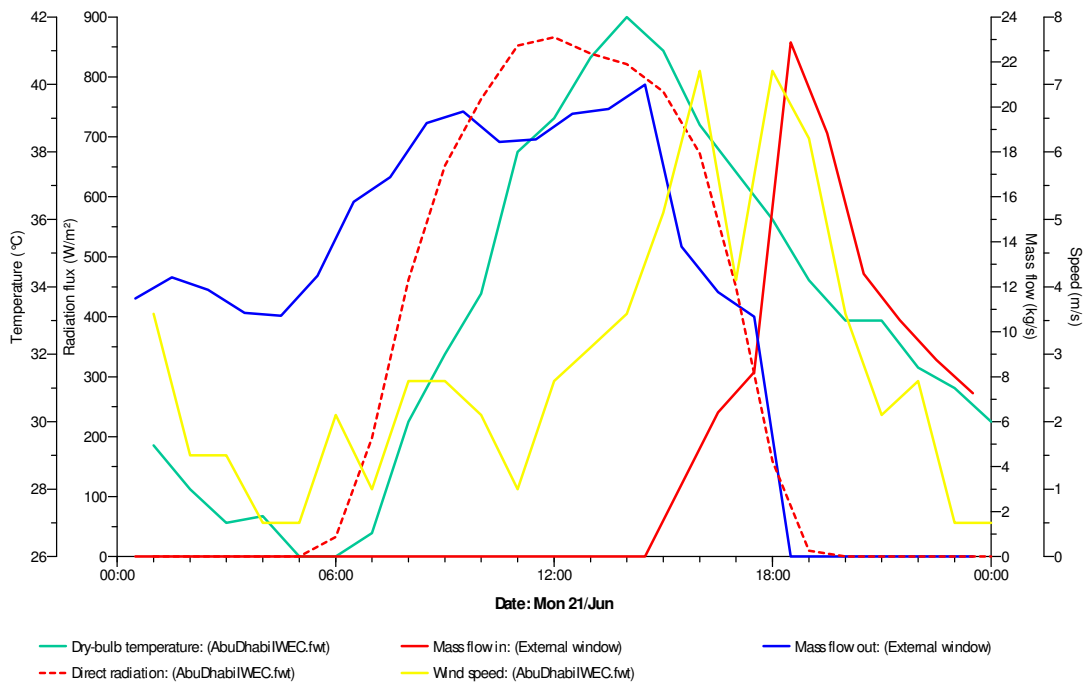
Figure 4.8: Variable1 Configuration Reference Monthly Energy Consumption

A monthly energy consumption total breakdown is illustrated in Figure 4.8. This shows that the south double skin façade and overhangs perform best from September to February which are typically the cooler months. During the peak summer months of June to August however, it

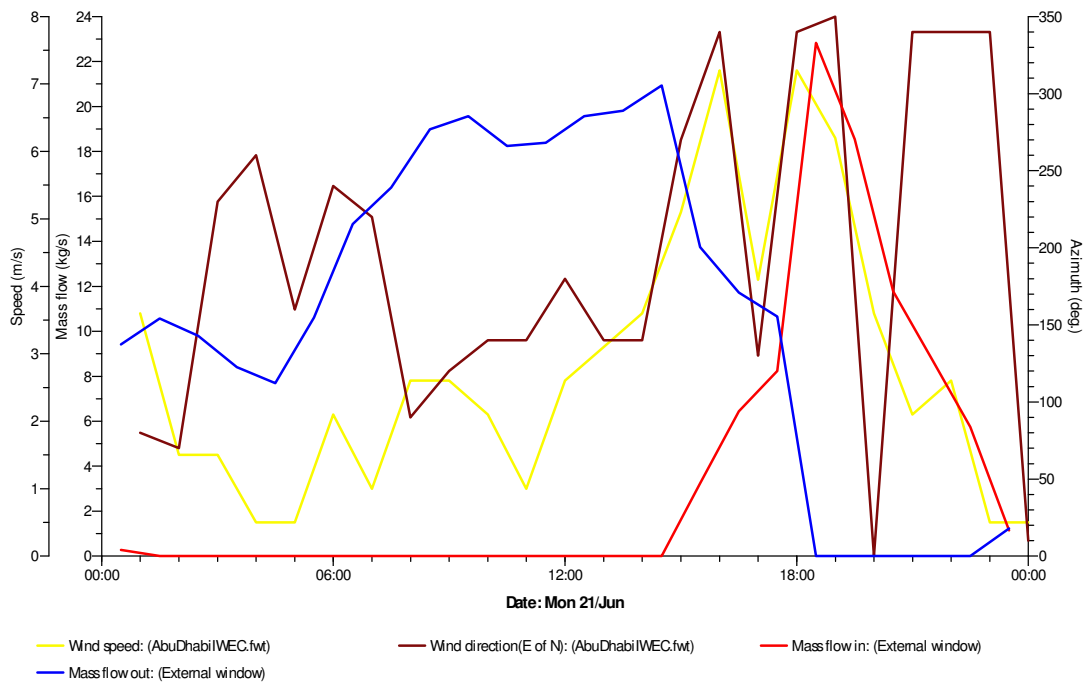
is noticeable that the south double skin façade is performing slightly better than the overhangs.

This is highly dependent on the specific solar location at certain times of the year. South overhangs would logically prevent direct solar rays that are dominantly steep south during winter. During summer, the overhangs have minimal benefit since the sun path is almost zenithal at noon and almost vertical at the sky. Double skin facades however, perform in both occasions because of the u value properties of the extra outer surface.

Figure 4.9 shows the summary performance of the Prototype model simulation with Macroflo under the two Design Day Scenarios of June 21 and Dec 21. The specific air flow results and graphs are detailed in Appendix F.

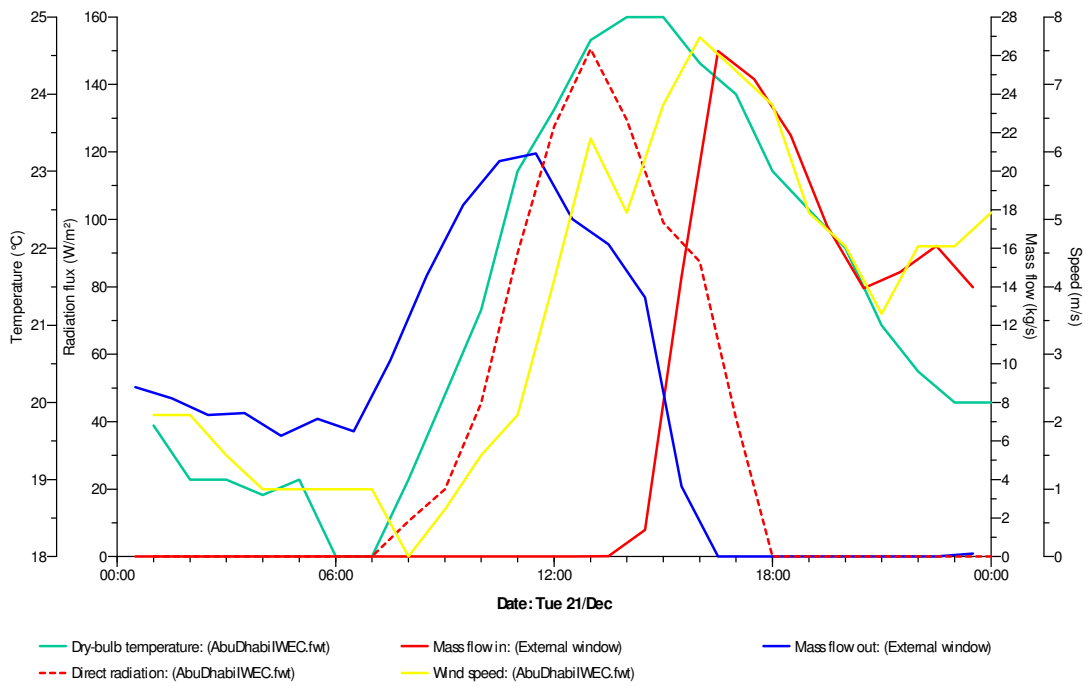


(a) Prototype mass air flow

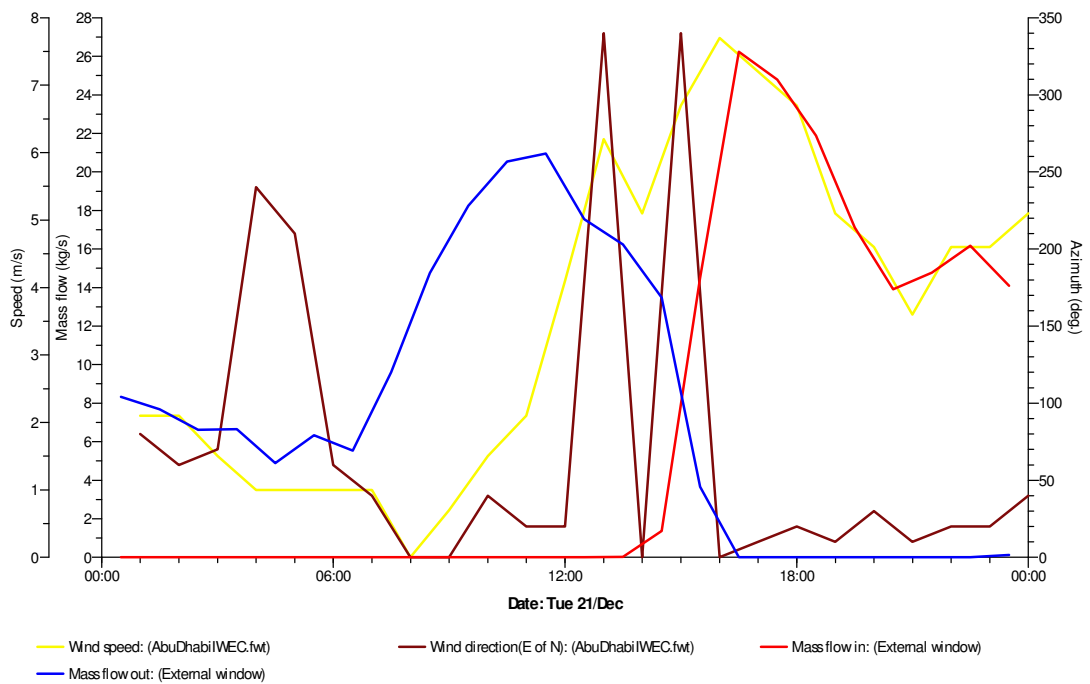


(b) Prototype mass air flow overlaid with wind direction

Figure 4.9 Prototype Air flow (June 21)



(a) Prototype mass air flow



(b) Prototype mass air flow overlaid with wind direction

Figure 4.10 Prototype Air flow (December 21)

In the **Prototype air flow**, there is a dominant outflow of air during the day through the upper opening in both design days. Figure 4.9 shows that during summer (June 21) the gradual outgoing increase of mass air flow peaks near the highest outdoor temperature reading, being continuously fueled by high direct solar radiation. The mass air out flow eventually drops with the decrease of solar radiation at around 6pm. The subsequent presence of wind however induces air movement within the cavity, but in the opposite direction. It is noted that external winds in this locality is predominantly coming from northwest, almost opposite to the cavity inlet which is located at the bottom of the double skin façade and placed at the other end of wind direction. Thus a likelihood of air entry from the top opening causes a reverse in mass air flow. Afterwards in the graph readings, the reverse mass air flow then behaves in the same slope as the external wind speed behavior.

In winter (Dec 21 at Figure 4.10), a continuous mass air out flow occurs during the day but drops earlier at around 2-3 pm as compared to the summer scenario. The lower radiation readings have caused a conservative mass out flow which is necessary to enhance stack effect. Zero net air flow occurs near the peak of external temperature around 3pm, this is the point on the graph where out flow and inflow meets. This behavior is similar to Hamza (2007) which stated that “the flow increases with increasing solar intensity but reduced with increasing external air temperature at any given value of solar intensity.” As this point in stagnation has weakened stack effect due to further loss of solar radiation presence of the peak in temperature, wind has taken over as a driving force for air movement. After 6pm, mass air outflow drops as wind speed has dropped and radiation supply has stopped.



A CFD illustration on the external wind relationship and the movement of the Prototype south doubles skin façade is shown below.

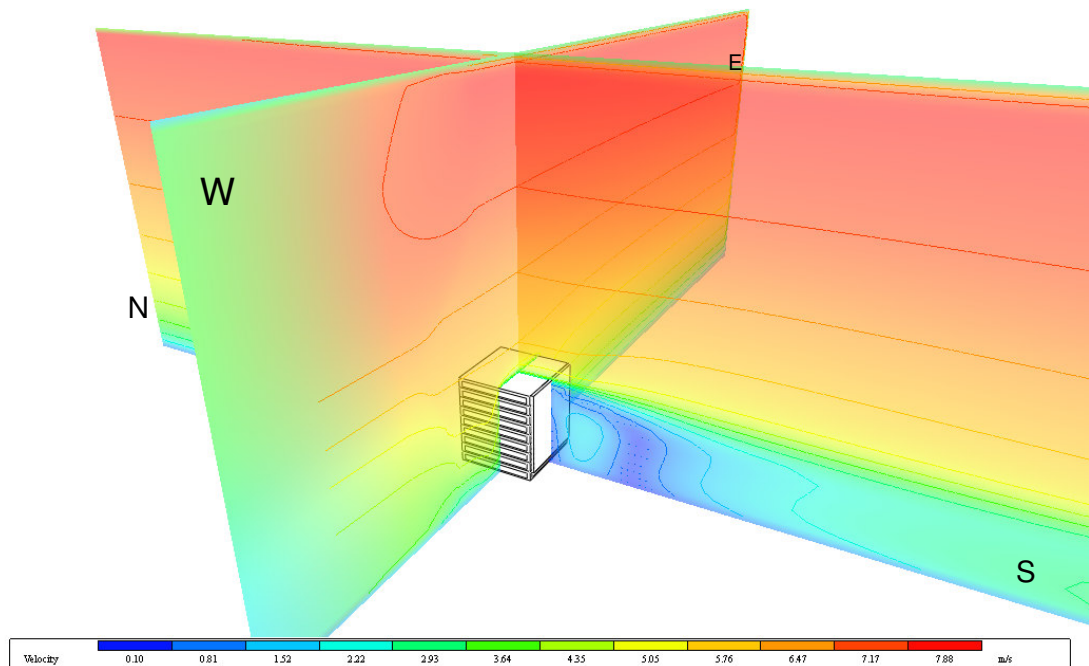


Figure 4.11: External Wind CFD

In Figure 4.11, a basic external CFD model is shown for the Prototype south façade on December 21 design day at around 6pm to analyze the influence of external wind on the downdraft air flow. The predominant north wind with a velocity of about 7.5 m/s shown in Figure 4.10, is used for the CFD simulation. The labeled axes indicates as reference for the sectional CFD slice.

The axis slices are represented through colored filled and contour readings against a velocity legend. Velocity vectors are also shown as arrows which depicts direction, the size however does not represent speed since its scale is exaggerated for readability.

This simulation however shows the whole building as a solid within the CFD boundary. A closer look at the internal CFD is also presented showing a spot detail on the slice within the cavity.

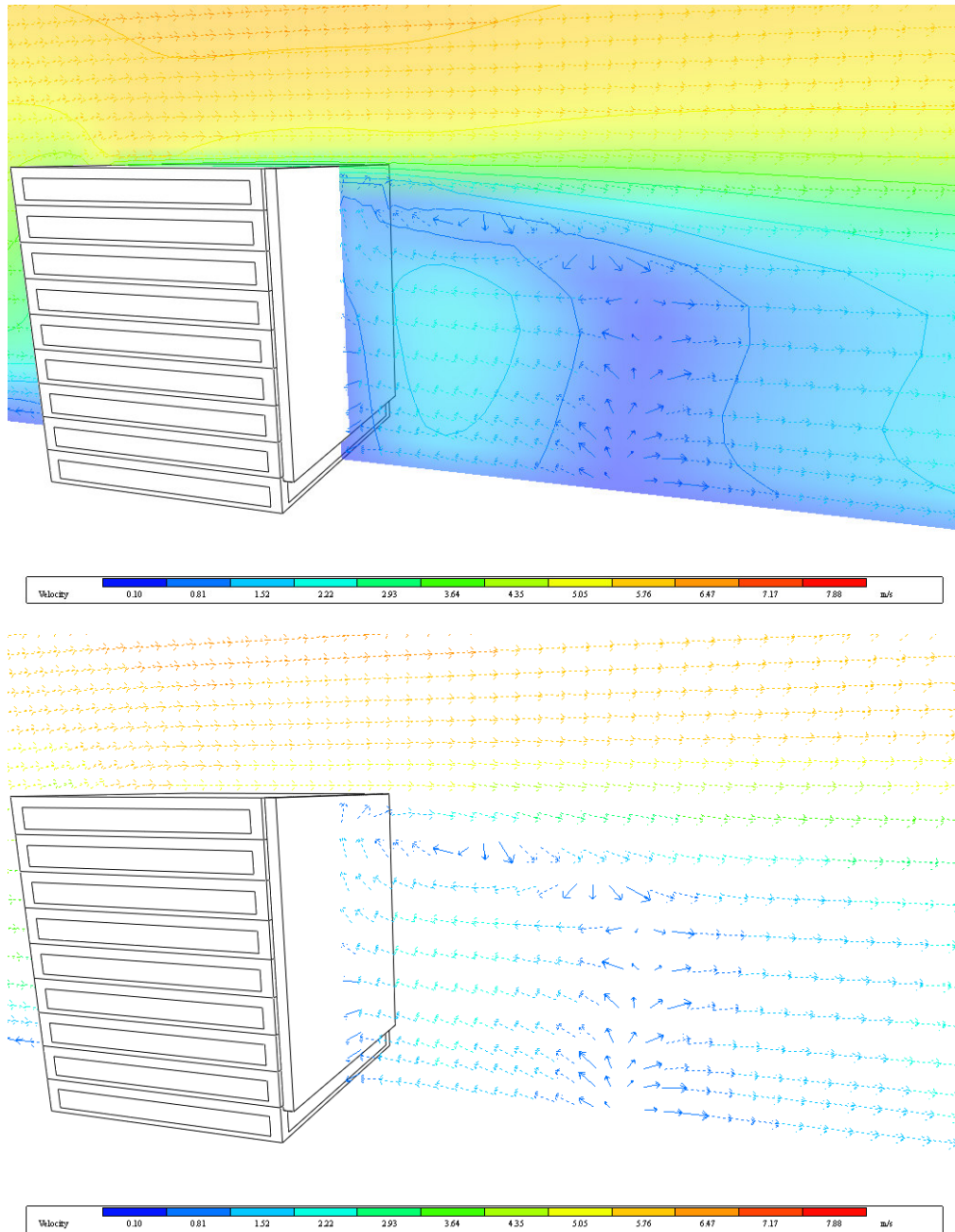
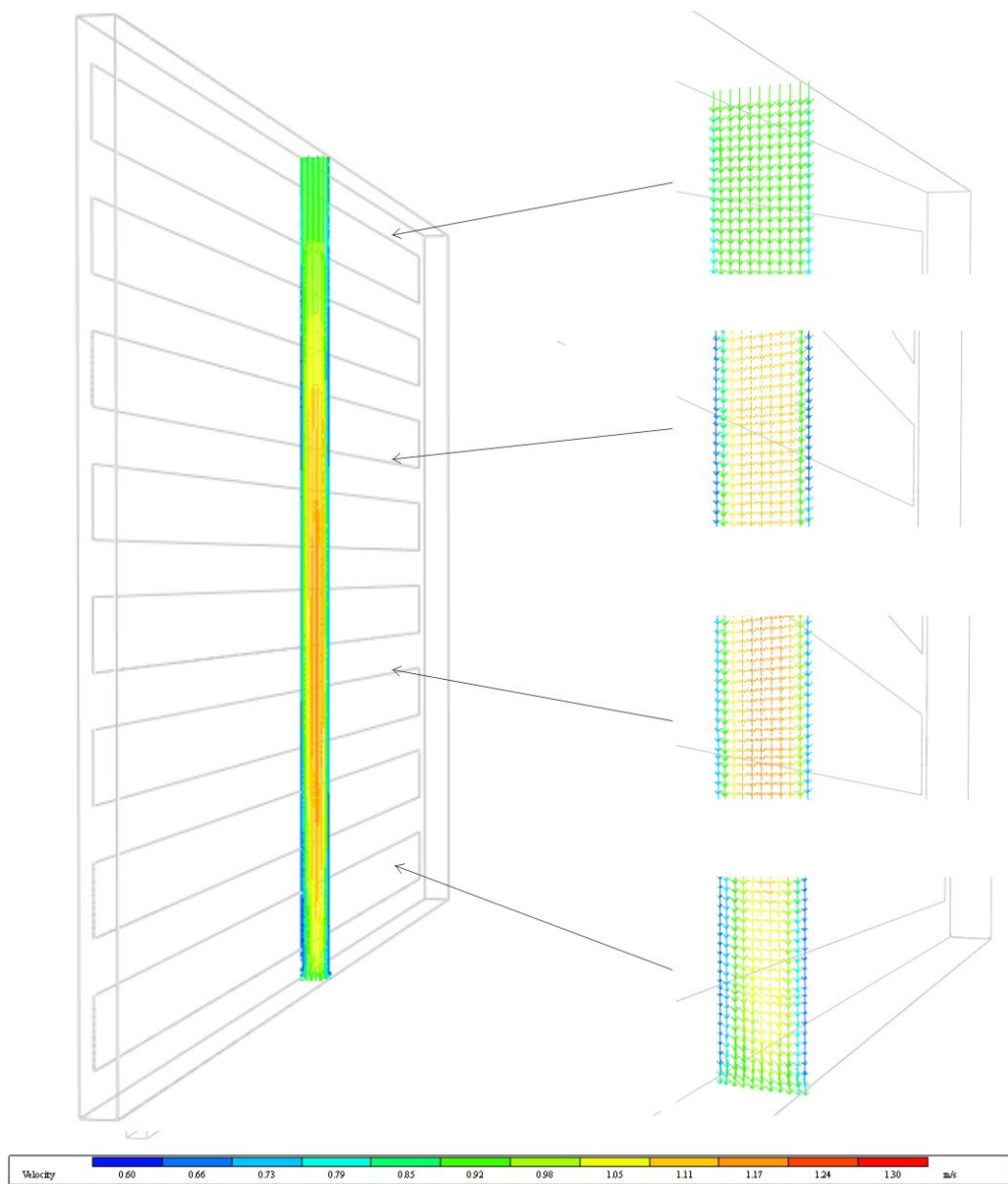


Figure 4.12 : Y Axis (South Facade)

Figure 4.12 shows that an eddy formation and negative pressure occurs on the south side or the wind leeward direction. This opposite end of the general external wind causes high velocity on the top part of the south double skin façade. There is almost no wind flow at the base of the cavity inlet where readings show an exaggerated directional arrow with negligible value of 0.1 m/s. The high velocity upper opening is drawn to a negative pressure area funnelled through the top opening.



*Figure 4.13 : Cavity Air Flow Y Axis (South Facade)*

Figure 4.13 illustrates the CFD vector velocity section along the y-axis through the median section of cavity. The direction is predominantly downwards with a maximum speed of 1.3 m/s. The downdraft velocity is not incremental showing a marginal increase in velocity towards the center, vertically and horizontally. Velocity is then reduced near the bottom opening as it mixes with outside air where a minor incoming velocity occurs as described earlier in Figure 4.10.

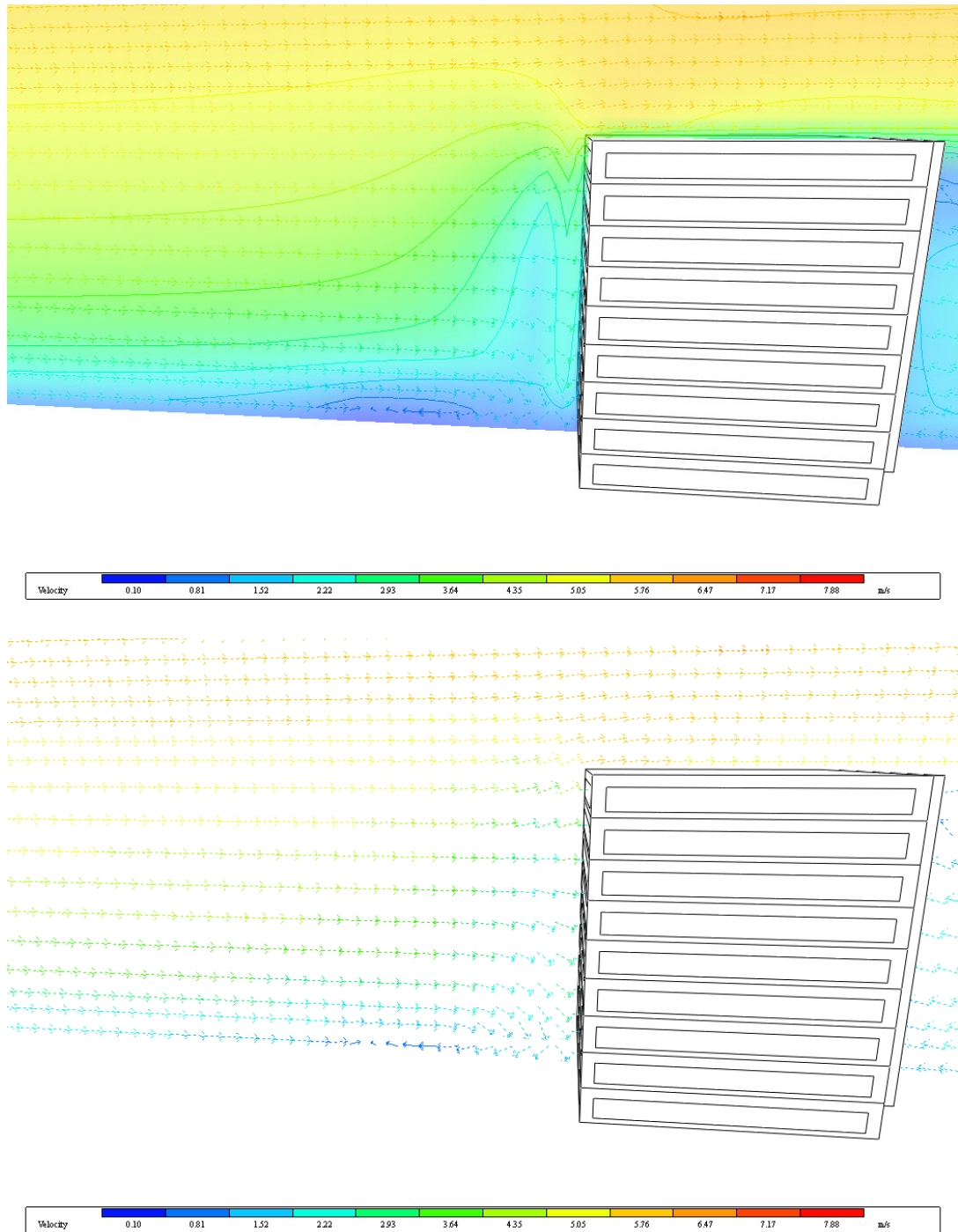
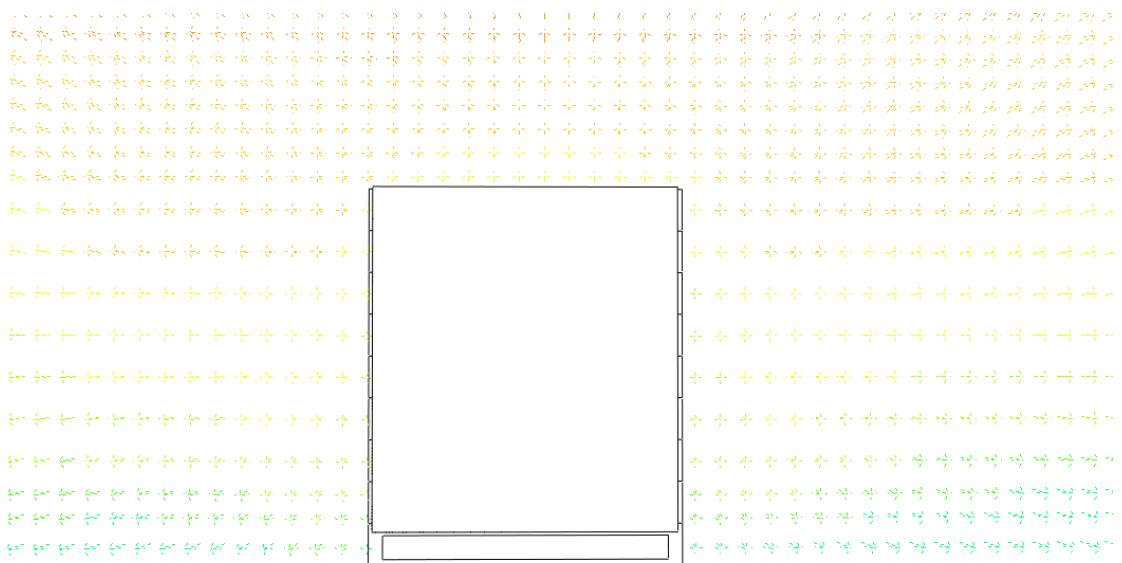
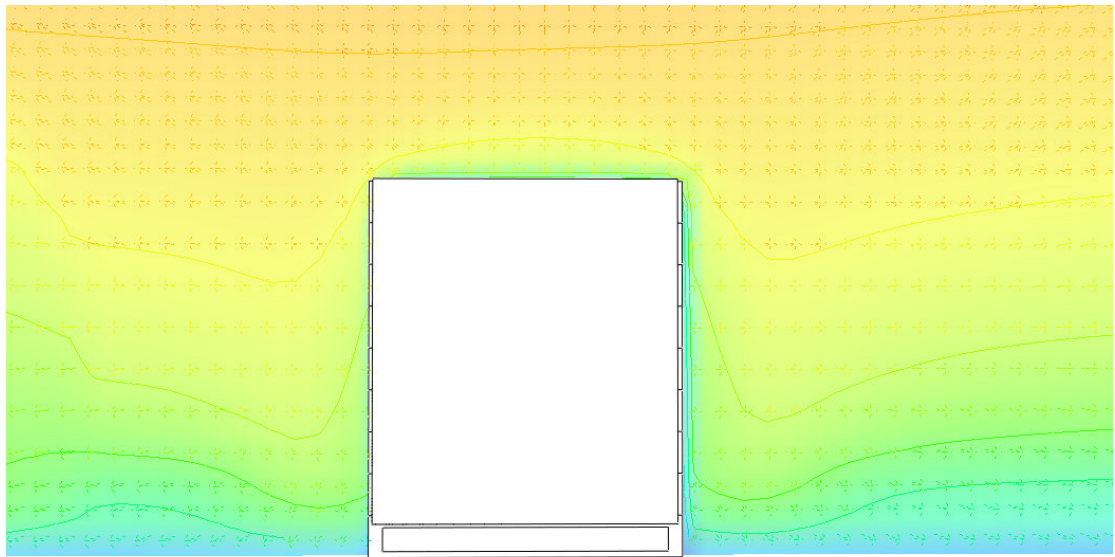


Figure 4.14 : Y Axis (North Façade)

In Figure 4.14, it is shown that the external wind flow directly hits the surface of the building, increasing pressure in this area and causing an upturn on the façade base. In the occasion that a north double skin façade is present, the bottom inlet would receive an incoming air that would enhance mass air flow.



*Figure 4.15 : X Axis*

Both east and west sides however are neutral and parallel to the external wind direction (Fig 4.15). In occasions where double skin facades are situated in these sides, any turn in wind direction that varies in slight degrees to the east and west throughout this design day, can affect mass air flow.

## Variable 2: Orientation

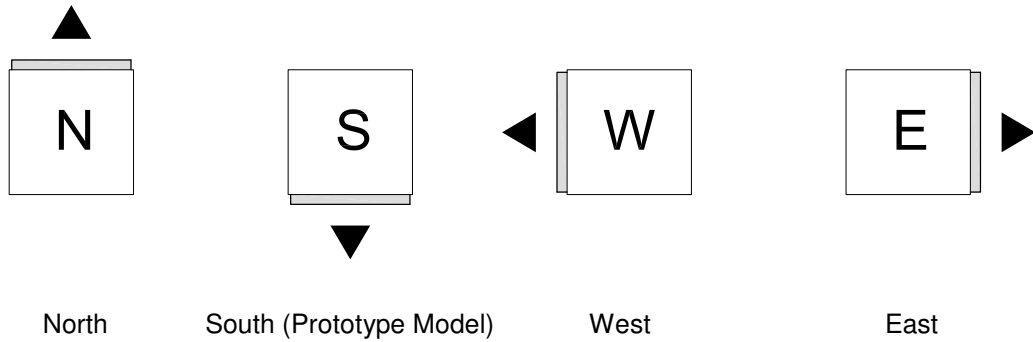


Figure 4.16: Variable2 Orientation Diagram

The effects of orientation are determined to identify the ideal location of the double skin façade assembly. The same Prototype Model is rotated and simulated to isolate the effects of orientation on energy consumption and air flow movement. The information from Variable 1 of the Prototype model and the Base Building without a double skin facade is also used for energy reduction reference. Detailed results of each scenario can be found in Appendix F while the summary can be read as follows.

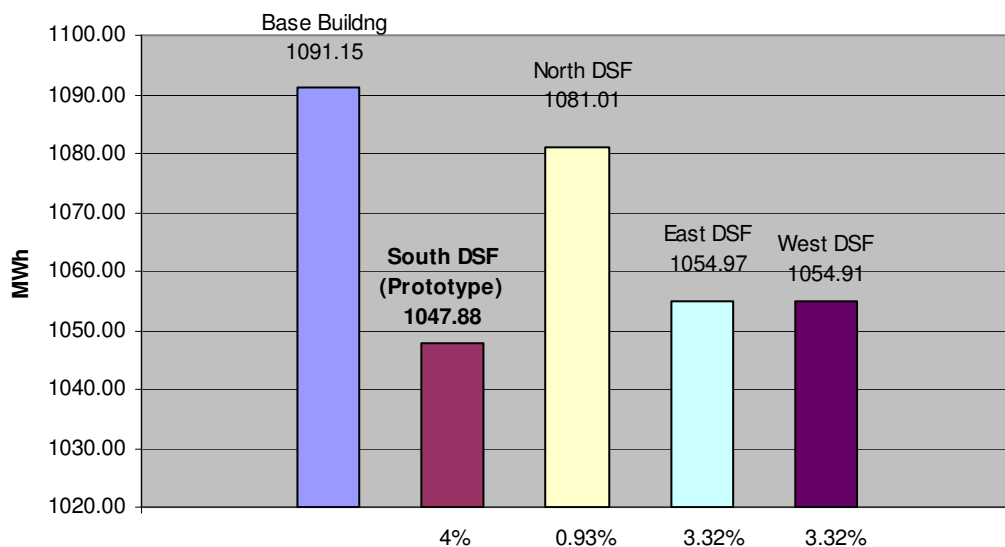


Figure 4.17: Variable2 Orientation Annual Energy Consumption

### Simulation 2: Orientation Monthly Energy Consumption Total

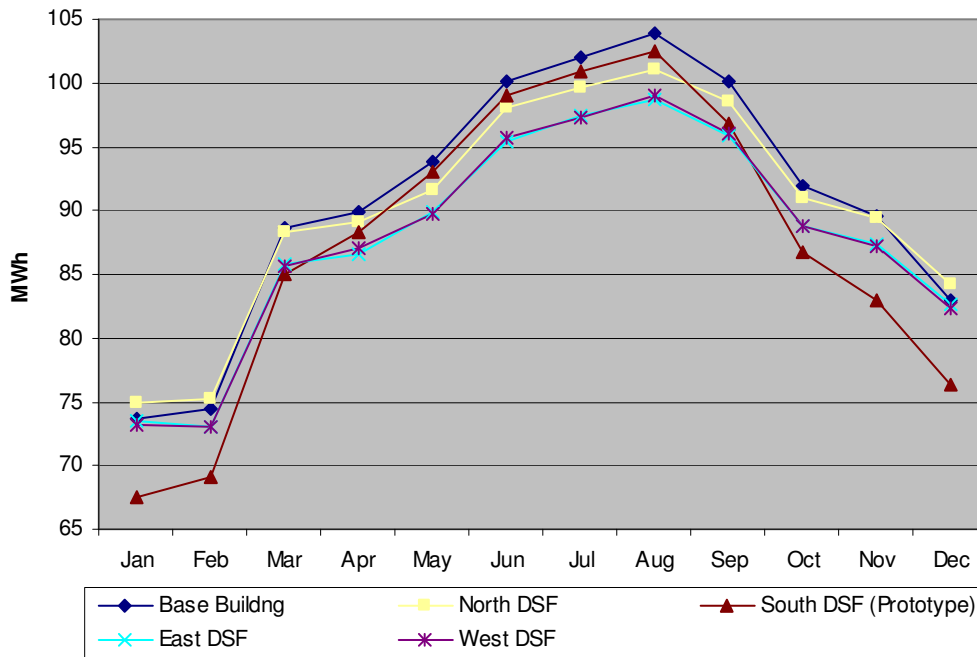


Figure 4.18: Variable2 Orientation Monthly Energy Consumption

In Figure 4.17, it is found that the four tested configuration has specific energy reduction compared to the same building without a double skin façade. The East and West façade have almost identical energy savings which accounts for their even share of daylight exposure. The north however has very minimal energy savings due to the fact that there is very little direct solar gain to protect the façade to start with. The South Façade or the Prototype model however still has the best energy consumption savings.

Figure 4.18 shows the monthly breakdown of the tested orientations. During the months of June to Aug, East and West façade has the highest margin of savings compared to the Base building. Due to the sun's angle to the summer sky, South façade has little exposure while the North façade is usually minimal and thus little potential for savings. The South façade's potential is more optimal during the winter months. As seen on

the same illustration there is greater difference in energy reduction for the South facade between October to February, which are the months where the sun is steep as temperature is cooling down around winter.

For specific and detailed air flow studies, the graphs in Appendix F show the North, East and West Orientation model simulated with Macroflo under the two Day Scenarios of June 21 and Dec 21.

It is initially assumed that in the North double skin façade, there would be lesser air movement since it has little solar exposure due to orientation. However, simulation results as per Appendix F show a substantial movement in air flow. In June, mass air out flow hints to drop early during the day, but is then picked up by the presence of external wind. Dominant northwest wind direction is more likely to enter the bottom inlet in this orientation. In December, although there is little solar exposure, increase in wind speed has also helped drive air movement.

Appendix F also shows that in the East façade, the peak in mass air out flow occurs in the early part of the June 21. This is due to the solar exposure from the rising sun while external temperatures are still low which is ideal for stack effect. Hamza (2007) also mentioned that buoyancy driven channel flow rate is said to be dependent on the temperature difference between the discharge and inlet. In this scenario, the external temperature serves as a heat sink to the accumulating solar gain within the cavity as influenced by early direct solar exposure. On the other hand in December, there is a continuous increase in air out flow movement within the cavity even if the day has progressed and where direct solar exposure is lessened. It would be imaginable that the thermal lag that started from the early sun is slowly released as the day



progresses. The strong correlation with the external wind also suggested that its influence that can be due to the parallel movement of air flow to the upper exhaust since according to Fig 4.10 and 4.12, external wind for this specific time and day is coming from the north.

Appendix F shows that in the West façade, peak in mass air out flow occurs in the afternoon highly due to the fact that the sun's position would substantially elevated temperatures only around this time of the day. Simultaneously, the presence of the afternoon external winds further increase mass air outflow where the highest reading in all orientation simulations is seen. A similar behavior can also be seen in the December design day.

Net air flow is calculated to identify the overall air mass flow effect of the double skin façade orientation under study. This shows the difference in airflow direction and determines the dominant air flow movement.

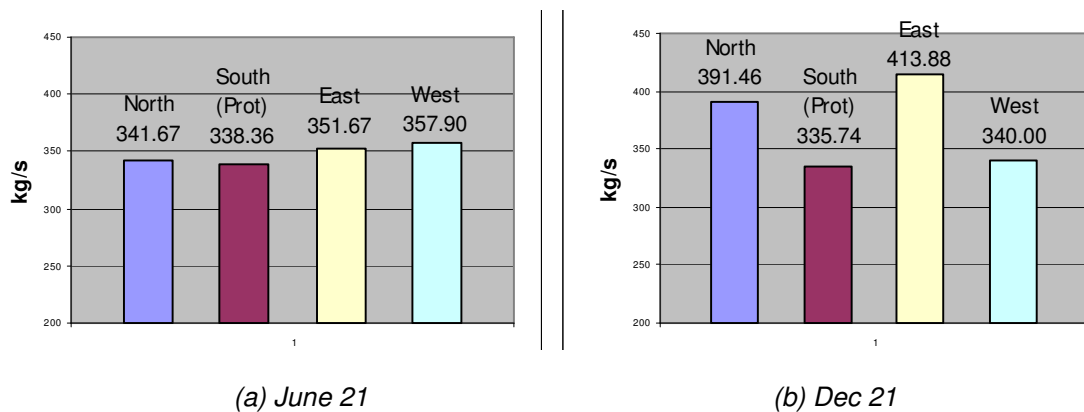


Figure 4.19 Variable 2 Orientation Net Mass Air Flow

The detailed mass air flow (kg/s) readings in Appendix F are on a 30 minute interval and multiplying each reading by a factor of 1800 (seconds in 30 minutes) equates to the volume of air for that time interval. The

units of the day sum in Figure 4.19 are still expressed in kg/s for manageable values, it can be multiplied to 1800s to get the total mass air movement for the whole day. The proportions however are the same between sum of mass air flow and total mass.

Figure 4.19a shows that in June 21 graphs the variation in orientation does not have a significant difference in providing net mass air flow values.

Figure (4.19 a & b) shows that the South orientation has the least net mass air flow for both June 21 and Dec 21 design days. Several initial assumptions have been drawn based on the logical position of the south façade where it is strategically placed in order for the assembly to receive maximum solar exposure. Inference for this relationship states that south façade can receive greater solar gains and thus higher mass air flow. However this is true, there are other factors that affect air flow.

Pasquay (2004) strongly emphasized the influence of wind speed and wind direction which may equal to a minimum the effect of temperature differences. In revisiting the climatic data of the design days as seen in Figure 4.9, it is clear that in June 21, the high external wind speed readings are coming from North some time in the afternoon. Also in Dec 21, the highest wind speed readings predominantly come from the same north direction. Due to this, as shown in (Figure 4.10), the south façade is situated in the side behind the wind direction where it cannot benefit from external wind as earlier illustrated in Figure 4.12 . While at the same time, any fall in speed and change in direction even reverses air flow.

### Variable 3: Cavity Depth (m)

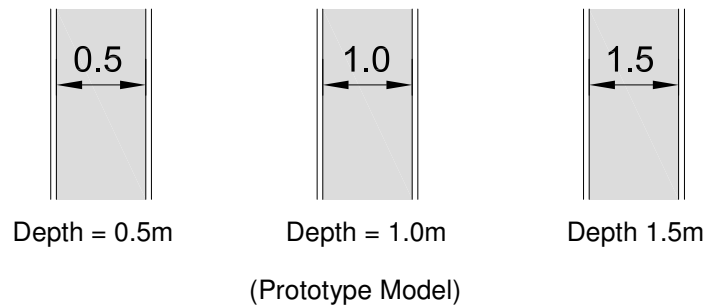


Figure 4.20: Variable3 Cavity Depth

The double skin façade is tested for different depth dimensions. The Base Case Model is altered to the mentioned double skin façade depth in order to study its effect on energy consumption and air flow movement.

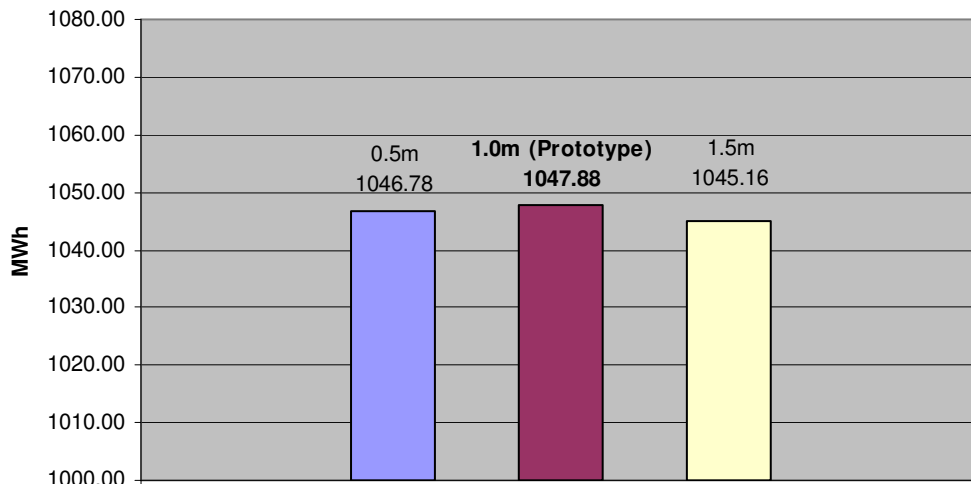


Figure 4.21 Variable 3 Cavity Depth Annual Energy Consumption

Based on Figure 4,21, there is almost negligible difference with energy consumption between the 3 depth variations. All results came close to 1047 MWh annual energy consumption. .

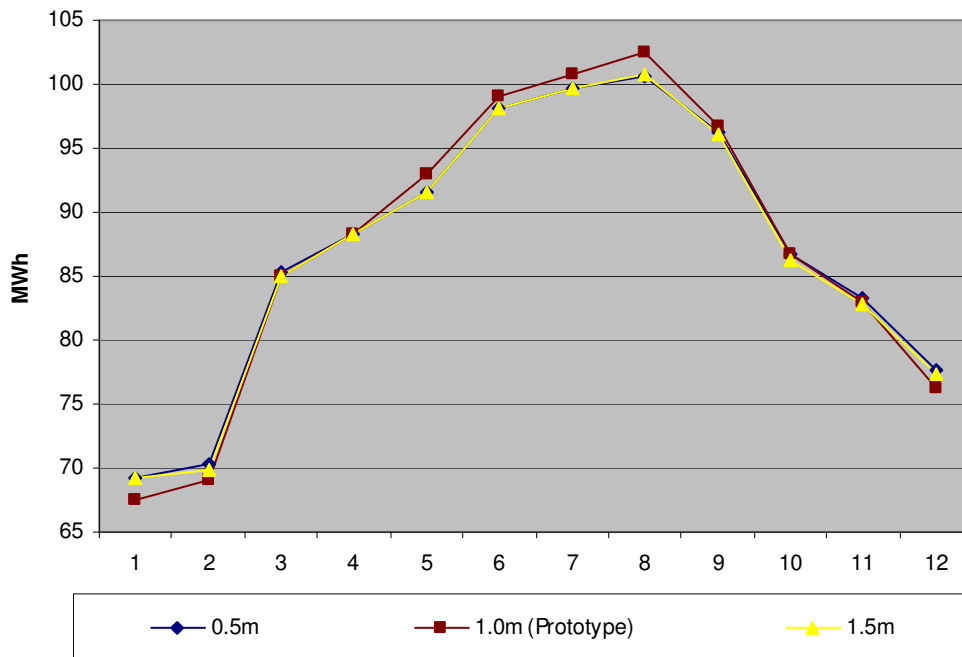


Figure 4.22 Variable 3 Cavity Depth Monthly Energy Consumption

Further on to Figure 4.22, monthly readings also illustrate similar pattern values that are almost identical to the Prototype model. The scale is adjusted to have closer look at these values. It reveals that the Prototype model is just 1 or 2 MWh higher during summer, with the same lower value in 2 months during winter

The detailed mass air flow (kg/s) readings in show the results of the Macroflo simulation based on the 2 variations of depth. The air flow in the depth variation for this simulation run exhibited similar trends with respect to the Prototype model. In June 21 (Appendix G), there is also an observable factor of increment due to the depth dimension variation of 0.5, 1.0 (Prototype) and 1.5m when the peak readings hit 12, 24 (Prototype) and 35 kg/s respectively.

In (Appendix G), December graphs slopes are also similar to the Prototype Case model however values are substantially increased with

every increase in cavity depth. In the three scenarios, mass air out flow increases with cavity depth. It is also noticeable that the net zero air mass flow, or where the mass flow lines intersect is at a similar time in all three scenarios.

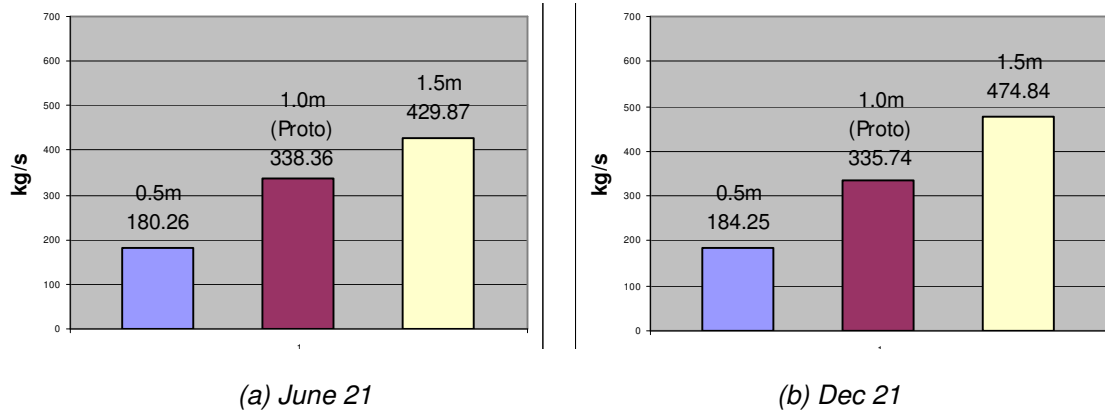


Figure 4.23 Variable 3 Depth Net Mass Air Flow

The net effective air mass out flow shown in Figure 4.23 also illustrates its progressive improvement in both design days as cavity depth increases. It is observed that for June 21 design day in Figure 4.23a, the difference between 0.5 and 1.0m depth is 180 while the difference between 1.0 and 1.5m depth is 90. In this case, subsequent 0.5 meter increase in cavity depth, increases mass air flow by half of the previous increment.

On the other hand, Figure 4.23b shows that in December 21 design day, the difference between 0.5 and 1.0m depth is 150 while the difference between 1.0 and 1.5m depth is 139. The Prototype net mass air flow is almost a median difference between the other two variables.

A wider cavity therefore is better for increased mass air flow, and thus, a high evaporative cooling potential for the water spray application. Essentially, it is a matter of design allowance to take into consideration permitted space for cavity depth. Keeping in mind also that one of the limitations on a narrower depth is the hindrance for maintenance access.

#### Variable 4: Height from Building Top

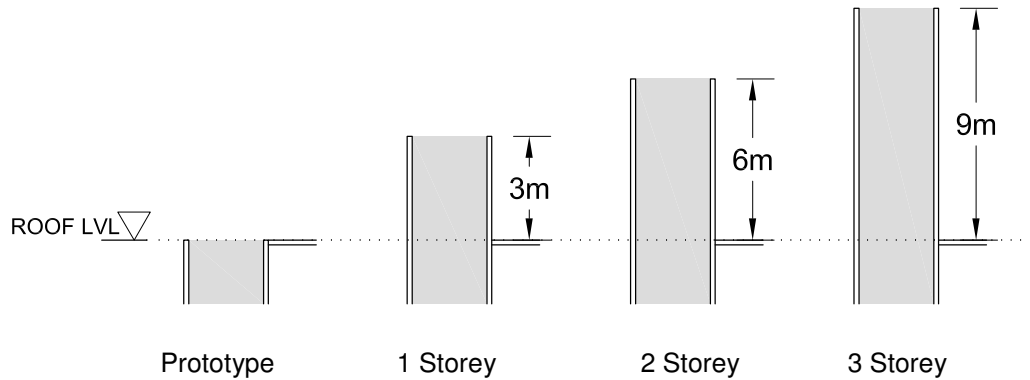


Figure 4.24: Variable4 Height from Top

The double skin façade is tested for the incorporation of a solar chimney in various height dimensions. The Prototype Model double skin top is extended in order to study its effect on energy consumption and air flow movement. The tested variables are 1 Storey (3m), 2 Storey (6m) and 3 Storey (9m) relative to the building top.

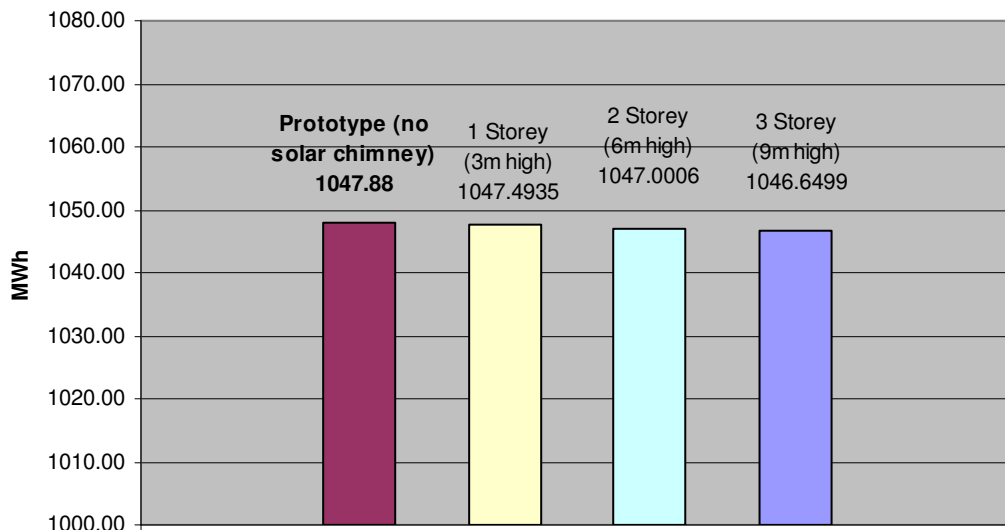


Figure 4.25: Variable4 Height from Top, Annual Energy Consumption Total

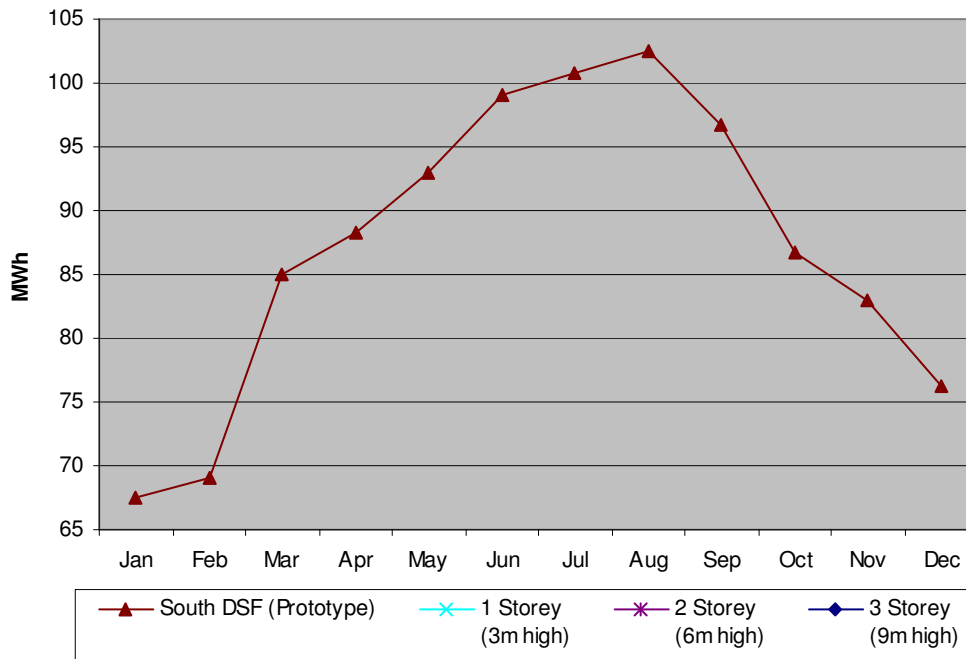


Figure 4.26: Variable4 Height from Top, Monthly Energy Consumption Total

Like most of the simulation variables, the annual energy consumption in Figure 4.25 is negligible showing figures that are close to the Prototype model without a solar chimney. The monthly energy consumption in Figure 4.26 also reveal close to identical values in monthly readings.

The detailed mass air flow (kg/s) readings are shown in Appendix G illustrating the results of the Macroflo simulation based on the 3 additional variations of height. The air flow in the height variation for this simulation run exhibited similar trends with respect to the Prototype model. In June 21 (Appendix XX), there is also an observable regular increment relative to the Prototype and due to the height variation of 3, 6, and 9m.

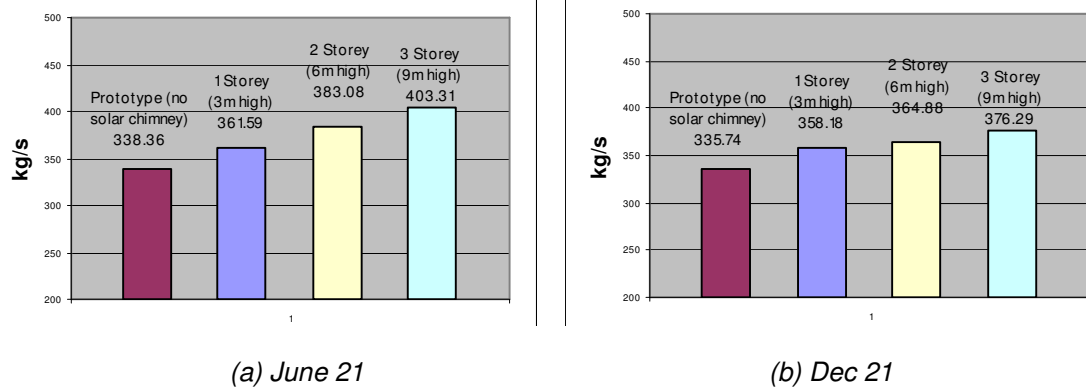


Figure 4.23 Variable 4 Height from Top Net Mass Air Flow

Figures 4.23 show that increasing the Solar Chimney height improved the mass air flow in the two design days. Although graphical behavior is still very similar to the Prototype trend, slopes and break points in net zero air flow, the high and low values differ per tested variable.

Since the double skin façade is situated in the south having little solar exposure during summer, increasing the height improves solar exposure and thus, more air movement in even in summer conditions. In Figure 4.23a, with the calculated net mass air flow for Jun 21, It is noticeable that between Prototype, 1, 2, and 3 Storey height, the differences are at close regular increments of 23, 22, and 21 kg/s respectively. Figure 4.23b also shows that in winter, however, there is some improvement in the net air mass flow. In terms of the net mass air flow, the difference of the increments between the tested variables are at an average of 13 kg/s.

In general, there is no direct energy consumption increase and savings with in the addition of double skin solar chimney height. In both summer and winter design days, an increase in solar chimney height increases mass air flow. These findings are consistent with Ding et al (2004) which mentioned that increasing the height generally increases air movement.



## **Chapter 5: Results and Discussion**

**5.1. Calculation Results: Water Spray Effect**

**5.2. Energy Reduction Synopsis**

## 5.0 Results and Discussion

After the exploration of configurations, the Prototype model is utilized as the basis of model for energy calculations. In the previous findings, it is shown that the Prototype configuration has the highest savings in exploration of orientation. The South Prototype façade on the other hand, has the least air flow movement in both design days. This would represent the minimum energy reduction due water spray application that in reality would account for efficiency setbacks.

A one meter depth on the other hand is a median cavity dimension. It is also illustrated that increase in depth is progressive with increased mass air flow however, thresholds and limitations for depth of a sample study is established out of practicality. The same consideration is also observed where an increased height improves annual energy reduction and higher mass air flow. Utilizing the Prototype double skin façade where there is no solar chimney establishes the minimum air flow movement in this typical configuration. Also keeping in mind that the increase in either width and height improving mass air flow, partly depends on which design configuration the project could afford.

Simultaneously, it is also informative to determine the maximum potential savings contributed by the cooling effect of the water spray as influenced by high mass air flow. In the simulation of configurations, it was determined that the highest yielding mass air flow from the tested set of variables is from the south double skin façade with the depth of 1.5 m. For comparative purposes, this is utilized to see further potential savings.

The energy reduction through evaporative cooling is derived by calculation method. It was earlier explained in the Methodology that the equations are fulfilled with figures from the simulation model and the Psychrometric Chart. The simulated model determines the cavity temperature, relative humidity and mass air flow while the rest are determined using the Psychrometric chart. The two basic equations can be revisited in the previous Chapter 3.3 Research Methodology.

Essentially, a higher  $\Delta E$  is ideal since this is the potential energy reduction that can be subtracted from actual energy consumption and therefore savings are quantified. This also corresponds to an amount of water consumed where the relationship of energy savings and water consumption can be weighed and analyzed. It is also important to note that although some entries of mass air out flow from the simulations are negative, the net absolute value is used since it still has the same potential regardless of air flow direction.

A spreadsheet of the computed tables can be found in Appendix I. The results are summarized and illustrated in graphical form to be seen in the following sections. It shows energy absorbed and water consumed between two Final conditions, where Relative Humidity = 90%, and where Relative Humidity is = 100%.

## 5.1 Calculation Results: Water Spray Effect on Prototype Model

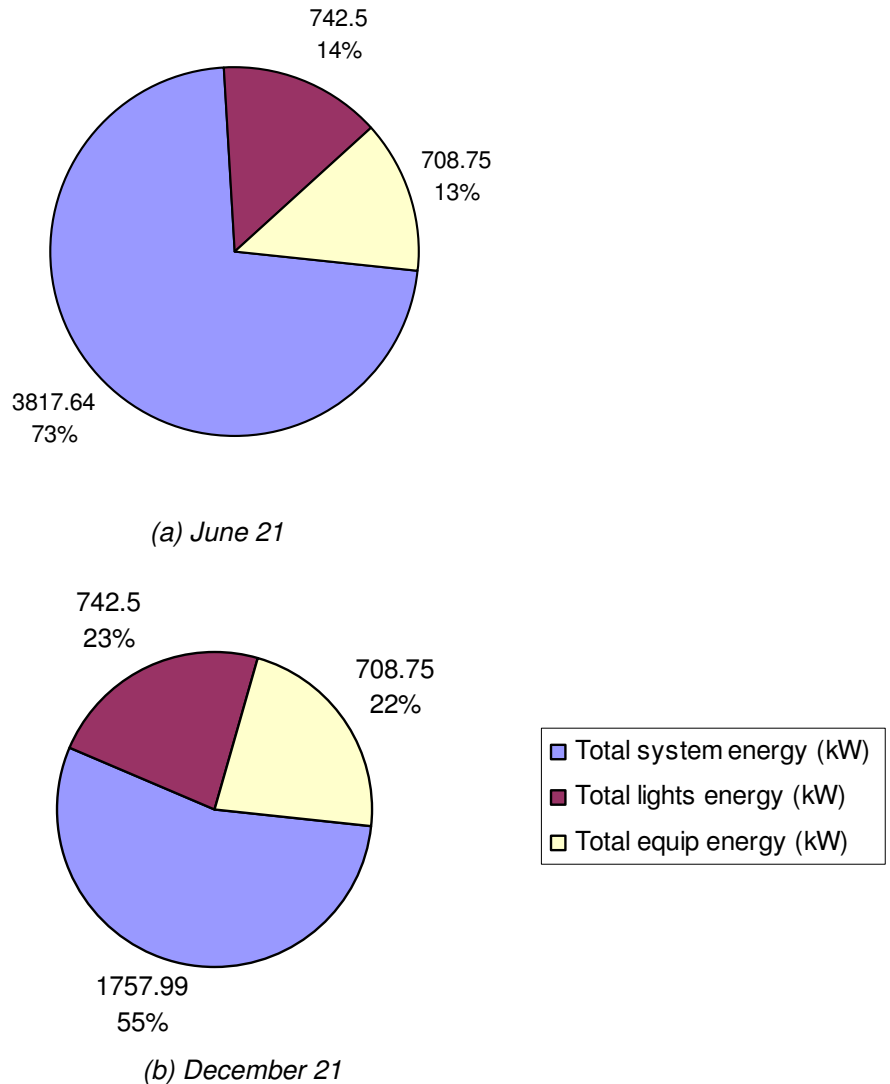
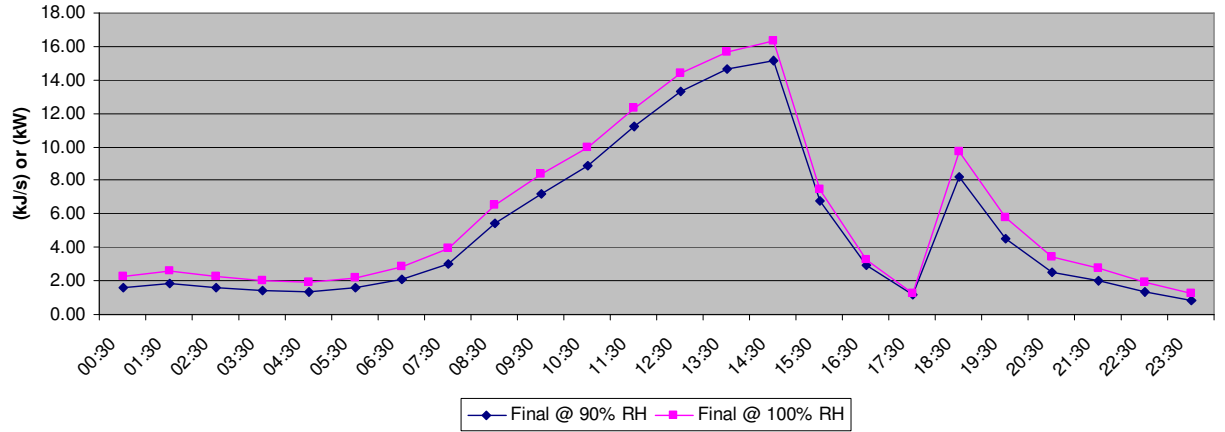


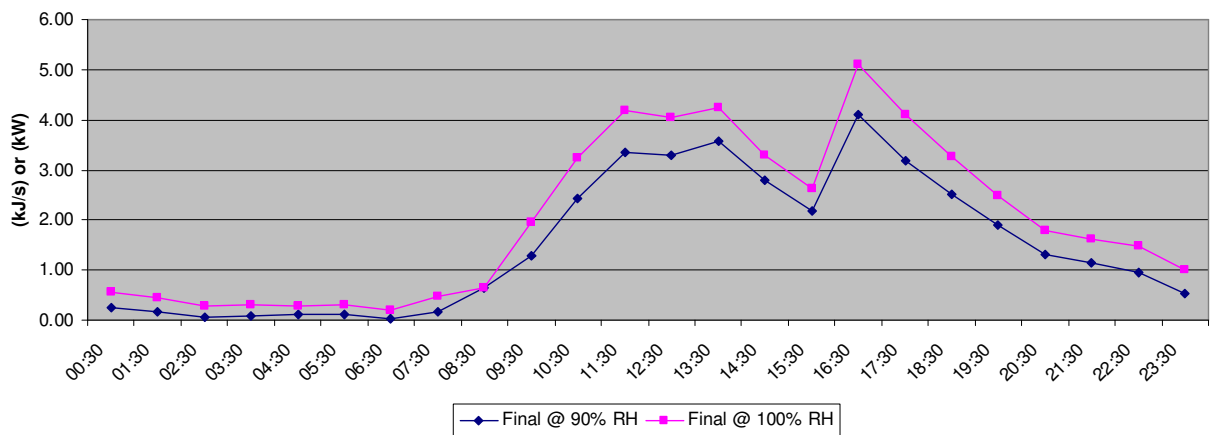
Figure 5.1 Energy Consumption Breakdown (kW)

Figures 5.1 (a & b) illustrate the energy breakdown between the two design days of the Prototype model. In both scenarios, lighting and equipment energy consumption are identical since operational patterns are common. The systems energy performance which includes HVAC system, chillers, fans and pumps is dependent on the climatic conditions and its users demands. The total systems energy therefore will serve as the basis of energy reductions

## Prototype Façade Absorbed Energy



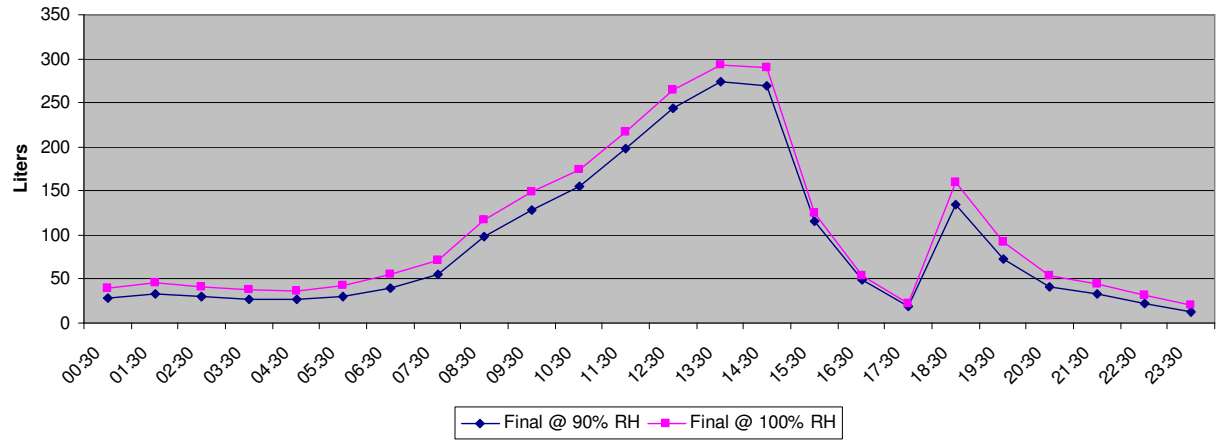
(a) June 21



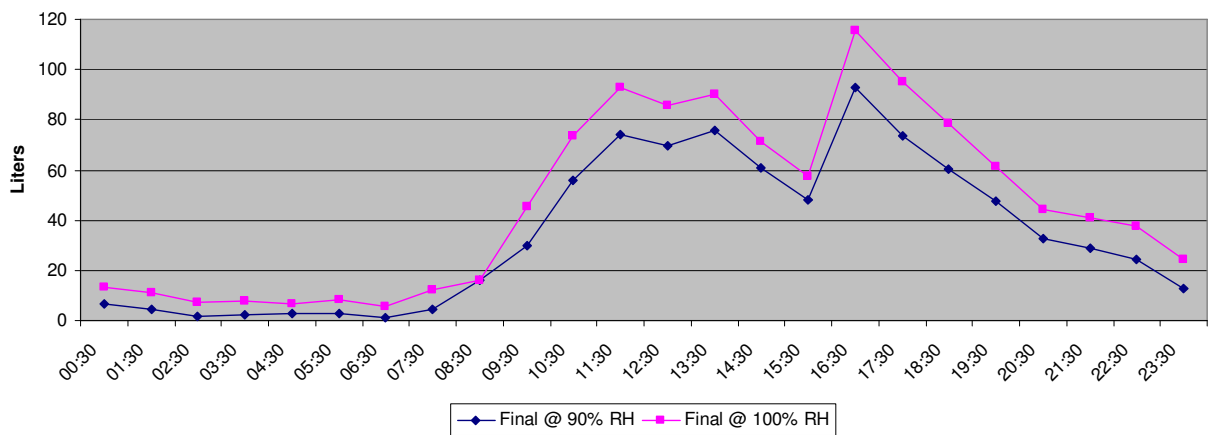
(b) December 21

Figure 5.2 Energy Absorbed through Spray Application - Prototype model (kW)

## Prototype Façade Water Consumed



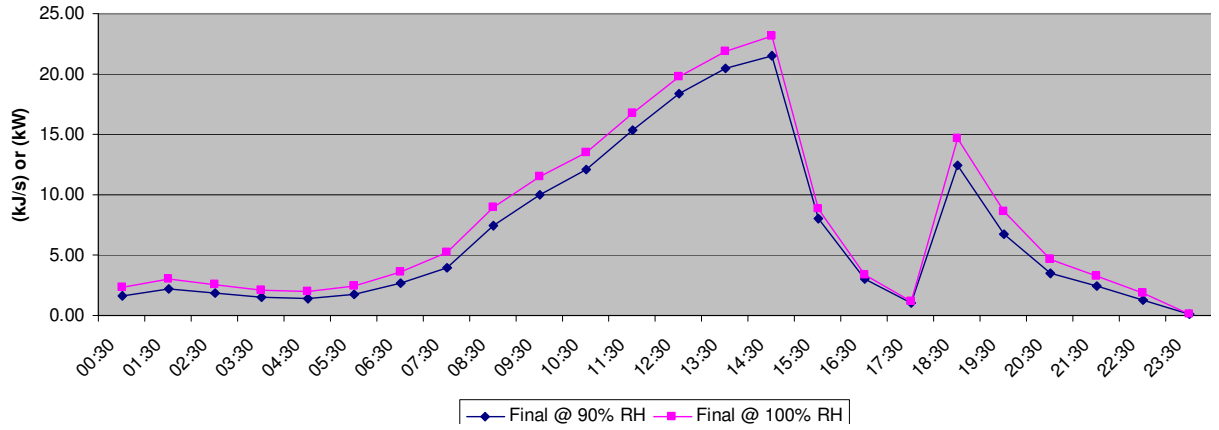
(a) June 21



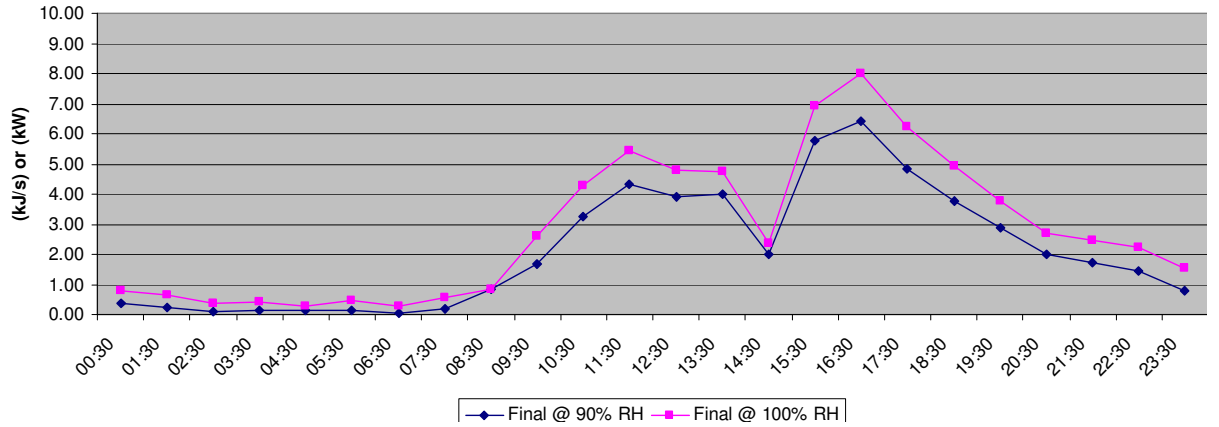
(b) December 21

Figure 5.3 Water Consumed through Spray Application - Prototype model (liters)

1.5m Depth South Façade Absorbed Energy



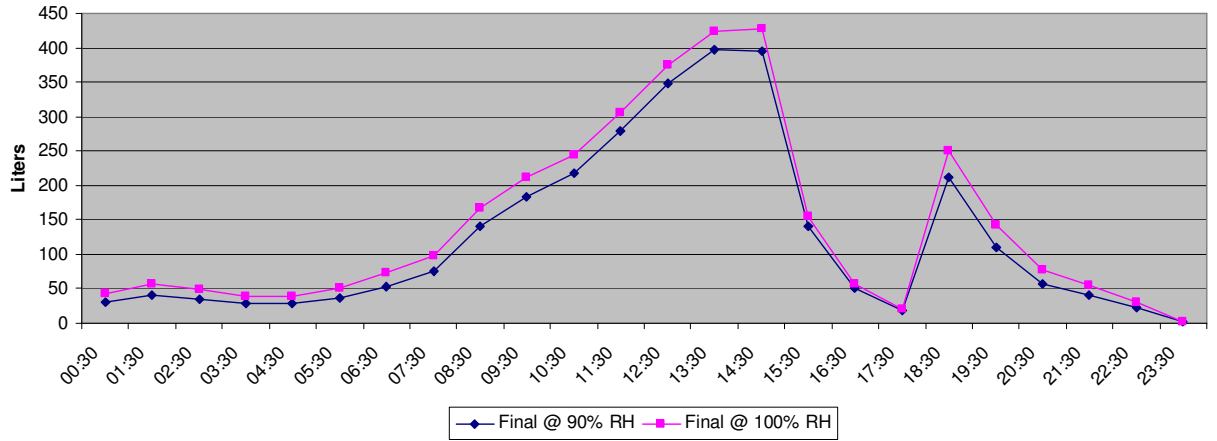
(a) June 21



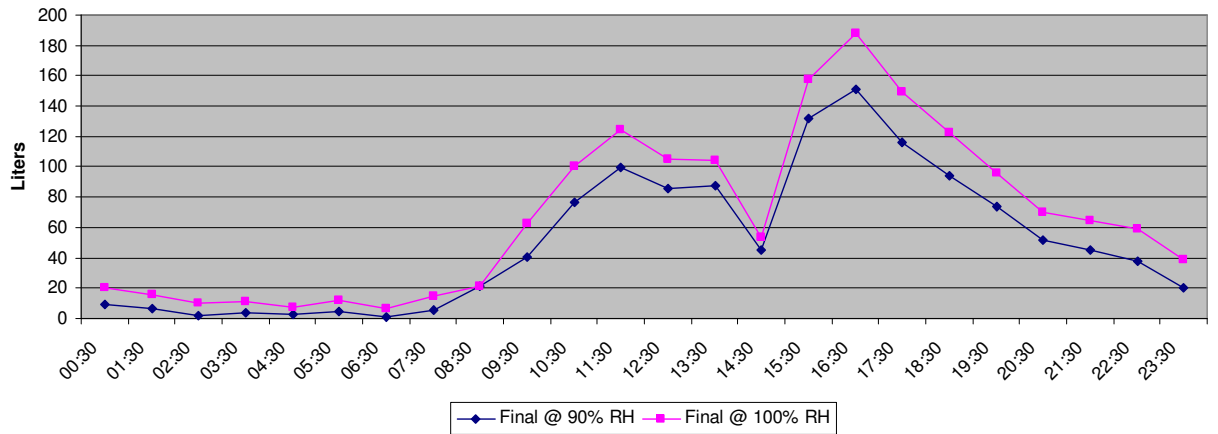
(b) December 21

Figure 5.4 Energy Absorbed through Spray Application – 1.5m Cavity (kW)

1.5m Depth South Façade Water Consumed



(a) June 21



(b) December 21

Figure 5.5 Energy Absorbed through Spray Application – 1.5m Cavity (kW)



The distinctive dip in values seen in the graphs directly corresponds to the low net mass air flow during that period.

In general however, it is observed that this typical Summer design day is the period where evaporative cooling is ideal due to the high temperatures and low relative humidity. Figure 5.2b and 5.4b show that the energy reduction potential for December is lower since humidity cannot be raised further due to relatively low temperatures and higher relative humidity values, near saturation. Detailed numbers are illustrated in Appendix I.

Figures 5.3 and 5.5 show the corresponding water consumption used to achieve the added humidity to reach the Final conditions of RH @ 90%, and RH @ 100%. The graph peaks and troughs are similar to the slopes of the absorbed energy. As expected, water consumption is high during the day. It is also noticeable that the differences of values between the two Final conditions are predominantly apart throughout.

In comparison with the 1.5m Depth Façade seen in Figures 5.4 and 5.5, there is a substantial increase in potential energy savings. However, there is also a high amount of water consumption associated with it.

## 5.2 Energy Reductions Synopsis

The tables in this section highlight the synopsis of the calculation results showing the potential Energy reductions and the amount of water used, against the two Design days and two Final Conditions. It is imperative to note that these reduction values are with respect to the Prototype model without a water spray, savings are extensively higher if it is compared against the Base building without a double skin façade. Also, instead of utilizing the whole day readings, only the effective hours are used due to the nature of the office operational profile.

*Table 5.1 Energy Reduction – Prototype*

Energy Reductions Summary: Effective Office Hours (7:00am - 6:00pm)			
June 21 Systems Energy =		3817.64 kW	
Dec 21 Systems Energy =		1757.99 kW	
	Energy Reductions		Water Consumed
	kW	%	liters
RH @ 90%	86.72	2.27%	1549.60
RH @ 100%	95.43	2.50%	1704.40

	Energy Reductions		Water Consumed
	kW	%	liters
RH @ 90%	26.83	1.53%	596.49
RH @ 100%	33.42	1.90%	743.25

Through Table 5.1, it is observable that the amount of water consumed is relatively high which ranges from 1,550 to 1,704 liters in June 21 in order to achieve 2.27% and 2.5% energy reduction respectively. This equates to around 682 liters per percent of savings. In December 21, water consumption lower savings potential is lower starting from 596 to 743 liters in order to have 1.53% and 1.9% energy reduction respectively which uses at an average 390 liters for a percentage in the day energy savings.

Table 5.2 Energy Reduction – 1.5m Cavity Depth

Energy Reductions Summary: Effective Office Hours (7:00am - 6:00pm)

June 21 Systems Energy = 3817.64 kW

Dec 21 Systems Energy = 1757.99 kW

	Energy Reductions		Water Consumed
	kW	%	liters
RH @ 90%	117.20	3.07%	2097.71
RH @ 100%	128.92	3.38%	2306.25

	Energy Reductions		Water Consumed
	kW	%	liters
RH @ 90%	37.08	2.11%	826.74
RH @ 100%	46.25	2.63%	1031.50

In Table 5.2, a 1.5 meter cavity depth shows that the result of energy savings is relatively higher mainly due to the fact that this model has enhanced net mass air flow. Proportionately, the amount of water consumed is also increased. The summary shows that it takes around 683 liters of water to achieve a percentage of savings in the June 21 design day. On the other hand, it takes about 391 liters to improve a percentage of reduction during the December 21 design day.

As the findings above suggest, the rate of savings in the Prototype model is almost the same with the rate of savings in the 1.5 m cavity double skin façade for their corresponding design days. However, the maximum potential savings has a limit threshold where the calculation of the Final condition reaches 100% relative humidity. Therefore, any addition beyond 1,704 liters of water to the Prototype double skin façade during the June 21 design day for example does not contribute to additional cooling since this has already reached saturation. This cannot further contribute to the latent heat of evaporation as energy reduction potential.

Table 5.3 Energy Reduction – Prototype Residential

Energy Reductions Summary: (Residential whole day)  
 June 21 Systems Energy = 128.45 kW

	Energy Reductions		Water Consumed
	kW	%	liters
RH @ 90%	120.75	94.01%	2136.34
RH @ 100%	140.18	109.13%	2476.72

Dec 21 Systems Energy = 85.63 kW

	Energy Reductions		Water Consumed
	kW	%	liters
RH @ 90%	36.17	42.24%	828.36
RH @ 100%	47.92	55.96%	1102.46

In basic comparison, the Prototype model is simulated using a residential thermal template as shown in Table 5.3. Due to the nature of residential buildings, there are lesser users within the whole day occupational profile. A detailed energy breakdown can be seen in Appendix I. Each design day total however is significantly lower than that of an office building. Due to this, the whole day application of a spray component provides a substantial amount of energy reduction to a residential building. In June 21 it the potential savings could match and exceed actual energy consumptions at a rate of 23 liters per percentage reduction. In December, energy savings could go high around 50% in both Relative humidity conditions where it costs 20 liters per percentage reduction. If the energy savings potential are this high, then there is more allowance for reduce amount of water applied. It is also noted that the reduction is relative to the room thermal template applied in the simulation, different buildings types and actual occupancy patterns would produce alternative results.

The findings above will serve as indications for systems set point programs in the usage of an evaporative spray that can modify flow rates depending on cavity air flow conditions. It is important to note however that the energy consumed by operating the spray is not accounted for in this calculation. The basis of which is dependent on the actual model selection of the spray mechanism that is installed.

Due to the high volume of water needs determined from these calculations, other sources of water should be utilized. Grey water or recycled water can be substituted which also helps reduce sewage movement by releasing it as moisture into the atmosphere. A consideration for larger grey water holding tanks should be installed to accommodate for this use. It is also advantageous for this cavity configuration since the humidified air is not introduced into the occupied spaces. On the downside, it is not always pleasant in air flow downdraft occasions when grey water vapor is mixed with the external pedestrian breathing air. In relation to breathing air, extreme negative effect could be the propagation of bacteria causing illnesses such as legionnaire's disease. This may however be mitigated by proper storage that is common practice in grey water handling. The use of salt water may be considered but spray nozzles should be regularly checked for salt deposits that may accumulate and cause blockage and clogging.

Overall, the potential for energy reduction through the incorporation of water spray in the double skin cavity is promising. However, the usage of water and more practical alternative sources as mentioned above should be taken into consideration in order to improve energy reduction, without burdening high water consumption.

## **Chapter 6: Conclusions and Recommendations**

### **6.1 Conclusions**

### **6.2 Recommendations**

## **6.0 Conclusions and Recommendations**

In this research, double skin facades are studied in literature to understand its dynamics from its original context. Some international examples and local precedents are also reviewed and critiqued. The findings of this literature led to the proposal of incorporating a water spray to induce evaporative cooling within the cavity. The method for measuring the said proposal is done through simulations and calculation. Results are then drawn based on these findings.

### **6.1 Conclusions**

Energy reduction through the use of a double skin façade is considerable resulting to a 4% savings on a south façade Prototype model. It is discovered however that during the course of alternative strategy through the use of overhangs, a one meter overhang on the south side produced only 3% reduction while a 2 meter overhang on the same side can result to 4.74% savings. Also, an increase in overhang projection performs better in energy reduction than an increase in cavity depth without a spray component.

The air flow simulations are studied to input in the established equations and to understand the air movement from different scenarios. The results vary and produced dynamic patterns against the given variables. Similar to prior literature, It is seen that mass air flow is favorable with lower outside temperatures which means that there is less opportunity to enhance air flow when it is most needed, during summer.

The four tested orientations however showed nominal mass air flow differences during the June design day. In Dec 21, the East showed highest values in net mass air flow. The South façade however performed poorly even in Dec when it has all day solar exposure. It was earlier explained and illustrated that the dominant North wind during the December design day inhibits mass air out flow.

Increase in depth produce substantial net air flow movement at close to regular increments in both design days. The increase in solar chimney height however showed marginal increase in net mass air flow.

An updraft within the cavity is a common knowledge assumption of proper air movement due to stack effect. However external wind can facilitate and reverse air flow. A down draft due to pressure differences induced by wind can be beneficial to evaporative cooling potential as per the established equations. In these simulation scenarios, wind inhibited and reduced net mass air flow.

In terms of direct energy reduction, the change in orientation, depth, and height of a double skin façade does not contribute to increase nor reduction in energy consumption. Prior the application of a water spray, an increased air mass flow does not correspond to higher reduction in energy consumption. These can be due to the premise that although there's a high removal of accumulated air, it is still displaced by the ambient outside temperature since cavity temperature are shown to have close values with the external temperature, .



The application of a water spray in the double skin facade helped further reduce energy consumption on the established design days through the use of results from simulation and calculations. It is however accompanied by the cost of a substantial amount of water. It takes more water to achieve energy reduction in the July design day than it is in Dec. In a different approach, due to the change of the spatial function from an office to a residential, the Prototype reference is lowered and proportionately increasing savings and minimizing water consumed to achieve the same rate of reduction.

## **6.2 Recommendations**

In general, the findings of this research explored the behavior and performance of different double skin façade configurations and its effects on energy consumption. A basic procedure for quantifying an evaporative cooling effect for the cavity is used to measure the amount of water versus the energy savings it can yield. With discovered results, other opportunities are proposed for future study.

In literature review, it was earlier suggested that the proposed spray component of the double skin façade can aide in fire suppression. At the same time, the incorporation of a new type of glazing referred to as self cleaning glass is complemented by the spray application. These promising advantages can be further explored.

An extended interrelationship of different established variable can also be investigated, for example, the East façade that showed promising air flow during summer can be used as a Prototype model for exploration.

Detailed operational spray mechanisms is also an opportunity for testing where efficiency rates can be measured and quantified.

Most air flow studies for double skin facades focus on increasing stack effect due to thermal buoyancy, an attitude towards harnessing external wind similar to a vernacular wind tower should also be considered. There are strong correlations of external winds and air movement between North East and West façade. These orientations are strategic in funnelling air into the cavity and thus enhancing air flow.

It is seen to be more worthwhile to use a double skin façade water spray in a summer day while a typical winter day could be accompanied by other methods like day direct ventilation, mixed mode systems should be considered. At the same time, the effect of material alterations on mass air flow can be further examined.

Specific spray features tests can be extended with guidance from performance of cooling towers. This can also further focus on spray efficiencies, droplet radius, mechanisms and specific locations.

After construction and during occupancy of the local examples highlighted in the literature review, the actual performance of the built double skin façade in this country should be studied by conducting with post occupancy evaluations and performance testing.

With all the mentioned recommendations for research, this dissertation suggests the evolution a typical double skin façade into a hybrid wind and

evaporative cooling tower. With all the variations and complexities associated with the proposed double skin design, its characteristics warrants further opportunities for study.

## References

ADNOC, (2008). H.H. President reviews progress of new ADNOC Corporate Headquarters [online]. Available from [http://www.adnoc.ae/AdnocNews\\_Details.aspx?NewsID=2831faf0-b969-43b0-acb6-78efd9a981cc&newid=162&mid=162](http://www.adnoc.ae/AdnocNews_Details.aspx?NewsID=2831faf0-b969-43b0-acb6-78efd9a981cc&newid=162&mid=162) [Accessed 20 November 2008].

Arons, D.M., (2000). Properties and applications of double-skin building facades. M.Sc Thesis: Massachusetts Institute of Technology, Department of Architecture. Available from: <http://dspace.mit.edu/handle/1721.1/8724> . [Accessed 15 January 2009]

Arons, D.M., & Glicksman, L.R., (2001). Double Skin, Airflow Facades: Will the Popular European Model work in the USA? *Proceedings of ICBEST 2001, International Conference on Building Envelope Systems and Technologies*, Ottawa, Canada, Vol 1: pp. 203-207. Available from: <http://www.tjuu.com/ebook/doubleskin.pdf>. [Accessed 10 November 2009]

Arup. GSW Headquarters. [online]. Available from: <http://www.arup.com/germany/project.cfm?pageid=3592> [Accessed 5 March 2009].

BBRI, (2004). Ventilated double façades: Classification and illustration of façade concepts. Belgian Building Research Institute, Department of Building Physics, Indoor Climate and Building Services, Brussels, Belgium. [online] Available from <http://www.bbri.be/activefacades/new/download/Ventilated%20Doubles%20Facades%20-%20Classification%20&%20illustrations.dvf2%20-%20final.pdf>. [Accessed 2 December 2008]

Belarbi, R., Ghiaus, C and Allard, F., (2006). Modeling of water spray evaporation: Application to passive cooling of buildings. [online] Available from: [www.sciencedirect.com](http://www.sciencedirect.com) [Accessed 25 May 2008].

Cengel, Y.A., and Boles, M.A., (2008), *Thermodynamics, an Engineering Approach*, 6<sup>th</sup> Edition. McGraw Hill, Washington.

Chow, W.K., Hung, (2005). Effect of cavity depth on smoke spreading of double-skin façade. [online] Available from: [www.sciencedirect.com](http://www.sciencedirect.com) [Accessed 08 June 2008].

Chow, W.K., Hung, W. Y., Gao, Y., Zou, G. and Dong H., (2005b). Experimental study on smoke movement leading to glass damages in double-skinned façade. [online] Available from: [www.sciencedirect.com](http://www.sciencedirect.com) [Accessed 08 June 2008].

Crespo, A.M.L., (1999). History of the Double Skin Façade. [online] Available from: <http://www.civil.uwaterloo.ca/beg/ArchTech/History%20of%20Double%20Skin.pdf>. [Accessed 30 April 2009].

CYTSoft, CYTSoft Psychrometric Chart 2.2 [online] Available from: <http://www.cytsoft.com/> [Accessed 08 June 2008].

Ding, W., Masemi, Y., Yamada, T., (2004). Natural Ventilation performance of a double-skin façade with a solar chimney. [online] Available from: [www.sciencedirect.com](http://www.sciencedirect.com) [Accessed 13 July 2008].

Emirates.org. The country. [online] Available from: [http://www.emirates.org/the\\_country.html](http://www.emirates.org/the_country.html). [Accessed 30 Aug 2008].

Erell, E., Etzion, Y., Pearlmutter, D., Guetta, R., Pecornick, D., Zimmerman, H. Krutzler, F., (2005) International Conference "Passive and Low Energy Cooling 529 for the Built Environment", Santorini, Greece. A novel multi-stage down-draft evaporative cool tower for space cooling. Part 2: Preliminary experiments with a water spraying system. [online] Available from: [www.sciencedirect.com](http://www.sciencedirect.com) [Accessed 16 June 2008].

Gan, G., (2005). Simulation of buoyancy-induced flow in open cavities for natural ventilation. [online] Available from: [www.sciencedirect.com](http://www.sciencedirect.com) [Accessed 06 February 2008].

Givoni, B., (1976). *Man Climate and Architecture*. 2<sup>nd</sup> ed. London: Applied Science Publishers

Harrison, Kate, (2001). The Tectonics of the Environmental Skin. The Occidental Chemical Center [online] Available from: [http://www.architecture.uwaterloo.ca/faculty\\_projects/terri/ds/hooker.pdf](http://www.architecture.uwaterloo.ca/faculty_projects/terri/ds/hooker.pdf). [Accessed 1 February 2008].

Hamza, N. and Underwood, C., (2007). CFD supported modelling of double skin facades in hot arid climates. [online] Available from: [www.sciencedirect.com](http://www.sciencedirect.com) . [Accessed 02 April 2008].

Hamza, N., (2007). Double versus single skin facades in hot arid areas. [online] Available from: [www.sciencedirect.com](http://www.sciencedirect.com) [Accessed 06 February 2008].

High Performance Commercial Building Façade. Building Case Studies GSW Headquarters. . [online] Available from: [http://gaia.lbl.gov/hpbf/casest\\_f.htm](http://gaia.lbl.gov/hpbf/casest_f.htm). [Accessed 04 May 2009].

Kazim, A., (2005) Assessments of primary energy consumption and its environmental consequences in the United Arab Emirates. [online] Available from: [www.sciencedirect.com](http://www.sciencedirect.com) [Accessed 6 May 2008].

Konya, A., (1980). Design Primer for Hot Climates. London: The Architectural Press Ltd.

Manz, H., (2002). Numerical simulation of heat transfer by natural convection in cavities of facade elements. [online] Available from: [www.sciencedirect.com](http://www.sciencedirect.com) [Accessed 13 July 2008].

Masdar, [online] Available <http://www.masdar.ae/>



Middle East Electricity., (2008). New and Renewable Energy Regional News. [online] Available from: [www.middleeastelectricity.com/Renewable/NewandRenewableEnergyRegionalNews.html](http://www.middleeastelectricity.com/Renewable/NewandRenewableEnergyRegionalNews.html). [Accessed 12 July 2008].

Nippon Sheet Glass Co, (1999). RWE Tower-- a New Phase of Ecological and High-tech *Space modulator No. 86*. [online] Available from: [http://space-modulator.jp/sm81~90/sm86\\_contents/sm86\\_e\\_index.html](http://space-modulator.jp/sm81~90/sm86_contents/sm86_e_index.html). [Accessed 1 April 2009].

Pasquay, T., (2004). Natural ventilation in high-rise buildings with double facades, saving or waste of energy, *Energy and Buildings*, Volume 36, Issue 4, April 2004, Pages 381-389, Proceedings of the International Conference on Solar Energy in Buildings CISBAT 2001

Pilkington. [online] Available <http://www.pilkingtonselfcleaningglass.co.uk/>. [Accessed 10 October, 2008].

Poirazis, H., (2004) Double Skin Façades for Office Buildings – Literature Review. [online] Available from: [http://www.ecbcs.org/docs/Annex\\_43\\_Task34-Double\\_Skin\\_Facades\\_A\\_Literature\\_Review.pdf](http://www.ecbcs.org/docs/Annex_43_Task34-Double_Skin_Facades_A_Literature_Review.pdf) [Accessed 12 July 2008].

RMJM, (2007). *7457 Scheme Design Report-Vol 1 Architectural-15 March 2007-KJ1*. Dubai

RMJM, *DWTC Architectural Plans*.

RMJM, (2008). *RMJM Environmental Design Guide*. Cambridge.

Saelens, D and Hens, H., (2001), Experimental Evaluation of Airflow in Naturally Ventilated Active Envelopes. *Journal of Thermal Envelope and Building Science* [online] Available from: [www.sciencedirect.com](http://www.sciencedirect.com) . [Accessed 1 April 2009].

Saelens, D., (2002). Energy Performance Assessments of Single Storey Multiple-Skin Facades. [online] Available from:: [http://www.kuleuven.ac.be/bwf/common/data/PhD\\_2002\\_Saelens.pdf](http://www.kuleuven.ac.be/bwf/common/data/PhD_2002_Saelens.pdf) [Accessed 1 April 2009].

Soberg, T., (2008) Double Duty: A two-skinned façade combats intense heat. Goettsch Partners [online] Available from: [http://www.gpchicago.com/users/news\\_view.asp?FolderID=1849&NewsID=73](http://www.gpchicago.com/users/news_view.asp?FolderID=1849&NewsID=73). [Accessed 20 November 2008].

Stec, W.J., Van Paassen, A.H.C and Maziarz, A., (2004). Modelling the double skin façade with plants. [online] Available from: [www.sciencedirect.com](http://www.sciencedirect.com) [Accessed 08 June 2008].

Stec, W.J., and van Paassen. A.H.C., (2004). Symbiosis of the double skin façade with the HVAC system. [online] Available from: [www.sciencedirect.com](http://www.sciencedirect.com) [Accessed 08 June 2008].

Streicher et al, (2007) On the Typology, Costs, Energy Performance, Environmental Quality and Operational Characteristics of Double Skin Façades in European Buildings. *Advances in Building Energy Research 1*, pp.1-28. Earthscan: London. [online] Available from: <http://www.earthscan.co.uk/Portals/0/Files/Sample%20Chapters/9781844073894.pdf> [Accessed 4 April, 2009].

Sureshkumar, R., Kale, S.R., Dhar, P.L. et al, (2007a). Heat and mass transfer processes between a water spray and ambient air – I. Experimental data. [online] Available from: [www.sciencedirect.com](http://www.sciencedirect.com) [Accessed 25 May 2008].

Sureshkumar, R., Kale, S.R., Dhar, P.L. et al, (2007b). Heat and mass transfer processes between a water spray and ambient air – II. Simulations . [online] Available from: [www.sciencedirect.com](http://www.sciencedirect.com) [Accessed 25 May 2008].

Tsou, J.Y., (2001). Strategy on applying computational fluid dynamic for building performance evaluation. [online] Available from: [www.sciencedirect.com](http://www.sciencedirect.com) [Accessed 23 September 2008].

USGBC (2007), *LEED NC Version 2.2*, 3<sup>rd</sup> ed. Washington.

UAE Interact, (2003). Fujairah to harness wind power. [online] Available [http://www.uaeinteract.com/docs/Fujairah to harness wind power/9919.htm](http://www.uaeinteract.com/docs/Fujairah_to_harness_wind_power/9919.htm) [Accessed 10 October, 2008].

Wu, J.M., Huang, X and Zhang, H., (2006). Numerical investigation on the heat and mass transfer in a direct evaporative cooler. [online] Available from: [www.sciencedirect.com](http://www.sciencedirect.com) [Accessed 25 May 2008].

## **Appendix A**

Administrative Resolution No. (66) of 2003 Approving Regulations on the Technical Specifications for Thermal Insulation Systems and Control of Energy consumption for Air-conditioned Buildings in the Emirate of Dubai

## Appendix A: Resolution No. (66)

Administrative Resolution No. (66) of 2003 Approving Regulations on the Technical Specifications for Thermal Insulation Systems and Control of Energy consumption for Air-conditioned Buildings in the Emirate of Dubai

### Chapter One Elements of Design

#### Section One Building Design and Materials Selection

##### Article (7)

a. External Walls and Roof

Roof:  $U = 0.44 \text{ W/m}^2\cdot\text{K}$  (0.078 Btu/h.ft<sup>2</sup>. F)

Wall:  $U = 0.57 \text{ W/m}^2\cdot\text{K}$  (0.100 Btu/h.ft<sup>2</sup>. F)

b. Glass Openings

2. Glass area without a back insulated wall exceeds 40% of the external wall area

$U = 2.1 \text{ W/m}^2\cdot\text{K}$  (0.37 Btu/h.ft<sup>2</sup>. F)

Shading Coefficient (SC) 0.35

#### Section Two Calculation of Heat Load

Article (8) Head Load for buildings calculated on the following factors:

a. Outdoor condition of the building:

Dry Bulb Temp DB: 46°C (115°F)

Wet Bulb Temp WB: 29°C (85°F)

Dubai City location Latitude (North Latitude) 25°N

Outdoor Variation of day temp 13.8°C (25°F)

- b. Indoor Condition of the Building  
2. Commercial Buildings:

Dry bulb temperature                      DB: 25°C (77°F)

Relative Humidity                          RH: 55 ±5%

- d. Ventilation as per ASHRAE Standard 62 – Recommended Values

- f. Safety Factor
  - Sensible heat                      Max 10%
  - Latent heat                        Max 5%

## **Appendix B**

### IES VE 5.9 Modules

This section enumerates and describe the features of the IES VE 5.9 Simulation software.



## Appendix B: IES Modules

IES Modules: <http://www.iesve.com/Our-Software>

**VE-Ware** is a free building energy usage and carbon dioxide emission assessment software. It is suitable for all building types across worldwide locations, and can be set to either Imperial or Metric units.

### VE-Toolkits

Our **VE-Toolkits** are ideal for use at the very early stages of the design process as they give quick sustainability feedback at the click of a few buttons.

**Sustainability Toolkit** – Version 2 available (Energy, Carbon and 2030 Challenge Assessment, ASHRAE/CIBSE Loads Calculations, Daylight Assessments, Solar Shading Animations)

**LEED Toolkit** – Version 2 available (LEED NC 2.2 Daylighting Credit 8.1 consideration)

**BREEAM Toolkit** – Version 1 available 2009

**Greenstar Toolkit** – Version 1 available 2009

### VE Architectural Suites

All the tools are integrated around a central 3D model that can connect directly with Google SketchUp™, Autodesk® Revit® and via gbXML with other 3D design tools.

### VE Modelbuilder

**ModellT::** enables creation of a 3D <Virtual Environment> model without CAD data, or alternatively allows to create a 3D model from 2D CAD data.

## VE Energy



[< VE Compliance > ::](#) provides conservation of energy compliance solutions for all regions of the UK.



[ApacheCalc ::](#) provides heat loss and heat gain calculations based on the CIBSE Guide



[ApacheLoads ::](#) calculates design heating and cooling loads based on the ASHRAE Heat Balance Methods



[ApacheSim ::](#) is an advanced, dynamic thermal simulation application which can also perform carbon emissions calculations



[ApacheHVAC ::](#) simulates HVAC plant and control systems



[MacroFlo ::](#) enables to simulate natural ventilation and mixed mode systems

## VE Lighting and Daylighting



[RadianceIES](#) :: is a detailed 3D simulation tool designed to predict daylight and electric light levels, and the appearance of a space prior to construction.



[FlucsPro](#) :: calculates the number of luminaires required in a room and analyses light levels for defined lighting schemes.



[FlucsDL](#) :: performs lighting design calculations to determine the day-lighting levels in a room. It allows to perform point-by- point lighting analyses to give light level values within a room.



[LightPro](#) :: allows you to place luminaires anywhere in a room for subsequent analysis using FlucsPro, or a detailed simulation using RadianceIES.

## VE Solar



[SunCast](#) :: generates visual, graphical and numerical information that can be used to explain to colleagues, clients and planning authorities how the sun impacts on and inside the building, and on the site.

## VE Value & Cost



[Deft](#) :: provides a comprehensive value engineering approach to building design. Enabling usage of a range of building performance indicators to compare different design options at any stage of the design process



[CostPlan](#) :: enables to prepare customised capital cost estimates



[LifeCycle](#) :: enables to take into account the operating costs of a building during its lifetime. The three products are closely linked, offering a unique opportunity to perform structured Value Engineering analyses at any stage of the design process, or as part of facilities management.

### **VE-CFD**

CFD designed specifically for building applications. <VE> building model automatically supplies all the data required. Graphics make the results easy to understand, and enable to communicate effectively.



[MicroFlo](#) :: tailor-made for building design

### **VE-Egress**



[Simulex](#) :: enables to simulate the evacuation of a building and evaluate alternative escape routes.



[Lisi](#) :: enables o design and simulate lift options.

## VE Mechanical



[IndusPro](#) :: provides you with the facilities to draft your ductwork system and then size your ducts within the <Virtual Environment>.



[PiscesPro](#) :: for pipework systems, offering similar benefits to IndusPro.

## **Appendix C**

IES Training Certificate



< Virtual Environment >

**IES <VIRTUAL ENVIRONMENT>  
TRAINING CERTIFICATE**  
*Cost effective, sustainable building design from concept to completion and beyond*

**THIS IS TO CERTIFY THAT.**

Red Ventura

of

RMJM

attended and completed

**Face to Face Training**

in the following <Virtual Environment> software:

IES <VE> Product	Date Attended
ApacheSim	26 <sup>th</sup> May 2008
FlucsDL	26 <sup>th</sup> May 2008

Hans Dharqalkar  
Training Manager



[www.iesve.com](http://www.iesve.com)

## **Appendix D**

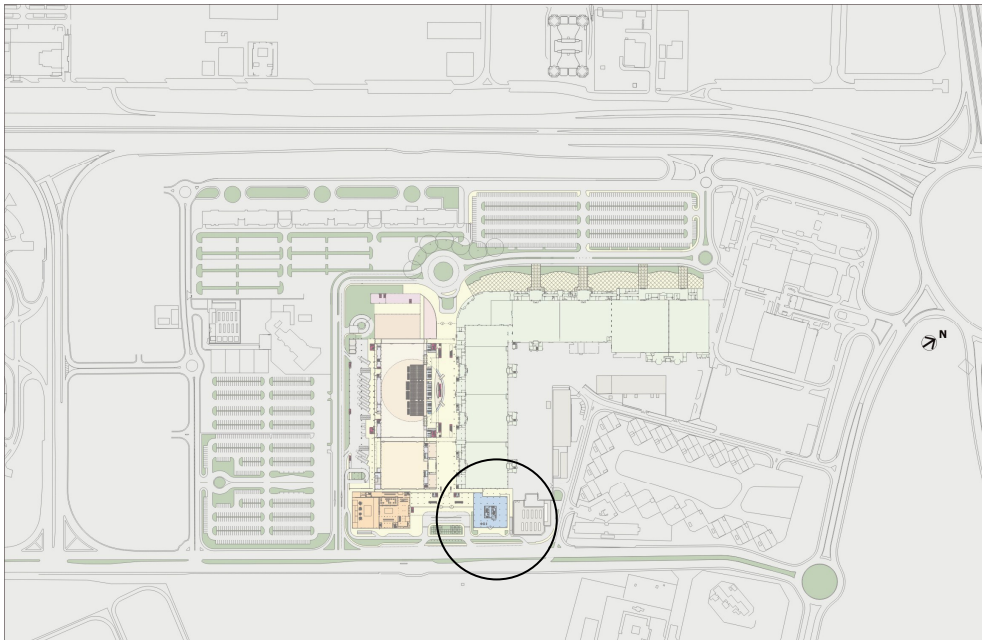
Dubai World Trade Center Office Block

Floor Plans

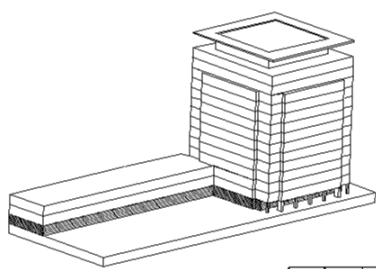
This section illustrates the architectural layout of the model used for Software Validation.



## Appendix D: Dubai World Trade Center Architectural Plans

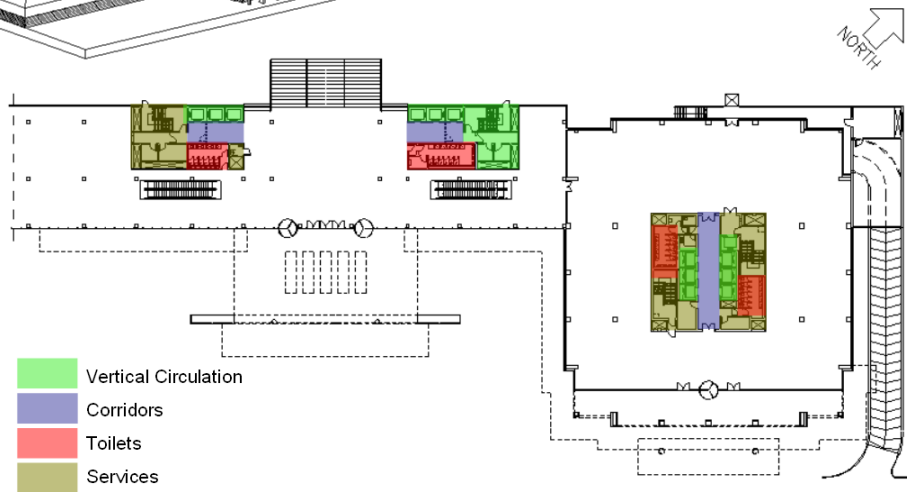


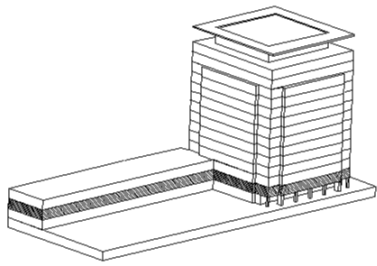
**LOCATION**



**GROUND FLOOR**

Gross Floor Area: 2183

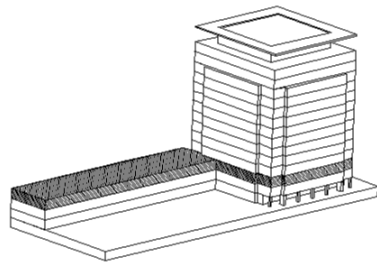
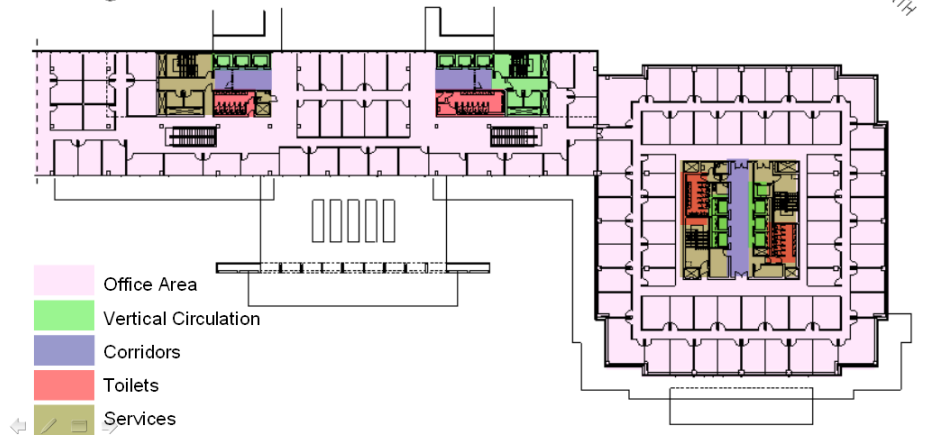




### 1<sup>ST</sup> FLOOR

Gross Floor Area: 2183

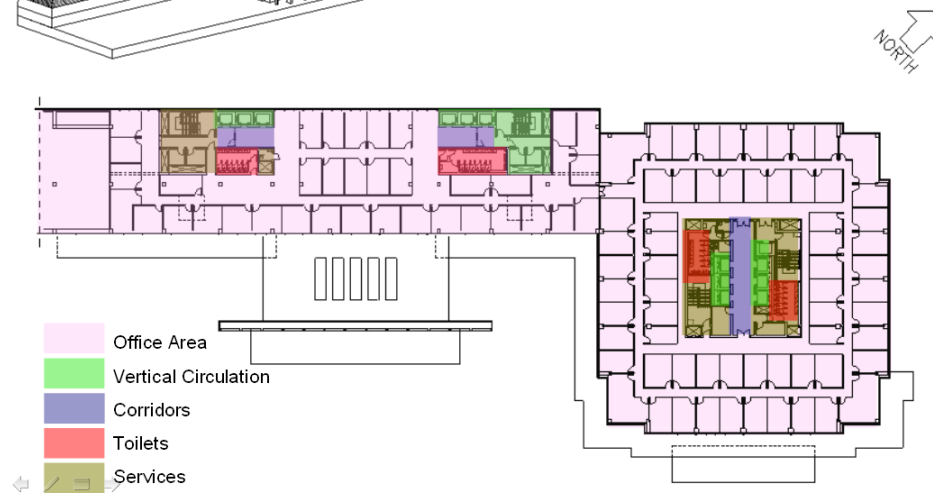
Lettable Area: 1840

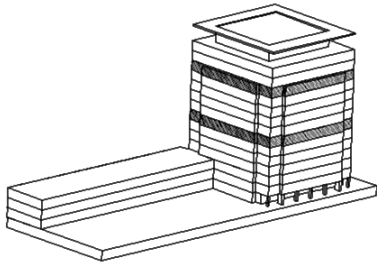


### 2<sup>ND</sup> FLOOR

Gross Floor Area: 2183

Lettable Area: 1840



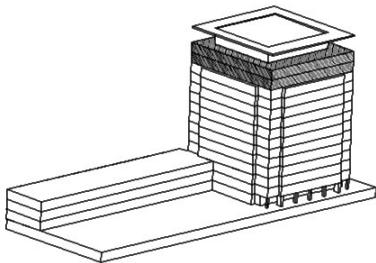
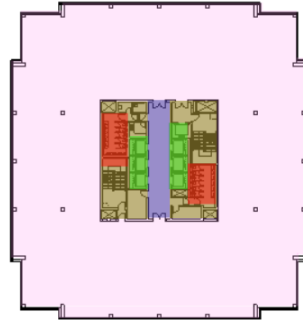


**5<sup>TH</sup>-11<sup>TH</sup> FLOOR (TYPICAL)**

Gross Floor Area: 2183  
Lettable Area: 1840



- Office Area
- Vertical Circulation
- Corridors
- Toilets
- Services

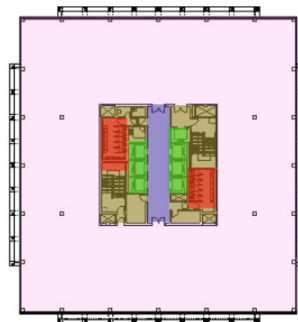


**12<sup>TH</sup>-13<sup>TH</sup> FLOOR**

Gross Floor Area: 1995  
Lettable Area: 1652



- Office Area
- Vertical Circulation
- Corridors
- Toilets
- Services



## **Appendix E**

### Variable 1 – Configuration Reference

This section lists the simulation results for Variable 1 which includes the Prototype model, Base Building (building without double skin), 1 meter overhang and 2 meter overhang building.

These are results derived from IES VE Apache V5.9 simulations and processed in an excel spreadsheet.

## Appendix E: Variable 1 Configuration References

### Variable 1 Configuration References Energy Consumption

<b>Base Building</b>		<b>1m South Overhang</b>	
	Total energy (MWh)		Total energy (MWh)
Date		Date	
Jan	73.6008	Jan 01-31	69.6782
Feb	74.4483	Feb 01-28	69.7632
Mar	88.6176	Mar 01-31	84.2164
Apr	89.9168	Apr 01-30	88.2082
May	93.8862	May 01-31	93.6272
Jun	100.07	Jun 01-30	100.0863
Jul	102.0282	Jul 01-31	101.888
Aug	103.951	Aug 01-31	103.1184
Sep	100.1474	Sep 01-30	96.7075
Oct	91.8539	Oct 01-31	86.9349
Nov	89.6319	Nov 01-30	84.8283
Dec	83.0029	Dec 01-31	79.0104
Summed total	1091.15	Summed total	1058.07
			<b>3.13%</b>

<b>South DSF (Prototype)</b>		<b>2m South Overhang</b>	
	Total energy (MWh)		Total energy (MWh)
Date		Date	
Jan	67.555	Jan 01-31	66.072
Feb	69.1399	Feb 01-28	66.5722
Mar	84.9786	Mar 01-31	83.4511
Apr	88.2289	Apr 01-30	87.9761
May	92.974	May 01-31	93.4702
Jun	99.0258	Jun 01-30	99.9379
Jul	100.8573	Jul 01-31	101.6912
Aug	102.453	Aug 01-31	102.9401
Sep	96.7745	Sep 01-30	96.5415
Oct	86.7179	Oct 01-31	84.9221
Nov	82.902	Nov 01-30	80.5397
Dec	76.27	Dec 01-31	75.286
Summed total	1047.88	Summed total	1039.40
	<b>3.97%</b>		<b>4.74%</b>

## **Appendix F**

### Variable 2 – Orientation

This section lists the simulation results for Variable 2 where the Prototype model is rotated to different orientations of North, South (Prototype), East and West.

These are results derived from IES VE Apache V5.9 simulations and processed in an excel spreadsheet.

## Appendix F: Variable 2 Orientation

### Energy Consumption

#### South DSF (Prototype)

Total energy (MWh)

Date	
Jan	67.555
Feb	69.1399
Mar	84.9786
Apr	88.2289
May	92.974
Jun	99.0258
Jul	100.8573
Aug	102.453
Sep	96.7745
Oct	86.7179
Nov	82.902
Dec	76.27
Summed total	1047.88
	<b>3.97%</b>

#### North DSF

Total energy (MWh)

Date	
Jan	74.9639
Feb	75.2966
Mar	88.232
Apr	89.142
May	91.5359
Jun	98.0113
Jul	99.5849
Aug	101.0071
Sep	98.565
Oct	91.041
Nov	89.4644
Dec	84.1637
Summed total	1081.01
	<b>0.93%</b>

#### East DSF

Total energy (MWh)

Date	
Jan	73.4704
Feb	73.0865
Mar	85.8091
Apr	86.5609
May	89.8228
Jun	95.4058
Jul	97.4549
Aug	98.7523
Sep	95.9175
Oct	88.7362
Nov	87.3613
Dec	82.5943
Summed total	1054.97
	<b>3.32%</b>

#### West DSF

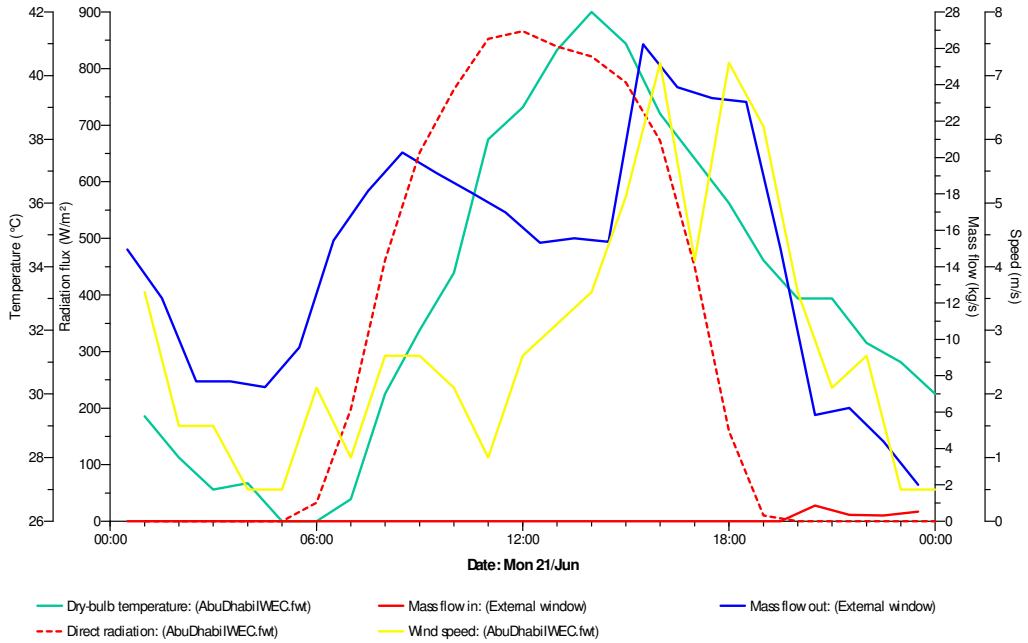
Total energy (MWh)

Date	
Jan	73.174
Feb	73.0502
Mar	85.6156
Apr	87.0204
May	89.6801
Jun	95.6628
Jul	97.3452
Aug	98.9981
Sep	96.045
Oct	88.7962
Nov	87.1426
Dec	82.377
Summed total	1054.91
	<b>3.32%</b>

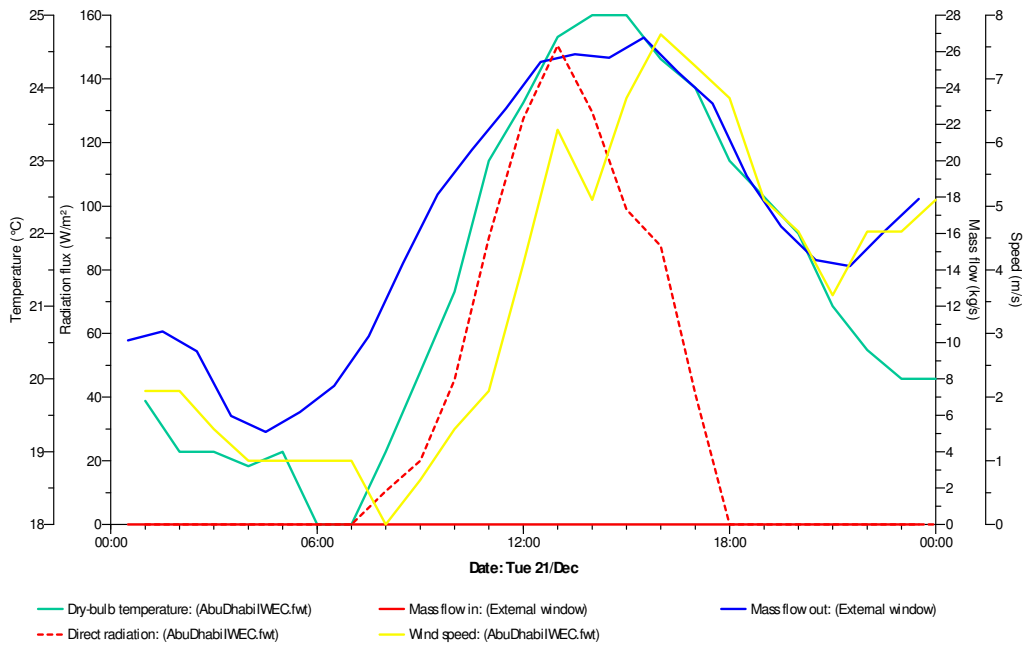
## Appendix F: Variable 2 Orientation

### Mass Air Flow

#### North Façade



(a) June 21



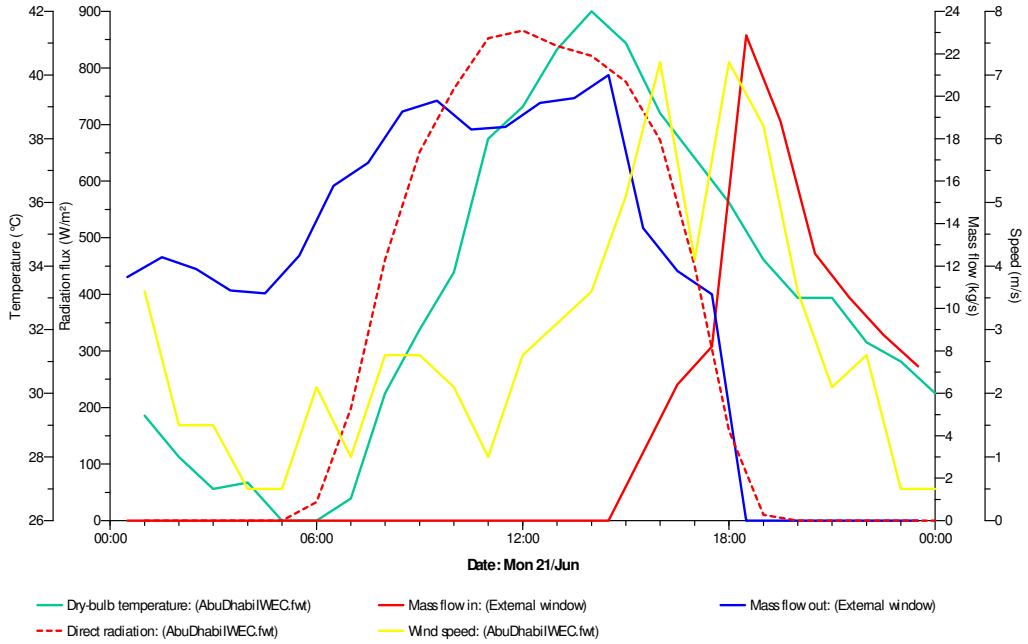
(b) December 21



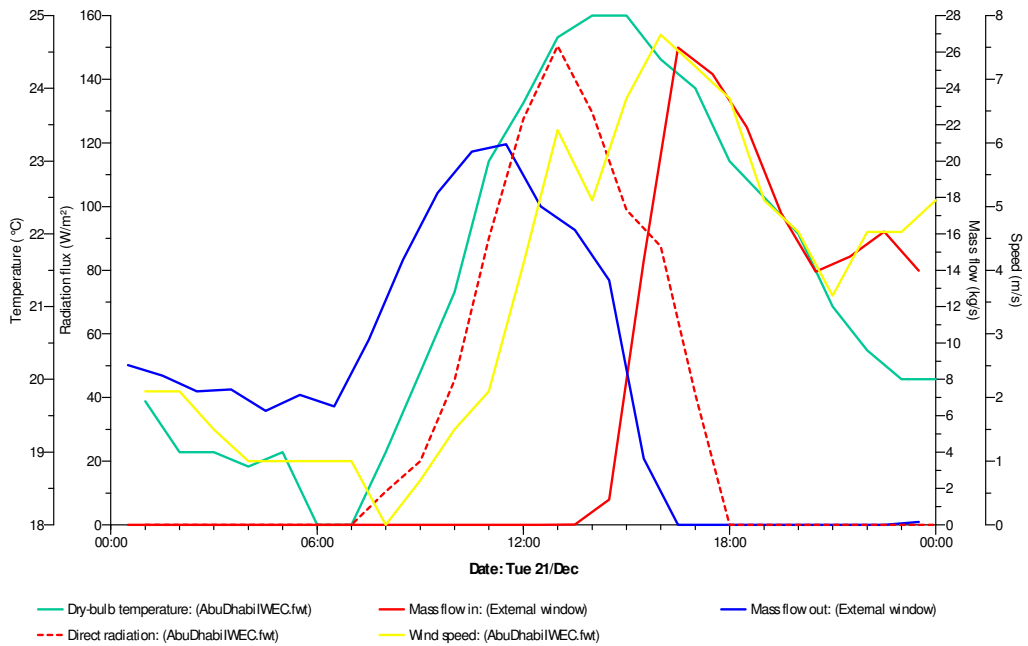
## Appendix F: Variable 2 Orientation

### Mass Air Flow

#### South Façade (Prototype)



(a) June 21

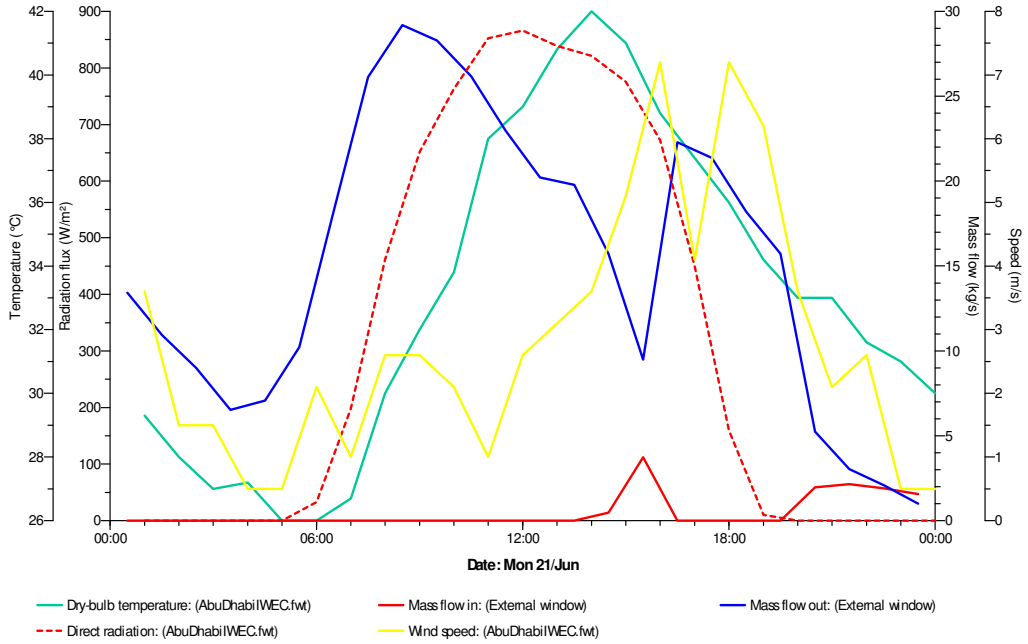


(b) December 21

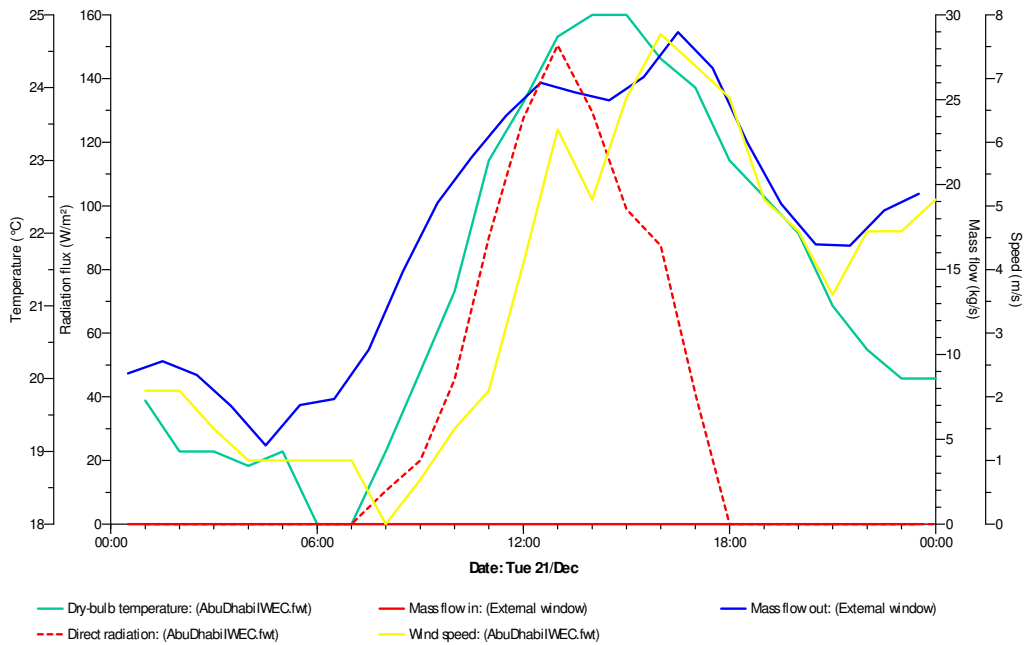
## Appendix F: Variable 2 Orientation

### Mass Air Flow

#### East Façade



(a) June 21

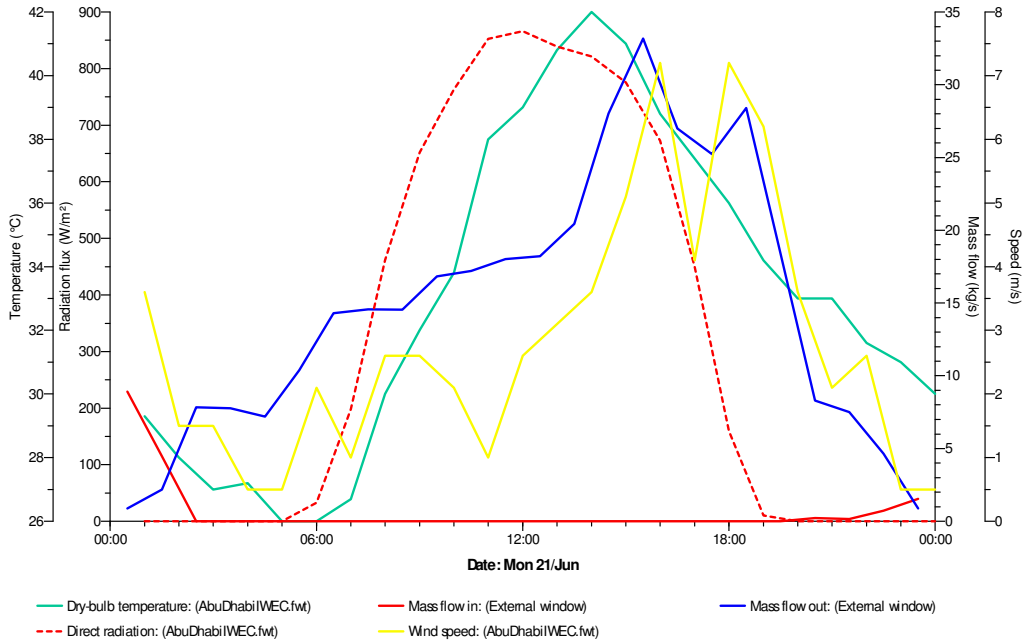


(b) December 21

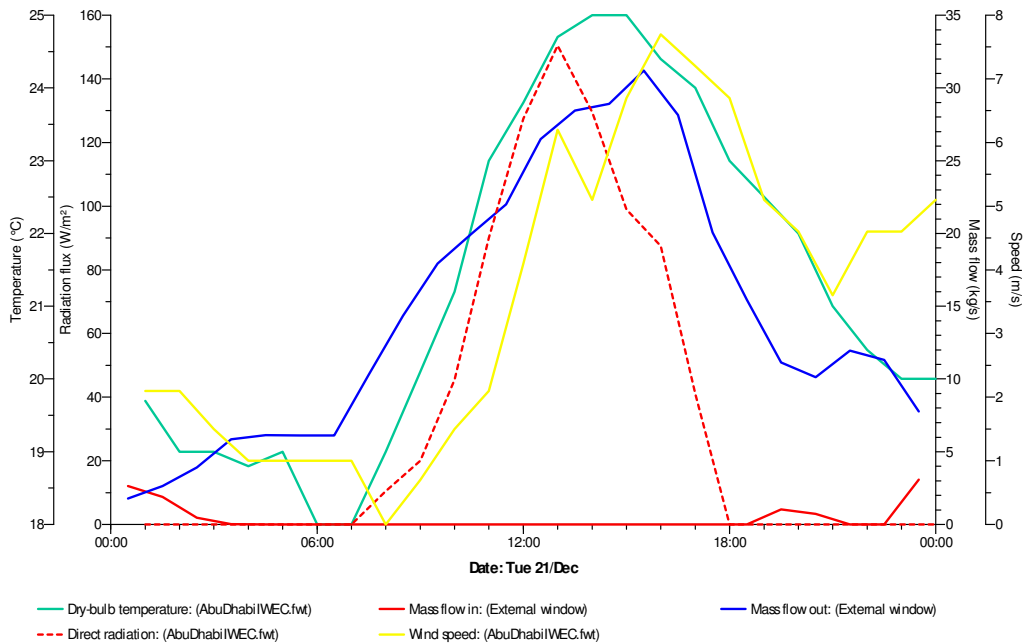
## Appendix F: Variable 2 Orientation

### Mass Air Flow

#### West Façade



(a) June 21



(b) December 21

## Appendix F : Variable 2 Orientation

### Mass Air Flow

#### North and South Values

North		Mass flow in	Mass flow	Net	
Date	Time	(kg/s)	out (kg/s)	Net	Absolute
Mon, 21/Jun		External window	External window		
	00:30	0.00	10.12	10.1166	10.1166
	01:30	0.00	10.62	10.6155	10.6155
	02:30	0.00	9.53	9.5281	9.5281
	03:30	<b>0.00</b>	<b>5.97</b>	5.9678	5.9678
	04:30	0.00	5.08	5.0839	5.0839
	05:30	0.00	6.18	6.1816	6.1816
	06:30	0.00	7.62	7.6226	7.6226
	07:30	0.00	10.36	10.3602	10.3602
	08:30	0.00	14.36	14.3568	14.3568
	09:30	0.00	18.15	18.147	18.147
	10:30	0.00	20.59	20.5869	20.5869
	11:30	0.00	22.88	22.8795	22.8795
	12:30	0.00	25.43	25.4276	25.4276
	13:30	0.00	25.86	25.8646	25.8646
	14:30	0.00	25.66	25.6581	25.6581
	15:30	0.00	26.77	26.7742	26.7742
	16:30	0.00	24.87	24.8674	24.8674
	17:30	0.00	23.14	23.1352	23.1352
	18:30	0.00	19.15	19.1453	19.1453
	19:30	0.00	16.39	16.3943	16.3943
	20:30	0.00	14.53	14.5327	14.5327
	21:30	0.00	14.21	14.2073	14.2073
	22:30	0.00	16.11	16.1111	16.1111
	23:30	0.00	17.90	17.8975	17.8975
				<b>391.46</b>	<b>391.46</b>

South (Prot)		Mass flow in	Mass flow	Net	
Date	Time	(kg/s)	out (kg/s)	Net	Absolute
Mon, 21/Jun		External window	External window		
	00:30	0.00	8.33	8.3317	8.3317
	01:30	0.00	7.68	7.6813	7.6813
	02:30	0.00	6.61	6.61	6.61
	03:30	0.00	6.66	6.6556	6.6556
	04:30	0.00	4.89	4.8883	4.8883
	05:30	0.00	6.33	6.3292	6.3292
	06:30	0.00	5.54	5.5384	5.5384
	07:30	0.00	9.61	9.6143	9.6143
	08:30	0.00	14.75	14.7479	14.7479
	09:30	0.00	18.25	18.2533	18.2533
	10:30	0.00	20.54	20.5426	20.5426
	11:30	0.00	20.95	20.9541	20.9541
	12:30	0.01	17.54	17.532	17.532
	13:30	0.02	16.23	16.2145	16.2145
	14:30	1.37	13.48	12.1015	12.1015
	15:30	14.51	3.66	-10.853	10.853
	16:30	26.24	0.00	-26.2437	26.2437
	17:30	24.79	0.00	-24.794	24.794
	18:30	21.88	0.00	-21.8835	21.8835
	19:30	-17.12	0.00	-17.1202	17.1202
	20:30	13.91	0.00	-13.9132	13.9132
	21:30	-14.78	0.00	-14.7791	14.7791
	22:30	16.18	0.00	-16.1758	16.1758
	23:30	14.10	0.11	-13.9813	13.9813
				<b>181.17</b>	<b>335.74</b>

North		Mass flow in	Mass flow	Net	
Date	Time	(kg/s)	out (kg/s)	Net	Absolute
Mon, 21/Jun		External window	External window		
	00:30	0.00	14.94	14.9359	14.9359
	01:30	0.00	12.28	12.2767	12.2767
	02:30	<b>0.00</b>	<b>7.69</b>	7.6933	7.6933
	03:30	0.00	7.70	7.7013	7.7013
	04:30	0.00	7.37	7.3736	7.3736
	05:30	0.00	9.56	9.5601	9.5601
	06:30	0.00	15.43	15.4322	15.4322
	07:30	0.00	18.16	18.1586	18.1586
	08:30	0.00	20.28	20.2767	20.2767
	09:30	0.00	19.12	19.1221	19.1221
	10:30	0.00	18.07	18.0691	18.0691
	11:30	0.00	16.99	16.9876	16.9876
	12:30	0.00	15.32	15.3202	15.3202
	13:30	0.00	15.56	15.5604	15.5604
	14:30	0.00	15.37	15.3737	15.3737
	15:30	0.00	26.23	26.2328	26.2328
	16:30	0.00	23.87	23.867	23.867
	17:30	0.00	23.27	23.267	23.267
	18:30	0.00	23.06	23.0607	23.0607
	19:30	0.00	15.00	15.0025	15.0025
	20:30	0.86	5.85	4.984	4.984
	21:30	0.35	6.23	5.8791	5.8791
	22:30	0.31	4.38	4.0719	4.0719
	23:30	0.54	2.00	1.4619	1.4619
				<b>341.67</b>	<b>341.67</b>

South (Prot)		Mass flow in	Mass flow	Net	
Date	Time	(kg/s)	out (kg/s)	Net	Absolute
Mon, 21/Jun		External window	External window		
	00:30	0	11.4744	11.4744	11.4744
	01:30	0	12.4208	12.4208	12.4208
	02:30	0	11.86	11.86	11.86
	03:30	0	10.8445	10.8445	10.8445
	04:30	0	10.7182	10.7182	10.7182
	05:30	0	12.4959	12.4959	12.4959
	06:30	0	15.774	15.774	15.774
	07:30	0	16.8751	16.8751	16.8751
	08:30	0	19.2818	19.2818	19.2818
	09:30	0	19.793	19.793	19.793
	10:30	0	18.4389	18.4389	18.4389
	11:30	0	18.5578	18.5578	18.5578
	12:30	0	19.6931	19.6931	19.6931
	13:30	0	19.909	19.909	19.909
	14:30	0	20.9959	20.9959	20.9959
	15:30	3.2066	13.7885	10.5819	10.5819
	16:30	6.404	11.7614	5.3574	5.3574
	17:30	8.2054	10.6667	2.4613	2.4613
	18:30	22.8724	0	-22.8724	22.8724
	19:30	18.8321	0	-18.8321	18.8321
	20:30	12.5751	0	-12.5751	12.5751
	21:30	10.5197	0	-10.5197	10.5197
	22:30	8.7529	0	-8.7529	8.7529
	23:30	7.2752	0	-7.2752	7.2752
				<b>338.36</b>	<b>338.36</b>

## Appendix F : Variable 2 Orientation

### Mass Air Flow

#### East and West Values

East			Net	
Date	Mass flow in (kg/s) External window	Mass flow out (kg/s) External window	Net	Absolute
Tue, 21/Dec	Time			
	00:30	0.00	8.8808	8.8808
	01:30	0.00	9.6001	9.6001
	02:30	0.00	8.7955	8.7955
	03:30	0.00	6.968	6.968
	04:30	0.00	4.6433	4.6433
	05:30	0.00	7.0115	7.0115
	06:30	0.00	7.3664	7.3664
	07:30	0.00	10.2724	10.2724
	08:30	0.00	14.8898	14.8898
	09:30	0.00	18.9298	18.9298
	10:30	0.00	21.6239	21.6239
	11:30	0.00	24.0574	24.0574
	12:30	0.00	26.0165	26.0165
	13:30	0.00	25.4394	25.4394
	14:30	0.00	24.9654	24.9654
	15:30	0.00	26.3356	26.3356
	16:30	0.00	28.9956	28.9956
	17:30	0.00	26.8652	26.8652
	18:30	0.00	22.5264	22.5264
	19:30	0.00	18.8755	18.8755
	20:30	0.00	16.4765	16.4765
	21:30	0.00	16.409	16.409
	22:30	0.00	18.4773	18.4773
	23:30	0.00	19.4589	19.4589
			<b>413.88</b>	

West			Net	
Date	Mass flow in (kg/s) External window	Mass flow out (kg/s) External window	Net	Absolute
Tue, 21/Dec	Time			
	00:30	2.65	-0.8569	0.8569
	01:30	1.89	0.7412	0.7412
	02:30	0.47	3.4485	3.4485
	03:30	0.02	5.8371	5.8371
	04:30	0.00	6.1424	6.1424
	05:30	0.00	6.111	6.111
	06:30	0.00	6.129	6.129
	07:30	0.00	10.3062	10.3062
	08:30	0.00	14.3504	14.3504
	09:30	0.00	17.9365	17.9365
	10:30	0.00	19.9971	19.9971
	11:30	0.00	22.0025	22.0025
	12:30	0.00	26.499	26.499
	13:30	0.00	28.4554	28.4554
	14:30	0.00	28.8966	28.8966
	15:30	0.00	31.1973	31.1973
	16:30	0.00	28.1439	28.1439
	17:30	0.00	20.0727	20.0727
	18:30	0.01	15.4406	15.4406
	19:30	1.03	10.1099	10.1099
	20:30	0.72	9.3887	9.3887
	21:30	0.00	11.9477	11.9477
	22:30	0.00	11.3082	11.3082
	23:30	3.08	4.685	4.685
			<b>340.00</b>	

East		Net	
Date	Mass flow in (kg/s) External window	Mass flow out (kg/s) External window	Net
Mon, 21/Jun	Time		
	00:30	0.00	13.4191
	01:30	0.00	10.937
	02:30	0.00	8.9889
	03:30	<b>0.00</b>	<b>6.5298</b>
	04:30	0.00	7.065
	05:30	0.00	10.2294
	06:30	0.00	18.1927
	07:30	0.00	26.1367
	08:30	0.00	29.192
	09:30	0.00	28.2846
	10:30	0.00	26.1798
	11:30	0.00	22.9913
	12:30	0.00	20.2151
	13:30	0.00	19.7826
	14:30	0.47	15.2413
	15:30	3.73	5.7451
	16:30	0.00	22.2906
	17:30	0.00	21.3672
	18:30	0.00	18.2067
	19:30	0.00	15.7241
	20:30	1.95	3.2835
	21:30	2.14	0.8963
	22:30	1.90	0.1961
	23:30	1.57	-0.5746
			<b>350.52</b>

West		Net	
Date	Mass flow in (kg/s) External window	Mass flow out (kg/s) External window	Net
Mon, 21/Jun	Time		
	00:30	8.90	-8.0191
	01:30	4.47	-2.3068
	02:30	0.00	7.8399
	03:30	0.00	7.7746
	04:30	0.00	7.2091
	05:30	0.00	10.3767
	06:30	0.00	14.3054
	07:30	0.00	14.5702
	08:30	0.00	14.5511
	09:30	0.00	16.8305
	10:30	0.00	17.2002
	11:30	0.00	18.0205
	12:30	0.00	18.2167
	13:30	0.00	20.4364
	14:30	0.00	28.031
	15:30	0.00	33.1734
	16:30	0.00	26.9923
	17:30	0.00	25.2297
	18:30	0.00	28.4143
	19:30	0.00	18.4126
	20:30	0.22	8.0804
	21:30	0.16	7.3523
	22:30	0.72	3.9158
	23:30	1.54	-0.6409
			<b>357.90</b>

## **Appendix G**

### Variable 3 – Cavity Depth

This section lists the simulation results for Variable 2 where the Prototype model cavity depth is altered to 0.5m, 1m (Prototype), and 1.5m.

These are results derived from IES VE Apache V5.9 simulations and processed in an excel spreadsheet.

## Appendix G: Variable 3 - Cavity Depth

### Energy Consumption

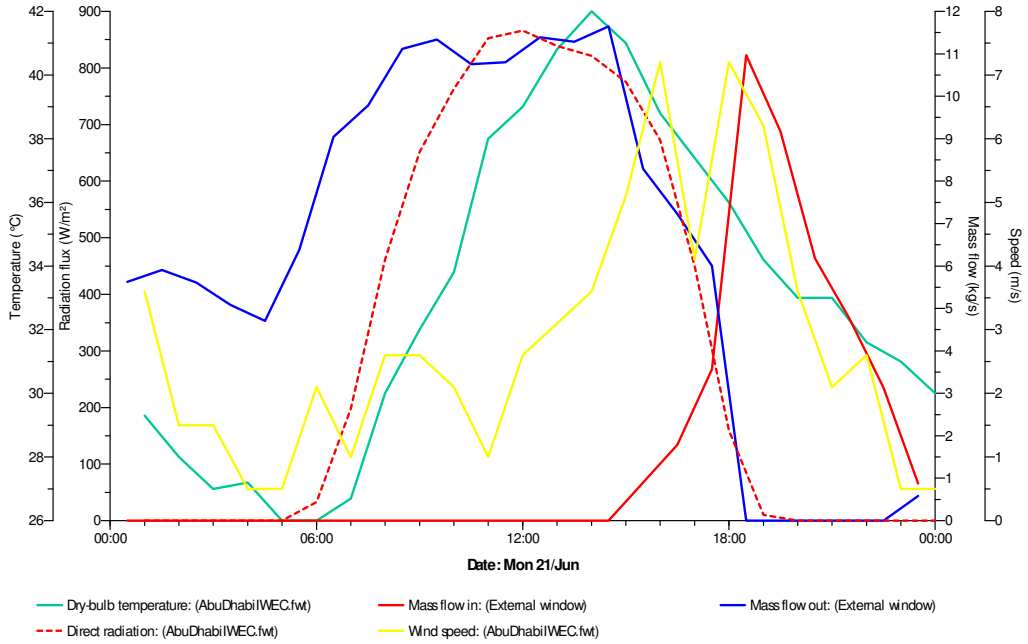
<b>1.5m</b>		<b>0.5m</b>	
Date	Total energy (MWh) annual.aps	Date	Total energy (MWh) annual.aps
Jan	69.2249	Jan	69.1641
Feb	69.8975	Feb	70.3421
Mar	85.0388	Mar	85.3025
Apr	88.2985	Apr	88.264
May	91.6375	May	91.5769
Jun	98.1228	Jun	98.1883
Jul	99.6511	Jul	99.6636
Aug	100.7173	Aug	100.566
Sep	96.1692	Sep	96.2327
Oct	86.2548	Oct	86.6566
Nov	82.8231	Nov	83.2082
Dec	77.326	Dec	77.6155
Summed total	1045.16	Summed total	1046.78

<b>1.0m (Prototype)</b>	
Date	Total energy (MWh) annual.aps
Jan	67.555
Feb	69.1399
Mar	84.9786
Apr	88.2289
May	92.974
Jun	99.0258
Jul	100.8573
Aug	102.453
Sep	96.7745
Oct	86.7179
Nov	82.902
Dec	76.27
Summed total	1047.88

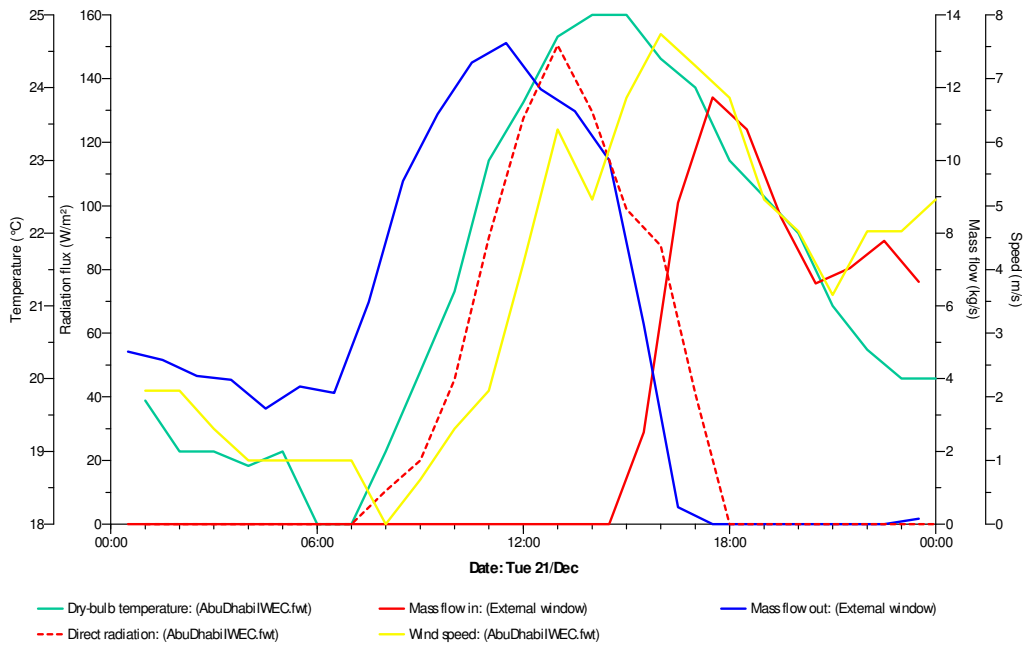
## Appendix G: Variable 3 - Cavity Depth

### Mass Air Flow

#### 0.5m Cavity Width



(c) June 21



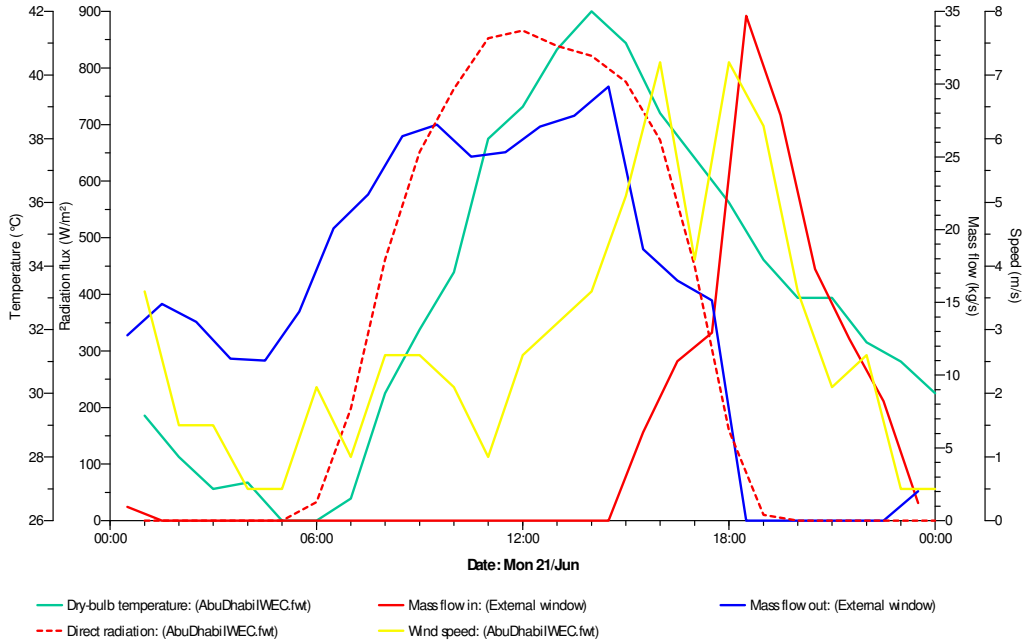
(d) December 21



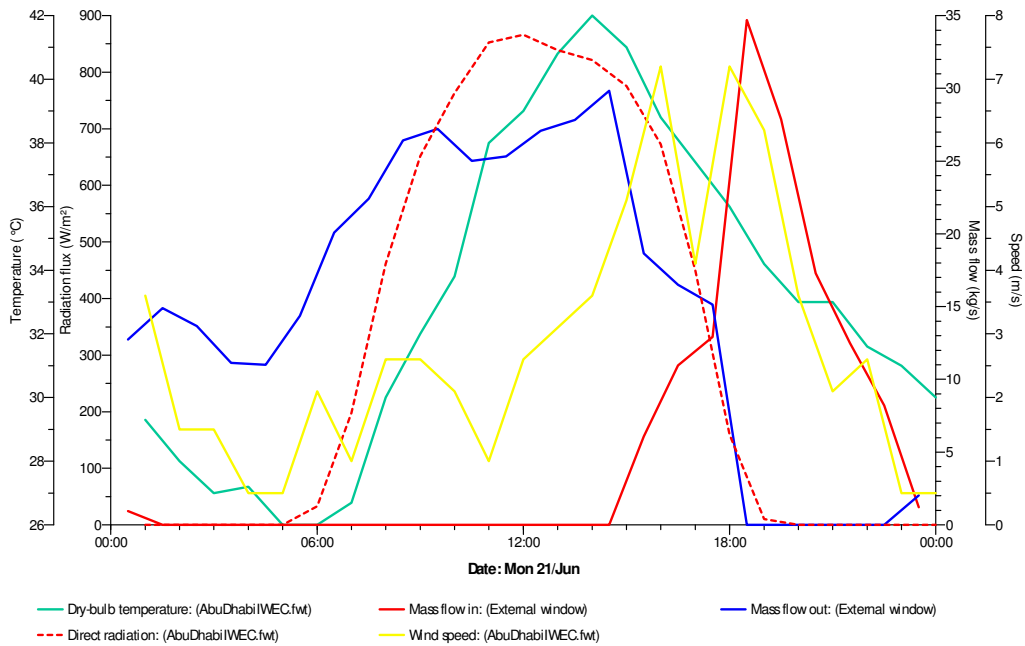
## Appendix G: Variable 3 - Cavity Depth

### Mass Air Flow

#### 1.5m Cavity Width



(a) June 21



(c) December 21

## Appendix G: Variable 3 - Cavity Depth

### Mass Air Flow

#### 0.5 and 1.0m Cavity Depth Values

0.5m					0.5m				
Date Mon, 21/Jan	Mass flow in (kg/s) External window	Mass flow out (kg/s) External window	Net	Net Absolute	Date Tue, 21/Dec	Mass flow in (kg/s) External window	Mass flow out (kg/s) External window	Net	Net Absolute
Time					Time				
00:30	0	5.6252	5.6252	5.6252	0.020833	0	4.7463	4.7463	4.7463
01:30	0	5.9097	5.9097	5.9097	0.0625	0	4.5152	4.5152	4.5152
02:30	0	5.6108	5.6108	5.6108	0.104167	0	4.0772	4.0772	4.0772
03:30	0	<b>5.0852</b>	5.0852	5.0852	0.145833	0	<b>3.974</b>	-3.974	3.974
04:30	0	4.7117	4.7117	4.7117	0.1875	0	3.1831	3.1831	3.1831
05:30	0	6.3826	6.3826	6.3826	0.229167	0	3.7854	3.7854	3.7854
06:30	0	9.0444	9.0444	9.0444	0.270833	0	3.6056	3.6056	3.6056
07:30	0	9.7807	9.7807	9.7807	0.3125	0	6.1079	6.1079	6.1079
08:30	0	11.119	11.119	11.119	0.354167	0	9.435	9.435	9.435
09:30	0	11.3344	11.3344	11.3344	0.395833	0	11.2724	11.2724	11.2724
10:30	0	10.756	10.756	10.756	0.4375	0	12.6861	12.6861	12.6861
11:30	0	10.7988	10.7988	10.7988	0.479167	0	13.221	13.221	13.221
12:30	0	11.3927	11.3927	11.3927	0.520833	0	11.9568	11.9568	11.9568
13:30	0	11.2835	11.2835	11.2835	0.5625	0	11.3575	11.3575	11.3575
14:30	0	11.6481	11.6481	11.6481	0.604167	0	10.0101	10.0101	10.0101
15:30	0.8979	8.288	7.3901	7.3901	0.645833	2.5267	5.493	2.9663	2.9663
16:30	1.7888	7.226	5.4372	5.4372	0.6875	8.8314	0.4632	-8.3682	8.3682
17:30	3.5689	6.0018	2.4329	2.4329	0.729167	11.7287	0	-11.7287	11.7287
18:30	10.9649	0	-10.9649	10.9649	0.770833	10.8483	0	-10.8483	10.8483
19:30	9.1739	0	-9.1739	9.1739	0.8125	8.433	0	-8.433	8.433
20:30	6.1805	0	-6.1805	6.1805	0.854167	6.6202	0	-6.6202	6.6202
21:30	4.7663	0	-4.7663	4.7663	0.895833	7.0433	0	-7.0433	7.0433
22:30	3.1328	0	-3.1328	3.1328	0.9375	7.7875	0	-7.7875	7.7875
23:30	0.8785	0.5817	-0.2968	0.2968	0.979167	6.665	0.148	-6.517	6.517
				<b>180.26</b>					<b>184.25</b>

1.5m					1.5m				
Date Mon, 21/Jan	Mass flow in (kg/s) External window	Mass flow out (kg/s) External window	Net	Net Absolute	Date Mon, 21/Jan	Mass flow in (kg/s) External window	Mass flow out (kg/s) External window	Net	Net Absolute
Time					Time				
00:30	0.9545	12.7479	11.7934	11.7934	00:30	0	11.8614	11.8614	11.8614
01:30	0	14.8975	14.8975	14.8975	01:30	0	11.0119	11.0119	11.0119
02:30	0	13.6587	13.6587	13.6587	02:30	0	8.6619	8.6619	8.6619
03:30	0	11.1376	11.1376	11.1376	03:30	0	9.0062	9.0062	9.0062
04:30	0	10.9967	10.9967	10.9967	04:30	0.0952	5.5373	5.4421	5.4421
05:30	0	14.3812	14.3812	14.3812	05:30	0	8.9389	8.9389	8.9389
06:30	0	20.0883	20.0883	20.0883	06:30	0	6.8327	6.8327	6.8327
07:30	0	22.4255	22.4255	22.4255	07:30	0	11.5723	11.5723	11.5723
08:30	0	26.4233	26.4233	26.4233	08:30	0	19.2618	19.2618	19.2618
09:30	0	27.2141	27.2141	27.2141	09:30	0	24.2871	24.2871	24.2871
10:30	0	25.0287	25.0287	25.0287	10:30	0	27.2429	27.2429	27.2429
11:30	0	25.3168	25.3168	25.3168	11:30	0	27.2447	27.2447	27.2447
12:30	0	27.0802	27.0802	27.0802	12:30	0.7443	21.5059	20.7616	20.7616
13:30	0	27.8393	27.8393	27.8393	13:30	1.4586	19.5967	18.1381	18.1381
14:30	0	29.8419	29.8419	29.8419	14:30	5.5886	14.2848	8.6962	8.6962
15:30	6.0776	18.6627	12.5851	12.5851	15:30	30.2716	1.5677	-28.7039	28.7039
16:30	10.9477	16.4922	5.5445	5.5445	16:30	41.1831	0	-41.1831	41.1831
17:30	12.9088	15.1477	2.2389	2.2389	17:30	37.7495	0	-37.7495	37.7495
18:30	34.6817	0	-34.6817	34.6817	18:30	32.9044	0	-32.9044	32.9044
19:30	<b>27.8761</b>	0	-27.8761	27.8761	19:30	<b>25.7736</b>	0	-25.7736	25.7736
20:30	17.2923	0	-17.2923	17.2923	20:30	21.12	0	-21.12	21.12
21:30	12.4917	0	-12.4917	12.4917	21:30	22.4556	0	-22.4556	22.4556
22:30	8.2076	0	-8.2076	8.2076	22:30	24.5365	0	-24.5365	24.5365
23:30	1.2015	2.0349	0.8334	0.8334	23:30	21.4945	0.0413	-21.4532	21.4532
				<b>429.87</b>					<b>474.84</b>

## **Appendix H**

### Variable 4 – Height from Building Top

This section lists the simulation results for Variable 4 where the Prototype model double skin facade is increased to different heights of 1 storey (3m), 2 storeys (6m) and 3 storeys (9m).

These are results derived from IES VE Apache V5.9 simulations and processed in an excel spreadsheet.

## Appendix H: Variable 4 – Height from Building Top

### Energy Consumption

<b>3 Storey (9m high)</b>		<b>Prototype (no solar chimney)</b>	
	Total energy (MWh)		Total energy (MWh)
Date		Date	
Jan	67.4446	Jan	67.555
Feb	68.6116	Feb	69.1399
Mar	84.8065	Mar	84.9786
Apr	88.131	Apr	88.2289
May	92.963	May	92.974
Jun	99.1518	Jun	99.0258
Jul	100.9529	Jul	100.8573
Aug	102.3412	Aug	102.453
Sep	96.651	Sep	96.7745
Oct	86.6292	Oct	86.7179
Nov	82.805	Nov	82.902
Dec	76.1623	Dec	76.27
Summed total	1046.65	Summed total	1047.88

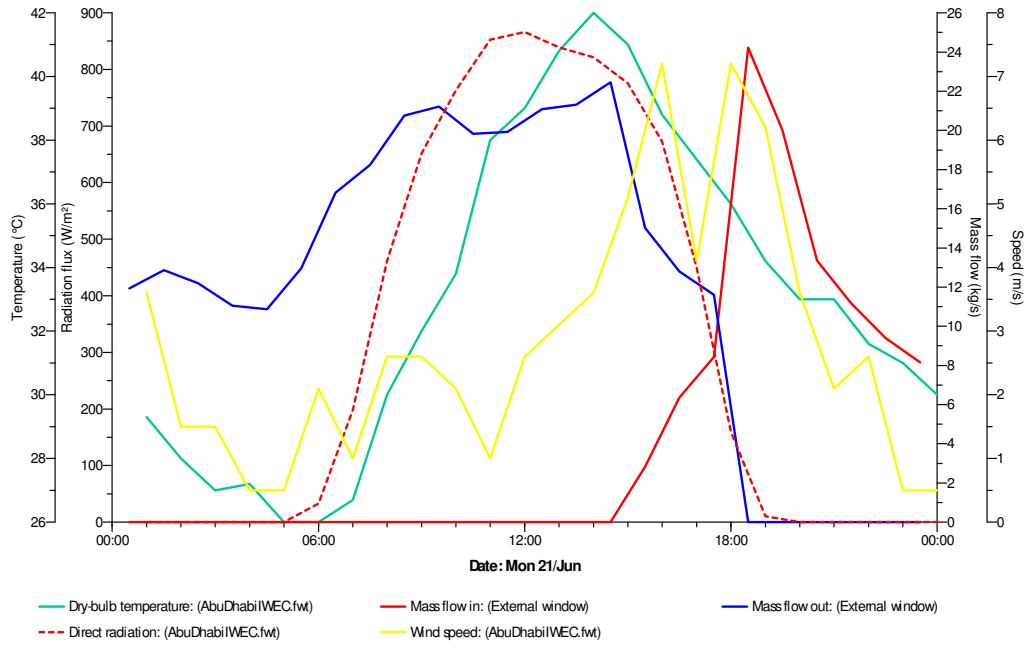
<b>2 Storey (6m high)</b>		<b>1 Storey (3m high)</b>	
	Total energy (MWh)		Total energy (MWh)
Date		Date	
Jan	67.5085	Jan	67.585
Feb	68.6715	Feb	68.7428
Mar	84.845	Mar	84.8832
Apr	88.1356	Apr	88.1557
May	92.9857	May	93.0084
Jun	99.1336	Jun	99.1116
Jul	100.9456	Jul	100.9363
Aug	102.3407	Aug	102.4057
Sep	96.6638	Sep	96.6799
Oct	86.6675	Oct	86.7214
Nov	82.8731	Nov	82.9529
Dec	76.23	Dec	76.3106
Summed total	1047.001	Summed total	1047.494

## Appendix H: Variable 4 – Height from Building Top

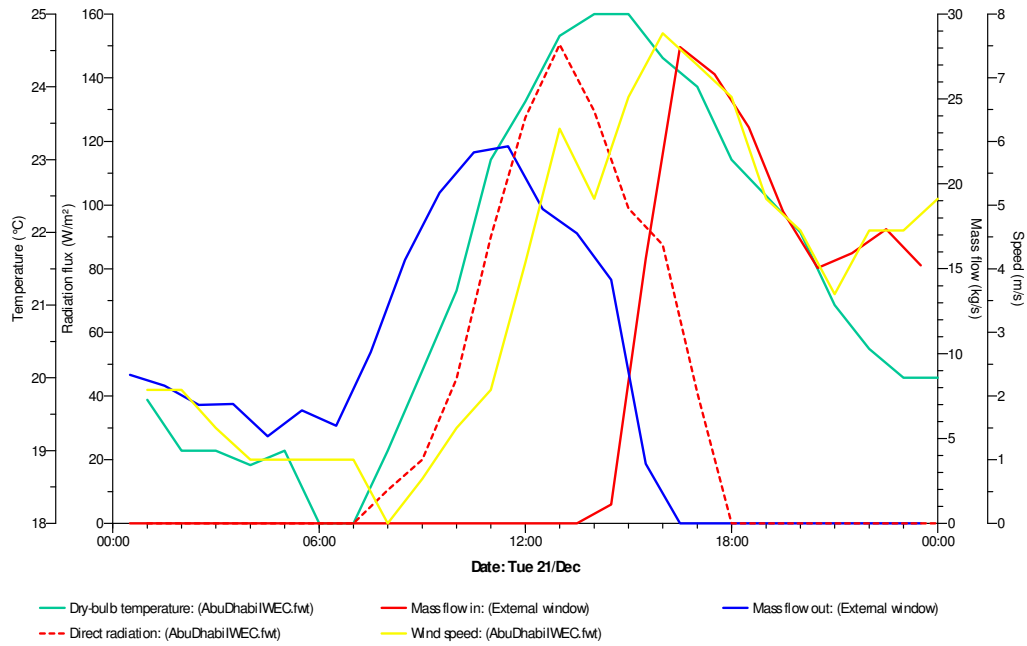
### Mass Air Flow

#### 1 Storey Height Solar Chimney

(3m from Building Top)



(e) June 21



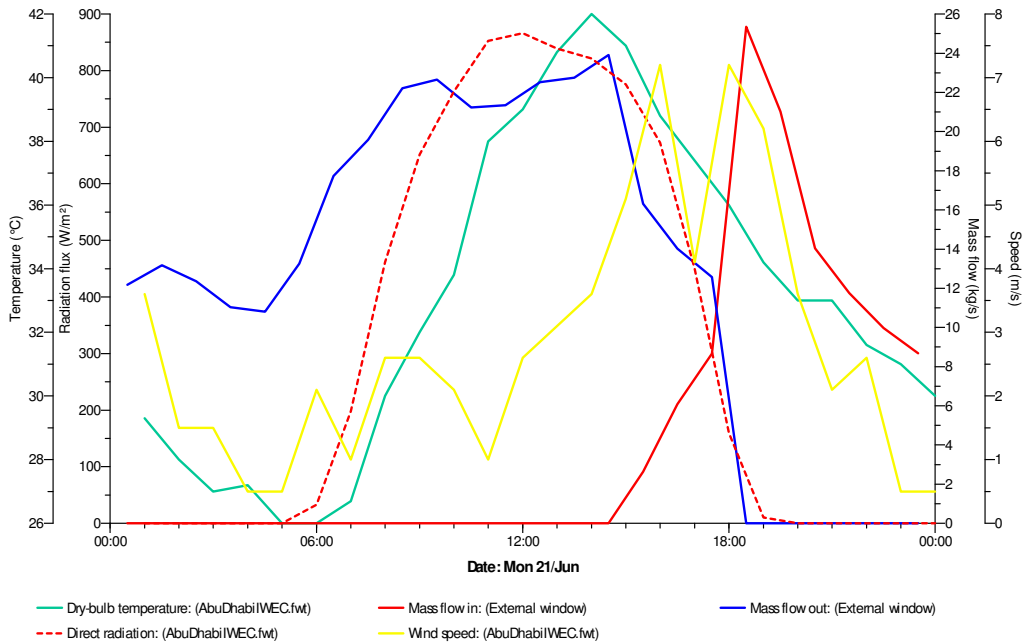
(f) December 21

## Appendix H: Variable 4 – Height from Building Top

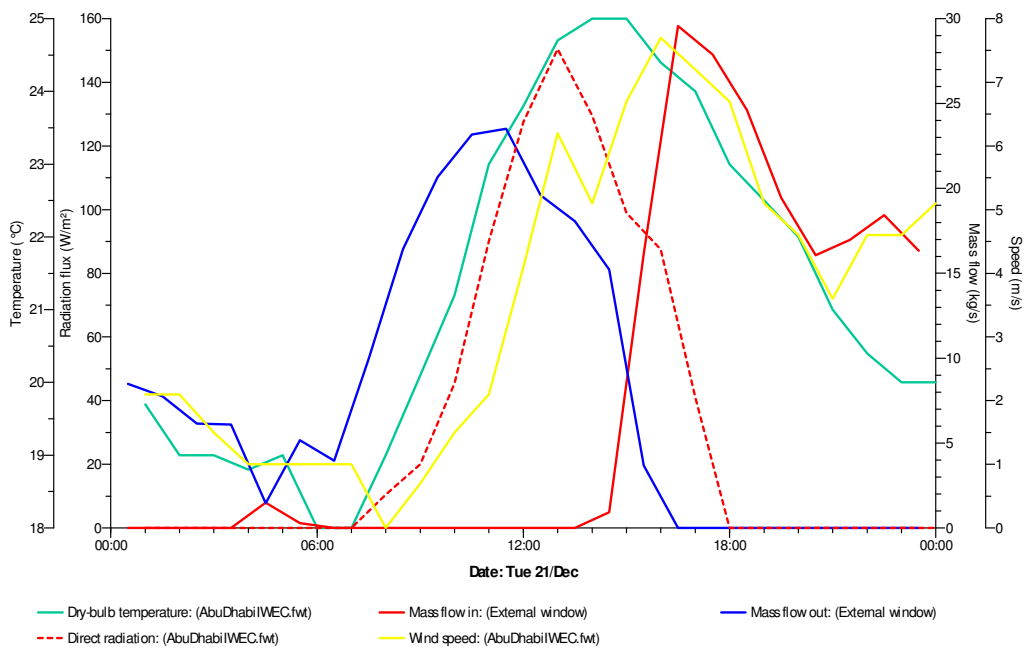
### Mass Air Flow

#### 2 Storey Height Solar Chimney

(6m from Building Top)



(a) June 21



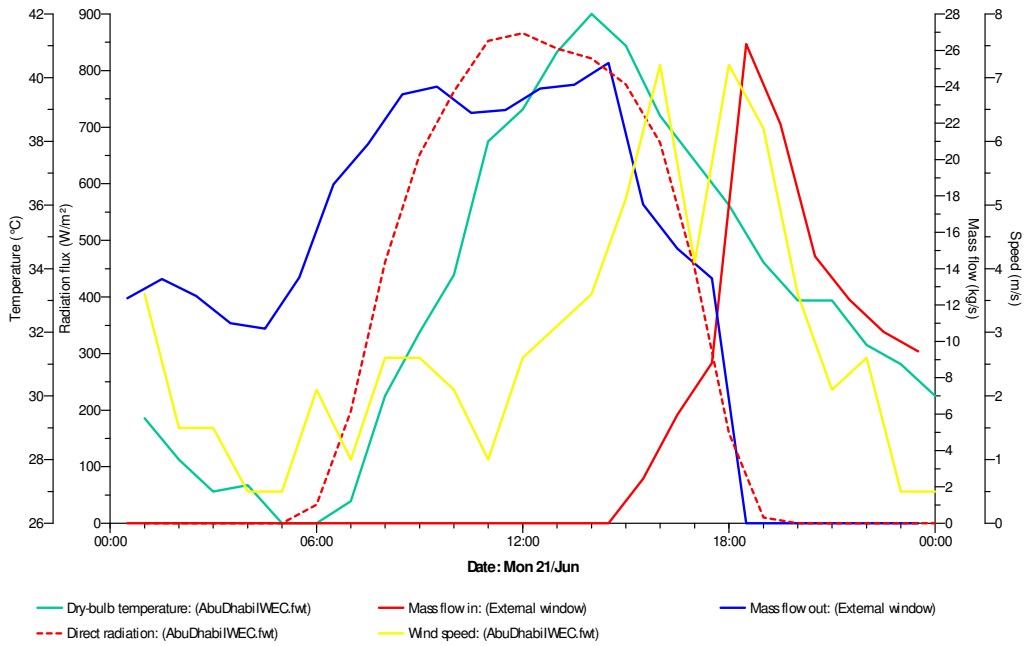
(d) December 21

## Appendix H: Variable 4 – Height from Building Top

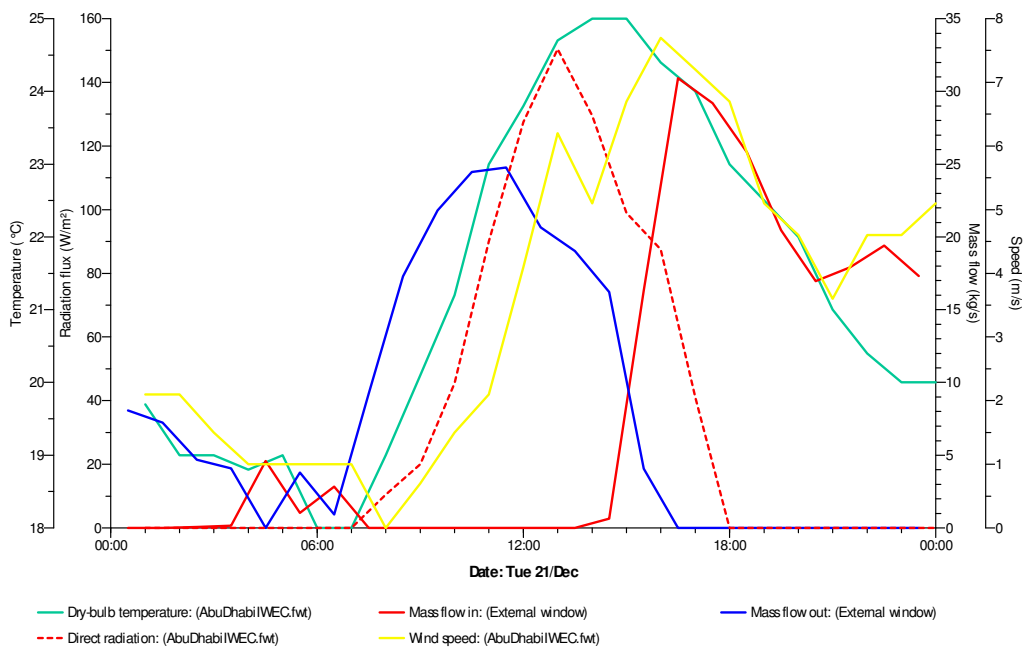
### Mass Air Flow

#### 3 Storey Height Solar Chimney

(9m from Building Top)



(a) June 21



(e) December 21

## Appendix H: Variable 4 – Height from Building Top

### Mass Air Flow

1 and 2 Storey Height Solar Chimney  
(3m and 9m from Building Top) - Values

1 Storey (3m high)					1 Storey (3m high)						
Date Mon, 21/Jun	Time	Mass flow in (kg/s) External window	Mass flow out (kg/s) External window	Net	Net Absolute	Date Mon, 21/Jun	Time	Mass flow in (kg/s) External window	Mass flow out (kg/s) External window	Net	Net Absolute
	00:30	0	11.926	11.926	11.926		00:30	0	8.7537	8.7537	8.7537
	01:30	0	12.8676	12.8676	12.8676		01:30	0	8.101	8.101	8.101
	02:30	0	12.191	12.191	12.191		02:30	0	6.9718	6.9718	6.9718
	03:30	0	11.0426	11.0426	11.0426		03:30	0	7.028	7.028	7.028
	04:30	0	10.864	10.864	10.864		04:30	0	5.1283	5.1283	5.1283
	05:30	0	12.9561	12.9561	12.9561		05:30	0	6.6557	6.6557	6.6557
	06:30	0	16.8127	16.8127	16.8127		06:30	0	5.7514	5.7514	5.7514
	07:30	0	18.2441	18.2441	18.2441		07:30	0	10.0869	10.0869	10.0869
	08:30	0	20.7518	20.7518	20.7518		08:30	0	15.5184	15.5184	15.5184
	09:30	0	21.2189	21.2189	21.2189		09:30	0	19.4744	19.4744	19.4744
	10:30	0	19.8251	19.8251	19.8251		10:30	0	21.8604	21.8604	21.8604
	11:30	0	19.9253	19.9253	19.9253		11:30	0	22.2189	22.2189	22.2189
	12:30	0	21.0917	21.0917	21.0917		12:30	0	18.5242	18.5242	18.5242
	13:30	0	21.3083	21.3083	21.3083		13:30	0.0006	17.0846	17.084	17.084
	14:30	0	22.4471	22.4471	22.4471		14:30	1.1057	14.3572	13.2515	13.2515
	15:30	2.837	15.0307	12.1937	12.1937		15:30	15.6019	3.5136	-12.0883	12.0883
	16:30	6.3542	12.802	6.4478	6.4478		16:30	28.0659	0	-28.0659	28.0659
	17:30	8.4417	11.5976	3.1559	3.1559		17:30	26.4469	0	-26.4469	26.4469
	18:30	24.2256	0	-24.2256	24.2256		18:30	23.3319	0	-23.3319	23.3319
	19:30	20.01	0	-20.01	20.01		19:30	18.3641	0	-18.3641	18.3641
	20:30	13.3556	0	-13.3556	13.3556		20:30	15.0511	0	-15.0511	15.0511
	21:30	11.1594	0	-11.1594	11.1594		21:30	15.9126	0	-15.9126	15.9126
	22:30	9.4036	0	-9.4036	9.4036		22:30	17.3247	0	-17.3247	17.3247
	23:30	8.1633	0	-8.1633	8.1633		23:30	15.1901	0	-15.1901	15.1901
					<b>361.59</b>						<b>358.18</b>
2 Storey (6m high)					2 Storey (6m high)						
Date Mon, 21/Jun	Time	Mass flow in (kg/s) External window	Mass flow out (kg/s) External window	Net	Net Absolute	Date Mon, 21/Jun	Time	Mass flow in (kg/s) External window	Mass flow out (kg/s) External window	Net	Net Absolute
	00:30	0	12.1693	12.1693	12.1693		00:30	0	8.485	8.485	8.485
	01:30	0	13.1712	13.1712	13.1712		01:30	0	7.7499	7.7499	7.7499
	02:30	0	12.3627	12.3627	12.3627		02:30	0	6.1593	6.1593	6.1593
	03:30	0	11.0382	11.0382	11.0382		03:30	0	6.0939	6.0939	6.0939
	04:30	0	10.81	10.81	10.81		04:30	1.4838	1.4604	-0.0234	0.0234
	05:30	0	13.2549	13.2549	13.2549		05:30	0.2912	5.1633	4.8721	4.8721
	06:30	0	17.7391	17.7391	17.7391		06:30	0.0029	3.9672	3.9643	3.9643
	07:30	0	19.5817	19.5817	19.5817		07:30	0	9.9784	9.9784	9.9784
	08:30	0	22.2018	22.2018	22.2018		08:30	0	16.4227	16.4227	16.4227
	09:30	0	22.6467	22.6467	22.6467		09:30	0	20.6717	20.6717	20.6717
	10:30	0	21.226	21.226	21.226		10:30	0	23.1791	23.1791	23.1791
	11:30	0	21.3531	21.3531	21.3531		11:30	0	23.5129	23.5129	23.5129
	12:30	0	22.5273	22.5273	22.5273		12:30	0	19.5948	19.5948	19.5948
	13:30	0	22.7434	22.7434	22.7434		13:30	0	18.0566	18.0566	18.0566
	14:30	0	23.9185	23.9185	23.9185		14:30	0.9249	15.2206	14.2957	14.2957
	15:30	2.6346	16.3124	13.6778	13.6778		15:30	16.164	3.6743	-12.4897	12.4897
	16:30	6.0864	14.0214	7.935	7.935		16:30	29.5777	0	-29.5777	29.5777
	17:30	8.6606	12.5645	3.9039	3.9039		17:30	27.888	0	-27.888	27.888
	18:30	25.3526	0	-25.3526	25.3526		18:30	24.6355	0	-24.6355	24.6355
	19:30	21.0241	0	-21.0241	21.0241		19:30	19.4649	0	-19.4649	19.4649
	20:30	14.0367	0	-14.0367	14.0367		20:30	16.0609	0	-16.0609	16.0609
	21:30	11.7479	0	-11.7479	11.7479		21:30	16.9615	0	-16.9615	16.9615
	22:30	9.9758	0	-9.9758	9.9758		22:30	18.4185	0	-18.4185	18.4185
	23:30	8.687	0	-8.687	8.687		23:30	16.3255	0	-16.3255	16.3255
					<b>383.08</b>						<b>364.88</b>



## Appendix H: Variable 4 – Height from Building Top

### Mass Air Flow

#### 3 Storey Height Solar Chimney

(9m from Building Top) - Values

3 Storey (9m high)					3 Storey (9m high)				
Date Mon, 21/Jun	Mass flow in (kg/s) External window	Mass flow out (kg/s) External window	Net	Net Absolute	Date Mon, 21/Jun	Mass flow in (kg/s) External window	Mass flow out (kg/s) External window	Net	Net Absolute
Time					Time				
00:30	0	12.3732	12.3732	12.3732	00:30	0	8.078	8.078	8.078
01:30	0	13.437	13.437	13.437	01:30	0	7.2419	7.2419	7.2419
02:30	0	12.4934	12.4934	12.4934	02:30	0.0695	4.6765	4.607	4.607
03:30	0	10.9981	10.9981	10.9981	03:30	0.1679	4.0849	3.917	3.917
04:30	0	10.694	10.694	10.694	04:30	4.6102	0	-4.6102	4.6102
05:30	0	13.5179	13.5179	13.5179	05:30	1.0355	3.8001	2.7646	2.7646
06:30	0	18.633	18.633	18.633	06:30	2.839	0.9241	-1.9149	1.9149
07:30	0	20.8613	20.8613	20.8613	07:30	0	9.2371	9.2371	9.2371
08:30	0	23.5859	23.5859	23.5859	08:30	0	17.3028	17.3028	17.3028
09:30	0	24.0143	24.0143	24.0143	09:30	0	21.8333	21.8333	21.8333
10:30	0	22.57	22.57	22.57	10:30	0	24.4608	24.4608	24.4608
11:30	0	22.721	22.721	22.721	11:30	0	24.7807	24.7807	24.7807
12:30	0	23.9009	23.9009	23.9009	12:30	0	20.6665	20.6665	20.6665
13:30	0	24.1101	24.1101	24.1101	13:30	0	19.0367	19.0367	19.0367
14:30	0	25.3126	25.3126	25.3126	14:30	0.6335	16.2252	15.5917	15.5917
15:30	2.4565	17.5299	15.0734	15.0734	15:30	16.3186	4.0828	-12.2358	12.2358
16:30	5.9731	15.0974	9.1243	9.1243	16:30	30.9092	0	-30.9092	30.9092
17:30	8.8142	13.4667	4.6525	4.6525	17:30	29.1862	0	-29.1862	29.1862
18:30	26.3514	0	-26.3514	26.3514	18:30	25.8226	0	-25.8226	25.8226
19:30	21.9455	0	-21.9455	21.9455	19:30	20.4678	0	-20.4678	20.4678
20:30	14.6706	0	-14.6706	14.6706	20:30	16.9769	0	-16.9769	16.9769
21:30	12.303	0	-12.303	12.303	21:30	17.9148	0	-17.9148	17.9148
22:30	10.5193	0	-10.5193	10.5193	22:30	19.4121	0	-19.4121	19.4121
23:30	9.4482	0	-9.4482	9.4482	23:30	17.3178	0	-17.3178	17.3178
				<b>403.31</b>					<b>376.29</b>

# **Appendix I**

## Calculation Spreadsheet

This section exhibits the spreadsheet tabulation of the established equations for this research.

The results derived from IES VE Apache V5.9 simulations and Psychrometric chart are post processed and filled in an excel spreadsheet.

# Appendix I: Latent Heat Calculation

## Prototype Model Calculations – June 21

### Water Spray Effect @ RH 90%

Date	Simulation Results							Psychrometric Chart				Calculations					
	Time	Mass flow in (kg/s)	Mass flow out (kg/s)	Mass flow - Net (kg/s)	Dry Bulb Air Temp (°C)	Relative humidity (%)	Wet Bulb Temp (°C)	Initial		Final @ 90% RH		$\Delta h$ (kJ/kg)	Energy (kJ/s) (kWatts)	Final @ 90% RH			
								Enthalpy $h_i$ (kJ/kg)	Absolute Humidity $W_i$ (g <sub>H2O</sub> /kg air)	Enthalpy $h_f$ (kJ/kg)	Absolute Humidity $W_f$ (g <sub>H2O</sub> /kg air)			Mass Water Rate (g <sub>H2O</sub> /s)	Mass Water (g <sub>H2O</sub> )	Volume Water (Liters)	
	00:30	0	11.4744	11.47	29.52	69.61	25.00	76.30	18.25	76.44	19.61	0.14	1.62	15.64	28,155	28	
	01:30	0	12.4208	12.42	29.04	67.59	24.24	73.14	17.20	73.29	18.69	0.15	1.87	18.49	33,287	33	
	02:30	0	11.86	11.86	27.91	68.49	23.36	69.67	16.30	69.80	17.69	0.14	1.61	16.46	29,623	30	
	03:30	0	10.8445	10.84	27.47	68.58	22.98	68.18	15.90	68.32	17.27	0.13	1.43	14.82	26,678	27	
	04:30	0	<b>10.7182</b>	10.72	27	68.53	22.55	66.54	15.44	66.66	16.80	0.13	1.37	14.51	26,124	26	
	05:30	0	12.4959	12.50	26.48	68.14	22.02	64.56	14.88	64.69	16.24	0.12	1.56	17.02	30,631	31	
	06:30	0	15.774	15.77	27.12	67.91	22.56	66.58	15.41	66.71	16.81	0.13	2.08	22.07	39,734	40	
	<b>07:30</b>	<b>0</b>	<b>16.8751</b>	<b>16.88</b>	<b>29.24</b>	<b>63.43</b>	<b>23.73</b>	<b>71.06</b>	<b>16.31</b>	<b>71.24</b>	<b>18.10</b>	<b>0.18</b>	<b>2.99</b>	<b>30.25</b>	<b>54,442</b>	<b>55</b>	<b>2.99</b> <b>54.77</b>
	08:30	0	19.2818	19.28	32.06	52.11	24.11	72.50	15.73	72.78	18.55	0.28	5.47	54.33	97,787	98	5.47 98.38
	09:30	0	19.793	19.79	34.11	44.89	24.32	73.24	15.19	73.60	18.78	0.37	7.23	71.15	128,067	129	7.23 128.84
	10:30	0	18.4389	18.44	37.12	36.99	24.83	75.26	14.76	75.74	19.41	0.48	8.90	85.58	154,045	155	8.90 154.98
	11:30	0	18.5578	18.56	39.77	28.53	24.49	73.73	13.10	74.34	19.00	0.61	11.23	109.33	196,793	198	11.23 197.98
	12:30	0	19.6931	19.69	41.16	22.39	23.55	69.84	11.04	70.52	17.89	0.68	13.32	135.03	243,061	245	13.32 244.53
	13:30	0	19.909	19.91	42.46	18.5	23.05	67.85	9.75	68.58	17.34	0.73	14.61	151.22	272,197	274	14.61 273.84
	14:30	0	20.9959	21.00	42.45	22.19	24.33	72.93	11.72	73.65	18.80	0.72	15.13	148.56	267,400	269	15.13 269.01
	15:30	3.2066	13.7885	10.58	41.07	29.04	25.57	78.20	14.32	78.85	20.31	0.64	6.79	63.42	114,159	115	6.79 114.85
	16:30	6.404	11.7614	5.36	39.01	35.61	25.91	79.80	15.77	80.34	20.76	0.54	2.89	26.71	48,086	48	2.89 48.38
	<b>17:30</b>	<b>8.2054</b>	<b>10.6667</b>	<b>2.46</b>	<b>37.28</b>	<b>41.21</b>	<b>25.99</b>	<b>80.25</b>	<b>16.64</b>	<b>80.71</b>	<b>20.86</b>	<b>0.46</b>	<b>1.13</b>	<b>10.39</b>	<b>18,710</b>	<b>19</b>	<b>1.13</b> <b>18.82</b>
	18:30	22.8724	0	22.87	35.34	49.54	26.32	81.79	18.03	82.15	21.29	0.36	8.21	74.69	134,440	135	
	19:30	18.8321	0	18.83	33.63	61.77	27.31	86.39	20.52	86.63	22.63	0.24	4.53	39.85	71,728	72	
	20:30	12.5751	0	12.58	32.85	65.66	27.33	86.53	20.89	86.73	22.66	0.20	2.54	22.31	40,159	40	
	21:30	10.5197	0	10.52	32.17	66.01	26.78	84.03	20.19	84.22	21.91	0.19	2.03	18.10	32,587	33	
	22:30	8.7529	0	8.75	31.17	69.6	26.50	82.78	20.11	82.94	21.53	0.16	1.38	12.41	22,332	22	
	23:30	7.2752	0	7.28	30.37	74.92	26.64	83.45	20.70	83.57	21.71	0.11	0.82	7.38	13,291	13	
				338.3604									<b>120.75</b>				<b>2,136</b> <b>86.72</b> <b>1549.60</b>

187

# Appendix I: Latent Heat Calculation

## Prototype Model Calculations – June 21

### Water Spray Effect @ RH 100%

Date	Simulation Results							Psychrometric Chart				Calculations						
	Time	Mass flow in (kg/s)	Mass flow out (kg/s)	Mass flow - Net (kg/s)	Dry Bulb Air Temp (°C)	Relative humidity (%)	Wet Bulb Temp (°C)	Initial		Final @ 90% RH		$\Delta h$ (kJ/kg)	Energy (kWatts)	Final @ 100% RH				
								Enthalpy $h_i$ (kJ/kg)	Absolute Humidity $W_i$ (g <sub>H2O</sub> /kg air)	Enthalpy $h_f$ (kJ/kg)	Absolute Humidity $W_f$ (g <sub>H2O</sub> /kg air)			Mass Water Rate (g <sub>H2O</sub> /s)	Mass Water (g <sub>H2O</sub> )	Volume Water (Liters)		
	00:30	0	11.4744	11.47	29.52	69.61	25.00	76.30	18.25	76.44	19.61	0.20	2.30	22.08	39,743	40		
	01:30	0	12.4208	12.42	29.04	67.59	24.24	73.14	17.20	73.29	18.69	0.21	2.56	25.33	45,598	46		
	02:30	0	11.86	11.86	27.91	68.49	23.36	69.67	16.30	69.80	17.69	0.19	2.23	22.85	41,122	41		
	03:30	0	10.8445	10.84	27.47	68.58	22.98	68.18	15.90	68.32	17.27	0.18	1.98	20.61	37,089	37		
	04:30	0	<b>10.7182</b>	10.72	27	68.53	22.55	66.54	15.44	66.66	16.80	0.18	1.90	20.17	36,300	37		
	05:30	0	12.4959	12.50	26.48	68.14	22.02	64.56	14.88	64.69	16.24	0.17	2.16	23.52	42,330	43		
	06:30	0	15.774	15.77	27.12	67.91	22.56	66.58	15.41	66.71	16.81	0.18	2.87	30.40	54,715	55		
	<b>07:30</b>	<b>0</b>	<b>16.8751</b>	<b>16.88</b>	<b>29.24</b>	<b>63.43</b>	<b>23.73</b>	<b>71.06</b>	<b>16.31</b>	<b>71.24</b>	<b>18.10</b>	<b>0.23</b>	<b>3.91</b>	<b>39.42</b>	<b>70,954</b>	<b>71</b>	<b>3.91</b>	<b>71.38</b>
	08:30	0	19.2818	19.28	32.06	52.11	24.11	72.50	15.73	72.78	18.55	0.34	6.54	64.91	116,837	118	6.54	117.54
	09:30	0	19.793	19.79	34.11	44.89	24.32	73.24	15.19	73.60	18.78	0.42	8.35	82.07	147,721	149	8.35	148.61
	10:30	0	18.4389	18.44	37.12	36.99	24.83	75.26	14.76	75.74	19.41	0.54	9.97	95.89	172,593	174	9.97	173.64
	11:30	0	18.5578	18.56	39.77	28.53	24.49	73.73	13.10	74.34	19.00	0.66	12.29	119.62	215,308	217	12.29	216.61
	12:30	0	19.6931	19.69	41.16	22.39	23.55	69.84	11.04	70.52	17.89	0.73	14.38	145.69	262,242	264	14.38	263.83
	13:30	0	19.909	19.91	42.46	18.5	23.05	67.85	9.75	68.58	17.34	0.79	15.64	161.86	291,345	293	15.64	293.10
	14:30	0	20.9959	21.00	42.45	22.19	24.33	72.93	11.72	73.65	18.80	0.78	16.32	160.14	288,254	290	16.32	289.99
	15:30	3.2066	13.7885	10.58	41.07	29.04	25.57	78.20	14.32	78.85	20.31	0.70	7.44	69.44	124,998	126	7.44	125.75
	16:30	6.404	11.7614	5.36	39.01	35.61	25.91	79.80	15.77	80.34	20.76	0.60	3.23	29.79	53,618	54	3.23	53.94
	<b>17:30</b>	<b>8.2054</b>	<b>10.6667</b>	<b>2.46</b>	<b>37.28</b>	<b>41.21</b>	<b>25.99</b>	<b>80.25</b>	<b>16.64</b>	<b>80.71</b>	<b>20.86</b>	<b>0.52</b>	<b>1.29</b>	<b>11.81</b>	<b>21,258</b>	<b>21</b>	<b>1.29</b>	<b>21.39</b>
	18:30	22.8724	0	22.87	35.34	49.54	26.32	81.79	18.03	82.15	21.29	0.42	9.68	87.94	158,293	159		
	19:30	18.8321	0	18.83	33.63	61.77	27.31	86.39	20.52	86.63	22.63	0.31	5.81	51.02	91,831	92		
	20:30	12.5751	0	12.58	32.85	65.66	27.33	86.53	20.89	86.73	22.66	0.27	3.40	29.77	53,591	54		
	21:30	10.5197	0	10.52	32.17	66.01	26.78	84.03	20.19	84.22	21.91	0.26	2.72	24.27	43,681	44		
	22:30	8.7529	0	8.75	31.17	69.6	26.50	82.78	20.11	82.94	21.53	0.22	1.94	17.50	31,501	32		
	23:30	7.2752	0	7.28	30.37	74.92	26.64	83.45	20.70	83.57	21.71	0.18	1.29	11.63	20,936	21		
				338.3604									<b>140.18</b>		<b>2476.72</b>		<b>95.43</b>	<b>1704.40</b>

188

# Appendix I: Latent Heat Calculation

## Prototype Model Calculations – Dec 21

### Water Spray Effect @ RH 90%

Simulation Results							Psychrometric Chart				Calculations							
Date	Time	Mass flow in (kg/s)	Mass flow out (kg/s)	Mass flow - Net (kg/s)	Dry Bulb Air Temp (°C)	Relative humidity (%)	Wet Bulb Temp (°C)	Initial		Final @ 90% RH		Δh (kJ/kg)	Energy (kJ/s) (kWatts)	Final @ 90% RH				
							Enthalpy h <sub>i</sub> (kJ/kg)	Absolute Humidity W <sub>i</sub> (g-H <sub>2</sub> O/kg air)	Enthalpy h <sub>f</sub> (kJ/kg)	Absolute Humidity W <sub>f</sub> (g-H <sub>2</sub> O/kg air)	Mass Water Rate (g-H <sub>2</sub> O/s)			Mass Water (g-H <sub>2</sub> O)	Volume Water (Liters)			
Tue, 21/Dec																		
Date																		
Tue,	00:30	0.00	8.33	8.33	19.98	81.52	17.84	50.44	11.96	50.47	12.39	0.03	0.26	3.59	6,467	7		
	01:30	0.00	7.68	7.68	19.52	83.59	17.65	49.86	11.92	49.89	12.24	0.02	0.18	2.46	4,432	4		
	02:30	0.00	6.61	6.61	19.15	87.26	17.72	50.10	12.16	50.11	12.30	0.01	0.06	0.89	1,601	2		
	03:30	0.00	6.66	6.66	19.02	86.06	17.46	49.29	11.89	49.30	12.09	0.01	0.09	1.29	2,316	2		
	04:30	0.00	4.89	4.89	18.98	83.72	17.15	48.34	11.54	48.36	11.85	0.02	0.11	1.51	2,719	3		
	05:30	0.00	6.33	6.33	18.65	84.74	16.96	47.74	11.44	47.76	11.69	0.02	0.11	1.62	2,915	3		
	06:30	0.00	5.54	5.54	18.15	88.18	16.86	47.48	11.54	47.49	11.62	0.01	0.03	0.48	864	1		
	<b>07:30</b>	<b>0.00</b>	<b>9.61</b>	<b>9.61</b>	<b>18.78</b>	<b>85.06</b>	<b>17.12</b>	<b>48.23</b>	<b>11.58</b>	<b>48.25</b>	<b>11.82</b>	<b>0.02</b>	<b>0.16</b>	<b>2.32</b>	<b>4,169</b>	<b>4</b>	<b>0.16</b>	<b>4.19</b>
	08:30	0.00	14.75	14.75	20.28	78.4	17.74	50.13	11.72	50.17	12.31	0.04	0.65	8.83	15,888	16	0.65	15.98
	09:30	0.00	18.25	18.25	21.84	73.46	18.56	52.68	12.09	52.75	12.99	0.07	1.27	16.44	29,592	30	1.27	29.77
	10:30	0.00	20.54	20.54	23.69	64.39	18.97	53.97	11.85	54.09	13.35	0.12	2.44	30.73	55,305	56	2.44	55.64
	11:30	0.00	20.95	20.95	25.43	58.49	19.60	56.01	11.95	56.17	13.90	0.16	3.34	40.95	73,713	74	3.34	74.16
	12:30	0.01	17.54	17.53	26.89	56.06	20.46	58.91	12.49	59.09	14.69	0.19	3.30	38.57	69,431	70	3.30	69.85
	13:30	0.02	16.23	16.21	27.63	51.43	20.30	58.31	11.96	58.52	14.54	0.22	3.56	41.82	75,268	76	3.56	75.72
	14:30	1.37	13.48	12.10	27.66	48.78	19.85	56.79	11.35	57.02	14.13	0.23	2.79	33.61	60,498	61	2.79	60.86
	15:30	14.51	3.66	10.85	26.59	52.32	19.58	55.90	11.44	56.10	13.88	0.20	2.18	26.55	47,795	48	2.18	48.08
	16:30	26.24	0.00	26.24	24.9	58.09	19.08	54.30	11.49	54.45	13.44	0.16	4.10	51.27	92,281	93	4.10	92.84
	<b>17:30</b>	<b>24.79</b>	<b>0.00</b>	<b>24.79</b>	<b>23.74</b>	<b>62.12</b>	<b>18.69</b>	<b>53.03</b>	<b>11.46</b>	<b>53.16</b>	<b>13.10</b>	<b>0.13</b>	<b>3.18</b>	<b>40.63</b>	<b>73,137</b>	<b>74</b>	<b>3.18</b>	<b>73.58</b>
	18:30	21.88	0.00	21.88	22.8	63.42	18.05	51.01	11.05	51.13	12.56	0.11	2.51	33.22	59,792	60		
	19:30	17.12	0.00	17.12	22.29	62.92	17.53	49.40	10.62	49.51	12.14	0.11	1.91	26.12	47,024	47		
	20:30	13.91	0.00	13.91	21.57	66.21	17.35	48.86	10.69	48.95	12.00	0.09	1.31	18.15	32,669	33		
	21:30	14.78	0.00	14.78	20.78	69.73	17.11	48.14	10.73	48.21	11.81	0.08	1.13	15.94	28,697	29		
	22:30	16.18	0.00	16.18	20.28	74.1	17.21	48.47	11.06	48.53	11.89	0.06	0.95	13.38	24,078	24		
	23:30	14.10	0.11	13.98	20.08	80.1	17.76	50.20	11.82	50.23	12.33	0.04	0.52	7.08	12,742	13		
				335.7385									36.17			828	26.83	596.49

189

# Appendix I: Latent Heat Calculation

## Prototype Model Calculations – December 21

### Water Spray Effect @ RH 100%

Simulation Results								Psychrometric Chart				Calculations							
Date	Time	Mass flow in (kg/s)	Mass flow out (kg/s)	Mass flow - Net (kg/s)	Dry Bulb Air Temp (°C)	Relative humidity (%)	Wet Bulb Temp (°C)	Initial		Final @ 90% RH		Final @ 100% RH							
Tue, 21/Dec								Enthalpy $h_f$ (kJ/kg)	Absolute Humidity $W_f$ (g <sub>H2O</sub> /kg air)	Enthalpy $h_f$ (kJ/kg)	Absolute Humidity $W_f$ (g <sub>H2O</sub> /kg air)	$\Delta h$ (kJ/kg)	Energy (kJ/s) (kWatts)	Mass Water Rate (g <sub>H2O</sub> /s)	Mass Water (g <sub>H2O</sub> )	Volume Water (Liters)			
Date								(Absolute)											
Tue,	00:30	0.00	8.33	8.33	19.98	81.52	17.84	50.44	11.96	50.47	12.39	0.07	0.55	7.45	13,411	13			
	01:30	0.00	7.68	7.68	19.52	83.59	17.65	49.86	11.92	49.89	12.24	0.06	0.44	6.00	10,798	11			
	02:30	0.00	6.61	6.61	19.15	87.26	17.72	50.10	12.16	50.11	12.30	0.04	0.29	3.94	7,091	7			
	03:30	0.00	6.66	6.66	19.02	86.06	17.46	49.29	11.89	49.30	12.09	0.05	0.32	4.33	7,802	8			
	04:30	0.00	4.89	4.89	18.98	83.72	17.15	48.34	11.54	48.36	11.85	0.05	0.27	3.73	6,711	7			
	05:30	0.00	6.33	6.33	18.65	84.74	16.96	47.74	11.44	47.76	11.69	0.05	0.32	4.47	8,053	8			
	06:30	0.00	5.54	5.54	18.15	88.18	16.86	47.48	11.54	47.49	11.62	0.04	0.21	2.97	5,348	5			
	<b>07:30</b>	<b>0.00</b>	<b>9.61</b>	<b>9.61</b>	<b>18.78</b>	<b>85.06</b>	<b>17.12</b>	<b>48.23</b>	<b>11.58</b>	<b>48.25</b>	<b>11.82</b>	<b>0.05</b>	<b>0.47</b>	<b>6.67</b>	<b>12,011</b>	<b>12</b>	<b>0.47</b>	<b>12.08</b>	
	08:30	0.00	14.75	14.75	20.28	78.4	17.74	50.13	11.72	50.17	12.31	0.04	0.65	8.83	15,888	16	0.65	15.98	
	09:30	0.00	18.25	18.25	21.84	73.46	18.56	52.68	12.09	52.75	12.99	0.11	1.94	25.07	45,127	45	1.94	45.40	
	10:30	0.00	20.54	20.54	23.69	64.39	18.97	53.97	11.85	54.09	13.35	0.16	3.22	40.56	72,999	73	3.22	73.44	
	11:30	0.00	20.95	20.95	25.43	58.49	19.60	56.01	11.95	56.17	13.90	0.20	4.18	51.16	92,079	93	4.18	92.64	
	12:30	0.01	17.54	17.53	26.89	56.06	20.46	58.91	12.49	59.09	14.69	0.23	4.05	47.32	85,171	86	4.05	85.69	
	13:30	0.02	16.23	16.21	27.63	51.43	20.30	58.31	11.96	58.52	14.54	0.26	4.25	49.87	89,761	90	4.25	90.30	
	14:30	1.37	13.48	12.10	27.66	48.78	19.85	56.79	11.35	57.02	14.13	0.27	3.29	39.55	71,183	72	3.29	71.61	
	15:30	14.51	3.66	10.85	26.59	52.32	19.58	55.90	11.44	56.10	13.88	0.24	2.61	31.84	57,305	58	2.61	57.65	
	16:30	26.24	0.00	26.24	24.9	58.09	19.08	54.30	11.49	54.45	13.44	0.19	5.11	63.86	114,956	116	5.11	115.65	
	<b>17:30</b>	<b>24.79</b>	<b>0.00</b>	<b>24.79</b>	<b>23.74</b>	<b>62.12</b>	<b>18.69</b>	<b>53.03</b>	<b>11.46</b>	<b>53.16</b>	<b>13.10</b>	<b>0.17</b>	<b>4.11</b>	<b>52.40</b>	<b>94,318</b>	<b>95</b>	<b>4.11</b>	<b>94.89</b>	
	18:30	21.88	0.00	21.88	22.8	63.42	18.05	51.01	11.05	51.13	12.56	0.15	3.28	43.41	78,143	79			
	19:30	17.12	0.00	17.12	22.29	62.92	17.53	49.40	10.62	49.51	12.14	0.15	2.49	33.98	61,162	62			
	20:30	13.91	0.00	13.91	21.57	66.21	17.35	48.86	10.69	48.95	12.00	0.13	1.78	24.50	44,098	44			
	21:30	14.78	0.00	14.78	20.78	69.73	17.11	48.14	10.73	48.21	11.81	0.11	1.61	22.64	40,748	41			
	22:30	16.18	0.00	16.18	20.28	74.1	17.21	48.47	11.06	48.53	11.89	0.09	1.48	20.73	37,308	38			
	23:30	14.10	0.11	13.98	20.08	80.1	17.76	50.20	11.82	50.23	12.33	0.07	1.00	13.54	24,369	25			
													<b>47.92</b>				<b>1,102</b>	<b>33.42</b>	<b>743.25</b>

335.7385

190



# Appendix I: Latent Heat Calculation

## 1.5m Cavity Model Calculations – June 21

### Water Spray Effect @ RH 100%

Date	Time	Mass flow in (kg/s)	Mass flow out (kg/s)	Mass flow - Net (kg/s)	Dry Bulb Air Temp (°C)	Relative humidity (%)	Wet Bulb Temp (°C)	Initial		Final @ 100% RH		Final @ 100% RH							
								Enthalpy $h_i$ (kJ/kg)	Absolute Humidity $W_i$ (g <sub>H2O</sub> /kg air)	Enthalpy $h_f$ (kJ/kg)	Absolute Humidity $W_f$ (g <sub>H2O</sub> /kg air)	$\Delta h$ (kJ/kg)	Energy (kJ/s) (kWatts)	Mass Water Rate (g <sub>H2O</sub> /s)	Mass Water (g <sub>H2O</sub> )	Volume Water (Liters)			
	00:30	0.9545	12.7479	11.79	29.52	69.61	25.00	76.30	18.25	76.50	20.17	0.20	2.36	22.69	40,848	41			
	01:30	0	14.8975	14.90	29.04	67.59	24.24	73.14	17.20	73.35	19.24	0.21	3.08	30.38	54,690	55			
	02:30	0	13.6587	13.66	27.91	68.49	23.36	69.67	16.30	69.85	18.23	0.19	2.57	26.31	47,359	48			
	03:30	0	11.1376	11.14	27.47	68.58	22.98	68.18	15.90	68.37	17.80	0.18	2.04	21.16	38,092	38			
	04:30	0	10.9967	11.00	27	68.53	22.55	66.54	15.44	66.71	17.33	0.18	1.95	20.69	37,243	37			
	05:30	0	14.3812	14.38	26.48	68.14	22.02	64.56	14.88	64.74	16.76	0.17	2.49	27.06	48,716	49			
	06:30	0	20.0883	20.09	27.12	67.91	22.56	66.58	15.41	66.76	17.34	0.18	3.65	38.71	69,680	70			
	<b>07:30</b>	<b>0</b>	<b>22.4255</b>	<b>22.43</b>	<b>29.24</b>	<b>63.43</b>	<b>23.73</b>	<b>71.06</b>	<b>16.31</b>	<b>71.30</b>	<b>18.65</b>	<b>0.23</b>	<b>5.19</b>	<b>52.38</b>	<b>94,292</b>	<b>95</b>	<b>5.19</b>	<b>94.86</b>	
	08:30	0	26.4233	26.42	32.06	52.11	24.11	72.50	15.73	72.84	19.09	0.34	8.96	88.95	160,110	161	8.96	161.08	
	09:30	0	27.2141	27.21	34.11	44.89	24.32	73.24	15.19	73.66	19.34	0.42	11.47	112.84	203,107	204	11.47	204.33	
	10:30	0	25.0287	25.03	37.12	36.99	24.83	75.26	14.76	75.80	19.96	0.54	13.53	130.15	234,276	236	13.53	235.69	
	11:30	0	25.3168	25.32	39.77	28.53	24.49	73.73	13.10	74.39	19.55	0.66	16.76	163.18	293,726	295	16.76	295.50	
	12:30	0	27.0802	27.08	41.16	22.39	23.55	69.84	11.04	70.57	18.44	0.73	19.77	200.34	360,612	363	19.77	362.79	
	13:30	0	27.8393	27.84	42.46	18.5	23.05	67.85	9.75	68.63	17.88	0.79	21.87	226.33	407,395	410	21.87	409.85	
	14:30	0	29.8419	29.84	42.45	22.19	24.33	72.93	11.72	73.70	19.35	0.78	23.19	227.61	409,702	412	23.19	412.17	
	15:30	6.0776	18.6627	12.59	41.07	29.04	25.57	78.20	14.32	78.91	20.88	0.70	8.85	82.59	148,660	150	8.85	149.56	
	16:30	10.9477	16.4922	5.54	39.01	35.61	25.91	79.80	15.77	80.40	21.33	0.60	3.34	30.83	55,490	56	3.34	55.83	
	<b>17:30</b>	<b>12.9088</b>	<b>15.1477</b>	<b>2.24</b>	<b>37.28</b>	<b>41.21</b>	<b>25.99</b>	<b>80.25</b>	<b>16.64</b>	<b>80.77</b>	<b>21.44</b>	<b>0.52</b>	<b>1.17</b>	<b>10.74</b>	<b>19,337</b>	<b>19</b>	<b>1.17</b>	<b>19.45</b>	
	18:30	34.6817	0	34.68	35.34	49.54	26.32	81.79	18.03	82.21	21.87	0.42	14.67	133.35	240,022	241			
	19:30	<b>27.8761</b>	0	27.88	33.63	61.77	27.31	86.39	20.52	86.70	23.23	0.31	8.60	75.52	135,932	137			
	20:30	17.2923	0	17.29	32.85	65.66	27.33	86.53	20.89	86.80	23.26	0.27	4.67	40.94	73,694	74			
	21:30	12.4917	0	12.49	32.17	66.01	26.78	84.03	20.19	84.28	22.50	0.26	3.23	28.82	51,869	52			
	22:30	8.2076	0	8.21	31.17	69.6	26.50	82.78	20.11	83.00	22.11	0.22	1.82	16.41	29,538	30			
	23:30	1.2015	2.0349	0.83	30.37	74.92	26.64	83.45	20.70	83.63	22.30	0.18	0.15	1.33	2,398	2			
				429.8745									185.39				3276.45	128.92	2306.25







